Preliminary Cruise Report, TicoFlux I Expedition

R/V *Maurice Ewing* 0104, 14 April - 19 May 2001

The thermal state of 20-25 Ma lithosphere subducting at the Costa Rica Margin: implications for hydrogeology, fluxes, and the seismogenic zone

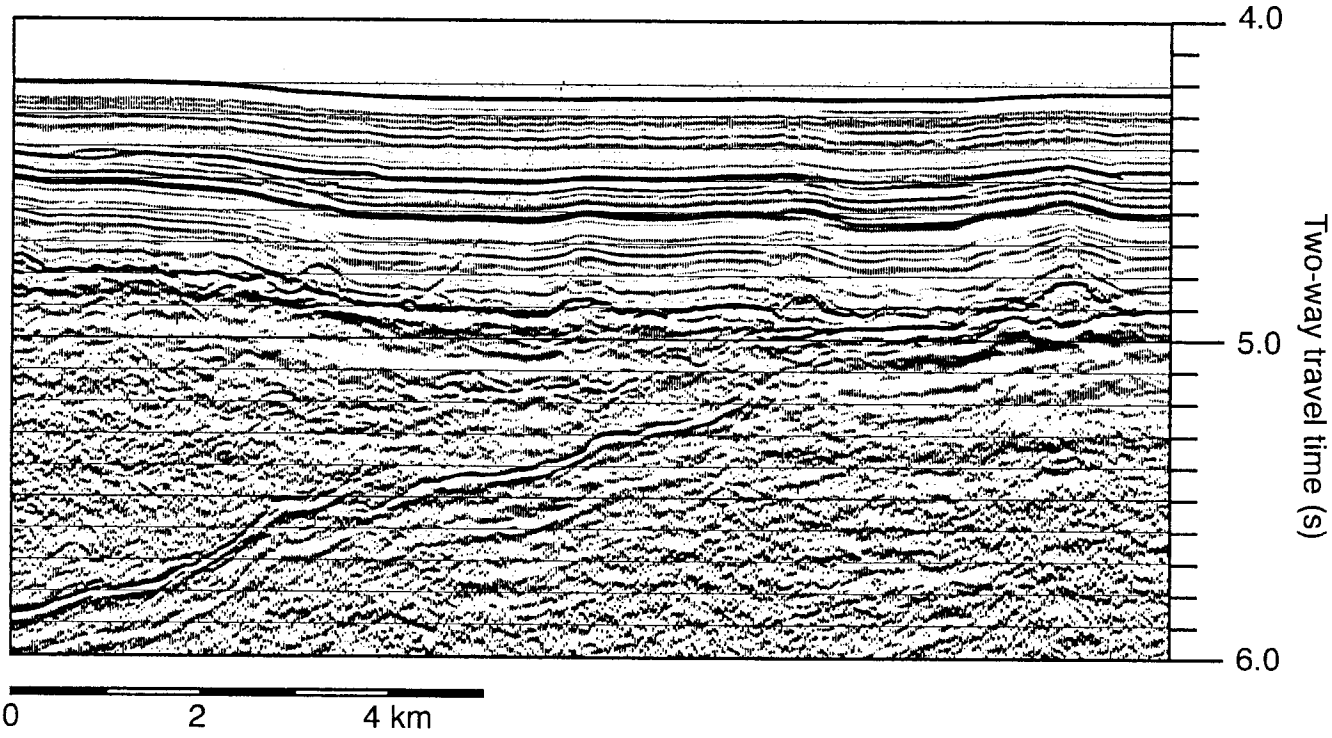

Scientific Participants: A. Fisher[1], E. Silver[1], G. Wheat[2], R. Harris[3], C. Stein[4], K. Wang[5], M. Underwood[6], C. Moser[7], M. Hutnak[1], A. Cherkaoui[1], R. Kelly[8], M. Pfender[9], P. Friedmann[1], R. Bodzin[1], R. Cleary[1], Y. Stewart[10], K. Jones[11]

[1] University of California, Santa Cruz
[2] University of Alaska Fairbanks
[3] University of Utah
[4] University of Illinois, Chicago
[5] Pacific Geoscience Center, Geological Survey of Canada
[6] University of Missouri
[7] Oregon State University
[8] Woods Hole Oceanographic Institution
[9] University of Bremen
[10] Maine Maritime Academy
[11] Indiana University of Pennsylvania

I. Introduction

This report provides an operational and scientific overview of the TicoFlux I expedition (*Maurice Ewing* cruise EW0104) to the incoming plate along the Costa Rica margin, eastern equatorial Pacific Ocean. This report was prepared during and at the end of scientific operations, so all analysis is preliminary. Greater detail regarding background, motivation and strategy is presented in the NSF proposal that funded this work, along with references to previous work in this area.

The TicoFlux I expedition was highly successful, both operationally and scientifically. We had some difficulties with equipment, but achieved all primary objectives. This success is directly attributable to the skill and dedication of the ship's crew and technical support staff and the outstanding facilities available on the *Maurice Ewing*. This report ends with some observations and recommendations concerning shipboard facilities and personnel.

A. Scientific Objectives

The TicoFlux I expedition was the first part of a field, lab and modeling program to investigate the nature of hydrothermal activity and its influence on lithospheric and subduction processes offshore of the Nicoya Peninsula, Costa Rica margin. Field and lab components comprise seismic, swath-mapping, heat flow, and geochemistry (coring) programs on 20-25 Ma lithosphere seaward of the Middle America Trench. These studies are to be based, in part, on data and samples collected during two marine expeditions, one during Spring 2001 and a second (to be scheduled) during 2002. Modeling components of this project includes numerical studies of the incoming plate and of the subduction zone. Collectively, these studies will help to resolve: (1) the nature and extent of hydrothermal circulation, and thus the likely thermal state and water content of the crust before it enters the trench; (2) the influence of these conditions on subduction processes; and (3) the significance of ridge-flank hydrothermal circulation for global solute fluxes. The field area is ideal for this work because it contains a fundamental transition in the structural, thermal and hydrogeologic state of the incoming plate. The region is the subject of numerous other studies emphasizing elemental fluxes and the seismogenic zone, but fluid and thermal conditions within the incoming plate are poorly understood. Considerable effort has focused on conditions and processes landward of, and immediately adjacent to, the trench; we are focusing observational efforts on a 120 nmi × 120 nmi (2° × 2°) region largely seaward of the trench (Fig I-1).

This work is intended to address these questions:

(1) What is the thermal state of the lithosphere being subducted below the Nicoya Peninsula?

(2) What are characteristic heat and fluid fluxes responsible for this thermal state, how does water enter and exit the crust in this area, and what are the characteristic length scales of flow?

(3) How do the thermal state, water content, sediment composition, and diagenetic state of the incoming plate influence the mechanics of the subduction zone?
(4) What are the chemical implications of extensive fluid circulation within the incoming plate, both to the subduction zone and to the overlying ocean, and how can these data be used to understand global fluxes?

The TicoFlux I expedition included regional and local goals. We wanted to map out regional crustal structures and define the various tectonic boundaries across the work area using a combination of seismic, thermal and geochemical tools. We also hoped to determine the nature of regional thermal conditions in basement within distinct seafloor areas. We planned to evaluate whether various tectonic boundaries (ridge jump, propagator trace, triple-junction trace, fracture zone, faults) were associated with thermal, chemical, seismic and hydrogeologic boundaries. We also wanted to establish the nature of thermal and chemical variations around basement outcrops, and evaluate directions and intensity of fluid flow within basement using thermal and chemical tracers. Field and lab work will be complemented by modeling to help us understand and extend these results to other areas.

C. Regional Setting

Costa Rica lies at the southern end of the Central American arc system, formed by subduction of the Cocos Plate under the Pacific Margin. The surface manifestation of this subduction - the Middle America Trench - has its southern end off southernmost Costa Rica, where it intersects the Panama fracture zone. The regional tectonic setting of southeastern Central America is controlled by the convergence of the Cocos, Caribbean, and South American Plates. The oceanic Cocos Plate subducts beneath the Caribbean Plate along the Middle American Trench at rates of 70 mm/yr off Guatemala to nearly 90 mm/yr off southern Costa Rica. The north-trending boundary between the Cocos and Nazca Plates is the right-lateral Panama Fracture Zone. West of this fracture zone is the Cocos Ridge, a trace of the Galapagos Hotspot, which subducts beneath southern Costa Rica and northern Panama.

The Cocos plate offshore northern Costa Rica is 20-25 Ma (early Neogene) in age, as interpreted on the basis of magnetic anomalies and other data. Drilling at ODP Site 1039 on Leg 170, near the axis of the trench, penetrated 180 m of diatom-rich hemipelagic claystones, with interspersed ash layers, overlying about 200 m of nannofossil-rich carbonate ooze. The base of the sedimentary section is a brown, metalliferous claystone, intruded by gabbroic sills. The oldest sediment recovered at Site 1039 was 16.5 Ma.

The incoming plate offshore Costa Rica can be subdivided into tectonically-distinct subregions (Fig. I-1). The region offshore of the northern Nicoya Peninsula has magnetic anomalies that strike approximately N40W and was produced along the East Pacific Rise. Towards

the middle of the Nicoya Peninsula there is a boundary across which the magnetic anomalies abruptly switch orientation by ~90°, to N45E. This boundary is thought to separate crust formed at the EPR from that formed at the Cocos-Nazca Spreading Center, making it the trace of the triple junction, and also corresponds (at least, in part) to an abrupt difference in the relief of upper basement, known as the "rough-smooth boundary" (RSB). Continuing to the southeast, there is another, more subtle, realignment of magnetic anomalies, which corresponds near the trench to the Fisher Ridge. The crust between the RSB and Fisher Ridge is referred to as the "smooth segment," while crust south of the Fisher Ridge is referred to as the "seamount segment". As suggested by the name, seamounts are much more common southeast of the Fisher Ridge than northwest of the ridge, although the oceanic crust still has a normal thickness of 6-7 km.

In fact, the area of the TicoFlux I survey northwest of the triple junction trace (Fig. I-1) has been known for some time to include significant areas of shallow water. It is identified on DMA charts at "Guardian Bank" and includes numerous "shoals" and other areas of shallow water. Bathymetry generated from a combination of satellite gravimetry and depth profiles prior to TicoFlux I suggested that there were several large seamounts within the planned work area, and some of these were targeted for mapping, seismic profiling, heat flow, and core sampling.

Although the transition in magnetic anomalies along the RSB is abrupt, the regional transition in basement relief appears to be more gradual. One possible explanation for this change in basement relief is that the orientation of the primary structural grain of the crust (as expressed by the orientation of magnetic anomalies), varies north and south of the RSB relative to the orientation of the subduction zone. To the northwest of the RSB, the magnetic anomalies are roughly parallel to the trench, while to the southeast of the RSB, magnetic anomalies are roughly perpendicular to the trench. This change in orientation of magnetic anomalies, and thus the structural grain of the crust, may have profound implications for the fluid and thermal evolution of the plate.

Heat flow data within and near the study area collected prior to TicoFlux I are sparse (typical spacing of 60-120 km), but there is a clear trend in the distribution of values. North of the RSB, heat flow is low (average = 31 mW/m^2), whereas heat flow to the south of the RSB is generally higher (average = 110 mW/m^2). The age contrast across the RSB is too small to account for the observed transition in seafloor heat flow. The global average of measured heat flow for this crustal age (20-25 Ma) is about 72 mW/m^2, corresponding to a heat flow fraction ($q_{observed}/q_{expected}$) of 0.67. This fraction indicates that, on average, 1/3 of heat flow through oceanic lithosphere of this age is lost by advection. The heat flow fraction north of the RSB is generally ≤ 0.25, suggesting an even larger fraction of advective heat loss, but the heat flow fraction south of the RSB is generally ≥ 1.0. Hence, heat flow north of the RSB is low compared to both lithospheric-conductive and global average values, whereas that south of the RSB is high

compared to both lithospheric-conductive and global average values. The latter situation is particularly unusual because most young-crust sites have heat flow significantly lower than that predicted by conductive lithosphere models, presumably because advected heat loss is not measured by heat flow probes.

II. Operational Summary

Table I-1 lists EW0104 operations, dates and times. The start of the port call in Colon, Panama was intended to begin on the morning of 4/12/01 but was delayed until the afternoon while the ship was at anchorage awaiting dock space. Scientists and crew were ferried out to the ship at anchorage in the afternoon of 4/12, and the ship was brought to the dock at 4:00 pm local time. Loading of scientific gear began immediately and continued until 9:00 pm. Loading continued the following morning and afternoon, and the ship left the dock and headed for the locks at 5:00 pm on 4/13. Passage through to the Pacific Ocean was completed at 3:00 am on 4/14, and the ship got underway for the work area after the canal crew left the ship.

The transit required 39 hours, and we stopped beyond the southern edge of the work area to collect a single gravity core, to test the equipment and establish deck and lab protocols for working with cored material. The seismic streamer and guns were deployed, and we began nine days of seismic/hydrosweep/3.5-kHz surveying at 4.86 kts. The survey went well and generated very good records of sediment and crustal structure and seafloor bathymetry. We had a computer problem while crossing one of the regional tectonic boundaries, resulting in loss of about 60 minutes of seismic data (Line 9), but coverage along the seismic lines was otherwise virtually complete. We learned after the survey was nearly over that we had not been receiving P-code GPS positions during most of the survey because the P-code antenna had been accidentally turned upsidedown on the roof of the A-deck winch shack. This resulted in degradation of navigation data during the seismic survey, with most positions being based on C/A code GPS locations, giving an uncertainty of 50-100 m rather than the anticipated P-code positioning uncertainty of 10-20 m. Hydrosweep records were generally of good quality, although edited files yielded reliable data within a swath only slightly greater in width than the water depth. XBTs were deployed and data recorded twice during TicoFlux I, in the western and southeastern parts of the survey area, to assist with processing of hydrosweep data. We also ran numerous additional small hydrosweep "surveys" as we transited between coring and heat flow stations later in the cruise, to fill gaps and complete coverage of specific targets.

After the seismic streamer was recovered, we moved to the next coring station and collected four gravity cores in 12 hours, then proceeded with the first heat flow station, which lasted 27 hours. Coring operations (gravity and piston) were run from the starboard rail using the trawl wire and winch, and heat flow operations were run from the fan tail using the 0.680 wire and traction

winch. A 12-kHz pinger was attached to the wire for all heat flow and gravity coring operations and was essential for determining instrument locations relative to the bottom because of problems with wire-out indicators. Once the instruments were placed in the water, winch control was transferred to the main lab. Coring and heat flow stations alternated in intervals of approximately 12 and 24 hours, respectively, with additional time occupied by transits and hydrosweep surveys. We worked around the field area in a clockwise direction, starting near the western edge and working towards the north and east, finally returning to the northeast and middle areas for the final stations.

We had problems with the heat flow probe during stations HF-03 and HF-04, with the thermistor tube breaking off at the support fin on the front of the lance. In each case, the probe was returned to the ship and repaired. We attribute this problem to not waiting long enough after moving the ship before making the next measurement, allowing the probe to drift too far behind the ship. During subsequent stations we waited 20-40 minutes for the probe to swing back under the ship after moving to a new measurement location, and we had no more problems with broken thermistor tubes. The batteries in the pinger used to telemeter heat flow data were drained and had to be replaced during station HF-07, requiring probe recovery and redeployment. We had to recover the probe a second time after a crimped wire in the pinger shorted out against the wall of the pressure case. We also had difficulty with the level wind mechanism on the trawl winch, the A-deck sheave for the traction winch, and with metering of both winch systems (wire out, rate, tension). Collectively, repair of the winch and gauge systems required about 24 hours over the length of the expedition.

TicoFlux I ended at 8:20 am on 5/17 with completion of a short heat flow station in the southeastern survey area. After recovering the gear, we transited to Balboa, Panama, arriving at anchorage at 6:00 am on 5/19. All scientific equipment was offloaded during the day and evening of 5/19, and most equipment was loaded into cargo vans for shipment back to the U.S.

III. Seismic Reflection Surveys

The objectives of the seismic survey were to delineate basement geometry and sediment thickness, determine the nature of subsurface crustal structures for lithosphere formed by East Pacific Rise spreading and by Cocos-Nazca Ridge spreading, evaluate differences in seismic velocities in upper basement, and support heat flow and coring operations. The seismic reflection survey required 9.6 days of ship time, including deployment and recovery of the streamer and guns. During the period of JD 107, 0245 (GMT) to JD 115, 0353 we obtained over 1800 km of seismic data resulting from over 48,000 shots. The shots were generated with a 10-gun array and were spaced 37.5 m apart. The hydrophone streamer array was 6000 m long and consisted of 480 channels spaced 12.5 m apart, giving a CDP spacing of 6.25 m and 80 fold subsurface coverage.

Survey parameters and locations and times of individual lines are listed in Tables III-1, III-2 and III-3. Locations of lines are shown in Figure III-1.

The streamer had been extensively repaired prior to our cruise, and QC observations showed data collected after these repairs to be of high quality. No channels were consistently bad; only one channel (51) showed consistent noise, but even that one was usable. A small fraction (about 0.1%) of the shots were lost (Table III-3). Some additional shots were not recorded due to problems with the P-code GPS antenna. Data were collected with the LDEO Syntron system on 3490 tapes and copied to DAT tapes for later processing. During acquisition, tapes were copied and a stack was made of the near 120 channels using the SIOSEIS processing system, and a continuous plot of the brute stack was produced on the Atlantek plotter. After each line was completed, the stack was migrated with SIOSEIS and plotted. Because of the time involved in migrating large data sets, most lines were migrated in sections of 40 km or less.

The results of the seismic survey were excellent overall, thanks to a combination of a source array that gave a sharp seismic signature, a streamer array that recorded virtually all channels well, and knowledge of the regional velocity structure that gave clear results with the initial brute stack. After the heat flow lines were collected, 2 to 3 hour segments of seismic data corresponding to the heat flow lines were printed page-sized (Figures III-2 to III-14), making it easy to see the details of the lines at a glance. Heat flow locations and preliminary values are plotted over the seismic data in these figures.

Following data acquisition, gathers were saved for most of the lines at an interval of 50 CDPs. Using a combination of SIOSEIS and Matlab, velocity analyses were carried out on a few line segments, and some of these gave significantly improved subsurface images. Regionally there is about 400-500 m of sediment covering a highly reflective basement. Drilling results from ODP Site 1039 documented that the upper 150 m of sediments are composed of hemipelagic mudstone and the lower section is largely pelagic nannofossil ooze. Each of Figures III-2 to III-14 shows signs of tectonic activity within the plate. In most cases ridges and seamounts are not simply draped with sediments, but they often show evidence of post depositional or syndepositional deformation. Figures III-2 and III-7 show good examples of stratigraphic pinchouts and overlap. In many cases the lowermost 0.15 s of strata appear to be deformed after they were deposited. The well-layered middle part (pelagic ooze) appears to be deformed during deposition (for example, see Figure III-11), and the upper hemipelagic layer generally covers the deformation. There are, however, many examples of deformation extending through to the surface and clearly affecting the hemipelagics (e.g., Figs. III-6, III-7, and III-10).

We show two examples of lines that are migrated after a full stack involving velocity analysis. Figure III-15 is from the NW part of seismic Line 11 and images a clear example of a reflection that cuts deeply through the oceanic crust, dipping at an angle of roughly 20 degrees to

the NW. Such through-crustal dipping reflections are not common here, but they are seen on parallel Lines 13 (Figure III-16) and 5 (Figure III-5). The dipping reflections in Figure III-16 are not restricted to a single plane. In Figure III-5 the reflection is sinuous. All of these low-angle reflections dip to the NW. A line crossing these at right angles shows deep crustal reflections that appear horizontal at about 1.5 s beneath the sediment-crust interface, suggesting that Lines 5, 11 and 13 are essentially dip lines.

Several examples are seen of a mantle reflection. The most notable is at the north end of Line 1, where a sharp reflection occurs 2 s beneath the sediment-crust interface. The seismic data also indicate that sill intrusion may be common in this region. We base this inference on the interpretation of seismic structure on these profiles and also on the fact that ODP Leg 170 bottomed in sills at two locations, the only two to bring up rocks from oceanic basement. The seismic structure indicates numerous regions where the base of the sediment section is a very smooth, high amplitude reflection. In addition, there are a number of regions where signs of youthful uplift occur (Fig. III-17).

IV. Heat Flow Surveys

The TicoFlux I heat flow program comprised two main components. Most measurements were made a 3.5-m, 11-thermistor, violin-bow heat flow system built and maintained at the Pacific Geoscience Center by Earl Davis and colleagues. This system provided real-time (analog) telemetry and in-situ thermal conductivity measurements. Internal power allowed stations to run 20-30 hours when fully charged, and most stations consisted of 8-15 measurements separated by 1.0 nmi (1.9 km; Fig. IV-1).

The second part of the heat flow program was based on autonomous outrigger thermistor probes banded to piston and gravity core barrels. These tools were developed through collaboration between the scientists at University of Bremen (led by Heiner Villinger) and Antares, a private company in Bremen, Germany. We also measured thermal conductivity at high resolution using the needle probe method in a single, 5-m piston core.

A. Multipenetration Heat Flow Stations

Multipenetration heat flow measurements were made by lowering the heat flow probe into the seafloor at 60 m/min. After a measurement was completed, the probe was raised to 600-2000 m above the seafloor while the ship transited at 1-2 kts to the next site. Tool penetration was typically followed by 7 minutes during which the thermistor tube was allowed to thermally equilibrate with the surrounding sediments (Fig. IV-2). A calibrated heat pulse was then fired, and the thermal response of the thermistor tube was monitored to determine in-situ thermal conductivity. Multipenetration heat flow data were parsed into individual penetration files and processed using

SlugHeat, a Matlab program based on the hfred/hflow set of processing programs (Fig. IV-3). Additional analysis will be required to finalize the heat flow values listed in this report (Table IV-1), but values are unlikely to change by more than a few percent as a result of reanalysis. No corrections have been applied for at this stage for instrument tilt (generally less than 5°), sedimentation, or local topography. We attempted 130 heat flow penetrations during TicoFlux I and completed 127 successful measurements (Table IV-1, Figure IV-1). Contour maps show the locations of heat flow measurements (Figs. IV-4 to IV-13) and data are plotted above seismic reflection profiles in Figs III-3 to III-14).

Heat flow station HF01 is collocated with seismic Line 7 and crosses a local basement high and outcrop (Fig. IV-4). To the northwest of the basement high, heat flow values are 50 to 60 mW m^{-2}. To the southeast of the basement high heat flow values drop to 29 and 24 mW m^{-2}, and then increase abruptly to 89 and 94 mW m^{-2}. This change in heat flow may be a manifestation of the transition between the warm and cold seafloor areas, or it may result from local fluid circulation patterns associated with nearby basement highs.

Heat flow station HF02 is also located along seismic Line 7 to the southeast of heat flow station HF01 (Figs. IV-1 and IV-5). This station traverses the ridge jump and was intended to investigate heat flow variations associated with this feature. Heat flow values are uniformly high, ranging between 114 and 129 mW m^{-2}.

Heat flow station HF03 lies along seismic Line 13 and is associated with a buried basement high (Figs IV-1 and IV-6). Heat flow values off the basement high are low, 16 to 28 mW m^2. Immediately adjacent to the basement high is a low heat flow value of 13 mW m^{-2}. Two penetrations were made over the basement high, and yielded values of 36 and 27 mW m^{-2}.

Heat flow station HF04 lies along seismic Line 5 and is to the northeast of heat flow station 3 (Figs. IV-1 and IV-7). This line is parallel to the trench axis and lies along the outer rise of flexing plate. Heat flow values are high ranging between 112 and 303 mW m^{-2}. High values are associated with a buried basement high that is the surface expression of the low-angle crustal reflector imaged in several seismic profiles (Fig. III-5).

Heat flow station HF05 lies along seismic Line 3 and is oriented perpendicular to the outer swell in an area of prominent normal faults (Figs. IV-1 and IV-8). Heat flow values are low, ranging between 14 and 35 mW m^{-2}. This profile is close to ODP Hole 1039 which has heat flow near the seafloor 17 mW m^{-2} and heat flow at depth of 9 mW m^{-2}.

Heat flow station HF06 is collocated with seismic Line 14 and crosses the propagator trace (Figs. IV-1 and IV-9). Heat flow values are high ranging between 109 and 128 mW m^{-2}. Two higher values, 203 and 214 mW m^{-2}, are associated with a buried basement high.

Heat flow station HF07 is collocated with seismic Line 13 and crosses the ridge jump (Figs. IV-1 and IV-10). Heat flow values vary between 127 and 148 mW m^{-2}. This station also crosses normal faults observed in seismic Lines 11, 13, and 14. The heat probe failed to penetrate the seafloor or partially penetrated during some measurements, so the seafloor in this area may be unusually hard compared to other areas in which we measured seafloor heat flow.

Heat flow station HF08 is collocated with seismic Line 11 and crosses the triple junction trace (Figs. IV-1 and IV-11). This station shows bimodal distribution of heat flow values. To the northwest, heat flow values are relatively low, ranging between 28 and 54 mW m^{-2}, with a trend to higher values approaching the triple junction trace. Over a distance of just 2 nmi, heat flow increases to values of 88 to 104 mW m^{-2}, with most of the increase occurring between two successive measurements. This transition in heat flow is displaced a short distance southeast of the mapped location of the triple junction trace and correlates with an abrupt (but small) decrease in basement depth and a thinning of sediments.

Heat flow station HF09 lies along seismic Line 13 and was intended to cross the triple junction trace and the transition from low to high heat flow in an area of relatively flat basement (Figs. IV-1 and IV-6). However the first measured value was relatively high, so we reoriented the line to the northwest. Heat flow along this station remained relatively high and consistent, with values of 102 to 111 mW m^{-2}.

Heat flow station HF10 fills the gap between heat flow stations HF03 and HF09, along seismic Line 13 (Figs. IV-1 and IV-6). The station runs northwest to southeast. The first two penetrations gave values of 28 and 35 mW m-2, respectively, and the next four penetrations yielded heat flow values between 89 and 100 mW m-2. Similar to HF08, the transition from low to high heat flow occurs in a relatively short distance, and correlates with a local basement high. However, the transition in heat flow is displaced to the northeast, well away from the mapped position of the triple junction trace.

Heat flow station HF11 is a continuation of heat flow station HF04 along seismic Line 5 (Figs. IV-1 and IV-7). This station was designed to help delineate the nature of the high heat flow region observed along heat flow station HF04. Heat flow values decrease from 640 to 48 mW m^{-2} with distance from the buried basement high.

Heat flow station HF12 lies along seismic Line 13 and was intended to delineate the transition from lower to higher heat flow values thought to be associated with the triple junction trace (Figs. IV-1 and IV-12). The first measurements indicated relatively high values (107-113 mW m^{-2}), so the probe was raised and the ship transited 11 nmi (20 km) to the northwest. The next four measurements documented an abrupt transition from lower to higher values (38 to 107 mW m^{-2}) from the northwest to the southeast, possibly associated with a large outcrop to the

northwest.

Heat flow station HF13 was located along seismic Line 8, near the edge of the trench east of the triple junction trace (Figs. IV-1 and IV-13). This station comprised only two measurements, heat flow values of 141 and 163 mW m^{-2}.

B. Autonomous Temperature Loggers on Cores

The autonomous data loggers are 175 mm in length, and have a nominal temperature measurement range of – 5 to + 60 °C, with higher sensitivity at lower temperatures. Instrument precision is 1 mK, and the absolute accuracy is on the order of several mK, based on laboratory calibration. The time constant of the thermistor fixed in the tip of the sensor tube, attached to the front of the data logger, is about 2 seconds. Non-volatile memory can hold up to 18 hours of measurements collected at a sample rate of 1 s, or data from a longer period recorded at a lower frequency.

The data loggers were mounted using fin-like attachments that extended from the core barrel. The attachments consist of a curved base, a longitudinal section of pipe, 12 cm in length and extending around 90° of arc; a plate welded to the base so that it projects away from the core barrel; and a cylindrical probe holder welded to the edge of the plate. The plate holds the logger and sensor 8 cm away from the outside of the core barrel, to avoid thermal disturbance from penetration of the core barrel, and the sensor tip extends 5 mm in front of the end of the probe housing. The data logger mounts were attached to the core barrels using a banding tensioner, seals, and crimper and stainless-steel banding (1.9 cm wide, 0.6 mm thick). The fins were attached on the core barrels in a spiral arrangement so that each logger would penetrate through undisturbed sediment.

Core barrels on which thermistor probes are attached are deployed and recovered using standard methods, with these exceptions. First, care must be taken so that the probes and probe mounts are not damaged during operations. The shallowest probes were attached far enough down the core barrel (about 1.5 m below the base of the weight stand) so that the would not be crushed or stripped off when the corer was moved into or out of the cradle support for the coring system. In addition, a braided cable that is used to assist in recovery of the corer is run along one side of the barrel, and probe attachments are positioned such that they will not interfere with this cable. When the core barrel penetrates the seafloor, it is left in place for several minutes to achieve partial thermal equilibration, and in-situ temperatures are extrapolated to equilibrium conditions.

At the start of the expedition we ran an empty support assembly to test the reliability of the banding straps, and after gaining confidence in the attachment method, we ran two to six tools on selected cores. The probes generally stayed in position, but we lost and damaged several

instruments and mounts when we cored thick ash layers or other lithologies that were difficult to penetrate. Seventeen cores were equipped with outriggers. One attachment including the data logger was lost and the sensor tips of four loggers were bent. Although the tools with bent tips continued to operate, they were not deployed again in order to prevent more damage. A tilt sensor deployed in the weight stand provided continuous tilt records during deployments; measured tilt was <5° in all deployments in which the probes penetrated the seafloor (i.e., the corer did not fall over).

Except from the first two deployments, which included empty probe mounts as an operational test, reliable gradients were determined from all deployments. The results are highly reproducible based on multiple measurements at one location, as PC18, 38 and 39 have shown, and are also confirmed by nearby measurements with the multipenetration heat flow probe. Instrumented gravity cores generally carried three temperature probes distributed over a length of 2.9 m. The number of outriggers on the piston cores varied with expected penetration depths and sediment types, but was as great as six probes over a depth range of 8.7 m.

A summary of results from all thermistor probe deployments is provided in Table IV-2, and an example of data from deployment on Core GC06 is shown in Figure IV-14. For this deployment, three probes were attached to the core barrel at distances of 1.58, 2.25 and 2.88 m from the base of the weight stand. The tools all penetrated the sediment and produced good temperature records, indicating a thermal gradient of 0.152 °C/m. Assuming a thermal conductivity of 0.74 W/m-K, based on data from nearby multipenetration probe measurements, heat flow at this site is 112 mW/m^2.

For coring sites GC03 and GC04, no reliable gradient can be given. In the first case, the upper sensor was knocked loose during deployment and had to be removed, and in the second case, the same tool did not penetrate into the sediment. Values from PC18, PC38 and PC39 indicated some of the highest heat flow values measured during the expedition, 570-605 mW/m^2, consistent with multipenetration measurements over a local basement high. Piston core PC19 penetrated completely with six temperature loggers attached to the core barrel, but one outrigger was lost and two others were damaged, probably during penetration of a thick ash layer.

C. Thermal Conductivity Measurements

We evaluated detailed thermal conductivity variations in PC18. These values were collected with two instruments, both using the transient, needle-probe technique. A University of Bremen instrument was used first to make measurements in 2-cm intervals with the pulse heating method. A UCSC instrument was used to collect additional data at a 2-cm interval, offset from the Bremen measurements by 1 cm, yielding a nominal 1-cm interval for the combined data set. We noted some

offset in values measured with the UCSC instrument on a needle-by-needle basis. We ran a series of tests with the UCSC instrument using a Jello standard and verified a consistent offset in apparent thermal conductivity values. We adjusted thermal conductivity values measured with the UCSC instrument to account for these offsets, greatly improving the self-consistency of the data (Fig. IV-15). Values vary from near 0.70 W/m °C near the seafloor to 0.75 W/m°C at 5 m depth. Small-scale variations are associated with changes in lithology, including a 10-cm-thick ash layer near 3 mbsf that resulted in higher thermal conductivities. These data will be used along with results of in-situ measurements to estimate final heat flow values from the autonomous thermistor probes.

In summary, heat flow measurements during the TicoFlux I expedition successfully delineated the transition between anomalously low and higher heat flow values along several transects. The primary transition is nominally associated with the triple junction trace, rather than any of the other tectonic boundaries, but is offset from the trace by tens of kilometers in some places. The transition is abrupt in several instances, suggesting that the cause of the generally-low heat flow in the northwestern part of the field area is a shallow process, most likely hydrothermal in origin. This interpretation is consistent with preliminary assessments of basement depths and lithospheric flexure northwest of the triple junction trace, which are normal for 20-25 Ma lithosphere.

TicoFlux I heat flow surveys also helped to delineate several areas within which heat flow is locally elevated or suppressed, generally in association with some kind of basement structure. One of the most interesting of these features (and associated thermal anomalies) is the low-angle structure crossed by seismic Line 5, above which heat flow values are at least 10x the "regional mean" for this area, and at least 20x greater than nearby values measured at ODP Site 1039.

V. Coring, Sediments and Geochemistry

Forty-three gravity and piston cores were collected during TicoFlux I for sedimentological and pore-fluid analysis (Fig. V-1 and Table V-1). Gravity cores were used in areas where sediment was expected to be particularly thin and where there was a danger of hitting bare rock. Piston cores were collected in areas where sediment was thicker and where collection of a longer sediment section was thought to be necessary. These cores were collected during twelve, 12-hour periods with each period focusing on a particular geologic feature or set of nearby features. Each feature that was targeted for coring had a seafloor expression of at least 20 m relative to the surrounding area. Most features had a surface relief of 100 m and some were up to 300 m higher than the surrounding region. Seismic lines provided information about sediment thickness near and on these features and most features had exposed basaltic basement. Eleven features were targeted to

determine (1) if the site is suitable for extensive coring and heat flow operations that will be the focus of our efforts in 2002, (2) if fluid flow is evident, and (3) if we can determine the composition of the fluid in basaltic basement. The basis for determining suitable future targets and fluid flow include core recovery and systematic variations in pore water chemical composition. We were limited at sea to measurements of pH, alkalinity, chlorinity, fluoride, calcium, magnesium, and phosphate in pore waters. A more extensive and comprehensive analytical program will be conducted ashore. Below we review the initial results from each of the eleven sites with recommendations for coring in 2002.

A. Sedimentology/stratigraphy

Sediment types found in each core are shown in Figs. V-2 To V-7 and core locations are shown with local bathymetry in Figs. V-8 to V-17. Piston cores are separated from gravity cores in Figs. V-2 To V-7 because of differences in depth scales. We placed the lithologies cored during TicoFlux I into five basic categories: hemipelagic mud, nannofossil chalk, mixed sediment, variegated clay, and volcanic ash. Gradations exist within each category, and many of the contacts between lithologies are transitional.

Hemipelagic Mud. This mixture of biogenic and siliciclastic debris (diatomaceous silty clay) is the most common lithology throughout the study area. The texture ranges from silty clay to clay, and the color is uniform dark olive gray. Mineral constituents consist largely of clay minerals and silt-sized plagioclase and quartz. Biogenic constituents include abundant diatoms and variable amounts of radiolarians and silica needles/spines. Carbonate content is low, consisting mostly of coccoliths. Other constituents in minor to trace quantities include volcanic glass shards and opaque grains. This lithology is typically homogeneous to mottled, with local trace fossils (Zoophycos).

Nannofossil Chalk. This fine-grained carbonate ooze is white to light gray or very pale brown in color and typically mottled. Coccoliths make up the primary grain type. Other biogenic particles include foraminifers, fragments of larger carbonate shells (pteropods?), diatoms, radiolarians, and discoasters. The content of clay minerals is low to very low in the chalk. This pelagic lithology also tends to be very firm, which inhibited coring.

Mixed Sediment. The category of mixed sediment differs from the typical hemipelagic mud by its relatively high content of calcareous microfossils, plus siliciclastic grains. Color ranges from gray to light olive brown and light yellowish brown. Primary constituents include clay minerals, quartz/plagioclase silt, coccoliths, and carbonate shell fragments, with lesser amounts of diatoms and radiolarians.

Variegated Clay. The variegated clay lithology ranges in color from brown to light olive brown, very pale brown, olive, olive gray, olive brown, yellowish brown, dark yellowish brown, and dark grayish brown. Clay minerals make up the bulk of these deposits; the amount of quartz/plagioclase silt ranges from trace to minor. The biogenic content is also unusually low. Clay-rich sediments are common in close proximity to basalt-sediment contacts. In many cases, fragments of basalt and Mn-oxide were recovered together with the clay. Reasons for the variability in color could not be determined by smear-slide examination, but the colors may be related to differences in clay mineralogy.

Volcanic Ash. There are two basic types of volcanic ash. The first type ranges in color from white to light gray, and the particles consist almost exclusively of clear, unaltered glass shards. Some such samples also contain crystals of fresh plagioclase and pyroxene. The light-colored layers probably originated through primary ash falls. The second type of ash ranges in color from dark gray to black. Fresh glass shards within the dark ash beds are brown in color, but heavily altered and devitrified glass shards are also common. Other constituents include vitric rock fragments, plagioclase and pyroxene crystals, opaque grains, clay minerals, and biogenic debris. The abundance of heavily altered grains indicates that older volcanic rocks were incorporated into the ash clouds during explosive eruptions. The ash layers range from less than 1 mm in thickness to more than 10 cm. Particle size ranges from medium sand to coarse silt. Most beds have sharp bases and sharp to diffuse tops. Normal size grading is common. In some cases, the ash deposits occur as irregular patches or as material filling vertical burrows.

B. Pore fluid chemistry

Gravity cores GC02-05 were taken from a small (<1 km) peanut shaped feature that extends about 250 m above the surrounding sediment (Figs. V-1 and V-8). GC02 was located on seismic Line 7 close to where basement may be exposed.Sediment recovered with this core is mostly calcareous ooze. We targeted GC03 at about the same depth but likely hit a steep cliff. This altered our plan for GC04 which was taken on the flat platform near the summit of the feature. No sediment was recovered, but the corer penetrated about 5 feet, based on thermal data recorded by the outrigger thermistor probes. GC05 was taken from the summit and included Mn nodules and an oxide layer. No fluid flow is indicated in these cores on the basis of chemical data from pore fluids; however, concentrations of phosphate decrease below bottom seawater concentrations. Given the low heat flow and the low expected temperature in basement, we may not expect to observe a change in Ca or Mg in pore fluids. The phosphate data are significant in that the low concentration is consistent with interaction with basaltic basement. Although we may not have flow

in the few cores from this site, this site will be a high priority for additional work next year. The cliff at GC03 should be targeted. In addition, cores from this area should be moved directly into the lab for processing as soon as possible after they are collected to avoid evaporation during sample handling.

Gravity cores GC06-GC09 were collected from a basement and seafloor high about 10 nautical miles northeast from the previous coring site, on seismic Line 4 (Figs. V-1 and V-9). The coring site was on a small topographic high, elevated 200 m above the surrounding seafloor, southeast of a larger basement edifice. The southeast corner of this feature needs to be surveyed before additional work is attempted at this site. Core recovery at this site was poor (Table V-1), although there is evidence that the corer successfully penetrated calcareous sediments. This evidence includes temperature data from thermistor probes mounted on the core barrels, mud on the inside and outside of the barrels, and inverted fingers in the core catchers. GC08 was taken with the 4" Benthos corer but only penetrated 16 cm. GC09, located near the summit, contained several prominent ash layers and a full barrel. Pore waters from this core have alkalinity, Mg, and phosphate concentrations that decrease with depth and Ca concentrations that increase with depth relative to bottom seawater. Pore waters from this core clearly indicate a basement influence, but an estimate of pore water flow rate through the section cannot be made. This site should be cored in 2002 after a more extensive seismic, bathymetric, and heat flow survey.

Gravity cores GC10-GC17 were collected above two basement highs close to seismic Line 12 (Figs. V-1 and V-10). Both features lie slightly off of the seismic line, and both show a thinning of sediment. The first feature (GC10 and GC11) is 40 m high and may be faulted along the southeastern side. The second feature, 4 nmi northwest of the first, extends 100 m above the surrounding sediment, but lies on the shoulder of a large seamount (at least 350 m high). Cores were collected on top of these features as well as along the base of fault-like structures (based on bathymetry). Sediment from each of these cores is greenish clay with several ash layers. Alkalinity and phosphate concentrations increase with depth in these cores. These data are consistent with the presence of sulfate reduction in or below the sampled section. Given the location of the cores, the lack of a basement component to the pore waters, and the low heat flow, these sites should not be considered for future work to find fluid flow or basement fluid compositions.

Piston cores PC18, PC19, PC38, and PC39 were collected near the trench along seismic Line 5 (Figs. V-1 and V-11). PC18, 38, and 39 were collected at the same location, which lies along a seismic line at a point where sediment thins to about 75 m. PC 19 was collected to the east of this line on a topographic high that rises about 25 m above the surrounding seafloor. This core was used primarily for physical properties testing. The location of PC18, 38, and 39 coincides with the highest heat flow measured on the cruise and with a shallowly-dipping reflector that appears to penetrate deeply into (and possibly through) the crust (Figs. III-5, III-15 and III-16).

Pore waters from these cores are consistent with the upwelling of a basement fluid at about 0.6 cm/yr (Fig. V-18). This fluid has a unique chemistry (98 mmol Ca/kg; 576 mmol chlorinity/kg; 1.3 mmol alkalinity/kg; 0.2 µmol phosphate/kg; 22 µmol F/kg; and a pH of 7.5). One particularly intriguing feature of this fluid is the high Ca concentration. Given such a high concentration one would expect there to be no alkalinity. This fluid is clearly coming from a source other than the upper most (200-500 m) permeable layer of basaltic crust. Two possibilities exist: a deep fault source or a subducting slab source. Given the existence of the deep fault and the high chlorinity, our initial interpretation is that these fluids come from a source deep within the crust or perhaps the upper mantle. Shore-based analytical programs will define the source of the fluids and will be a major focus of work for the remainder of the year. Because we collected good samples of this upwelling fluid in a controlled atmosphere, opportunities for work in this area next year will focus on the collection of samples for carbon-14 dating and determining the extent, magnitude, and pattern of fluid flow in reference to heat flow and geologic structure. Given the extent of fluid alteration and the fact that we collected the endmember fluid, data from gravity cores will provide the data needed to map the pattern of fluid flow. We should be able to collect four gravity cores in a 12-hour period compared to only two piston cores in the same time interval.

Gravity cores GC20-23 were collected along seismic Line 12 in the "warm" crust area, southeast of the triple junction trace, ridge jump, and propagator trace (Figs. V-1 and V-12). The seismic and hydrosweep data delineate a local topographical high that extends about 200 m above the surrounding seafloor. This high is associated with a bathymetric feature that runs perpendicular to the seismic line and additional bathymetric and seismic surveys of the this area will be required to resolve the geometry and nature of this structure. We targeted specific features where sediment thins and basement outcrops are likely. We recovered sediment with each of these cores and pore water data from GC23 are consistent with fluid upwelling (Fig. V-18). An upwelling rate of about 1 cm/yr is estimated from the data. This core is on the southeast side of the topographic high where sediments onlap a basaltic outcrop. An initial estimate of the composition of the basement fluid is 35 mmol Ca/kg, 553 mmol chlorinity/kg, 2.2 mmol alkalinity/kg, 2.6 µmol phosphate/kg, and a pH of 7.5. There appears to be a basement fault associated with the edge of the basement structure near where this core was collected, and this area will be a prime target for coring and heat flow studies in 2002.

Gravity cores GC24-27 were located at the southwestern and southern side of a conically-shaped seamount that extends about 450 m above the sediment plain to the south and 300 m above the sediment plain to the north along seismic Line 1 (Figs. V-1 and V-13). Seismic Line 1 crossed the southern portion of the outcrop and shows that sediment thins at the base. We targeted this area of thin sediment with two cores along the seismic track (GC24 and 25) and placed two additional cores at a similar location about 1.2 km south of the seismic line (Fig. V-13). We

selected the last location based on hydrosweep data, inferring that steep bathymetric contours in this area might indicate the presence of a fault. Although concentrations of chlorinity and alkalinity remained uniform with depth in these cores, concentrations of Ca increased (by less than 10%) and phosphate decreased. Although no flow was inferred in any of these cores this site is a possible coring target for 2002. There is an interesting basement and topographic high to the east of this site along seismic Line 1 where sediment thins to about 50-100 m.

Gravity cores GC28-31 were located on a topographic high that lies just south of seismic Line 11 in the southeastern part of the field area (Figs. V-1 and V-14). This feature was selected rather than another that lies about 2 km to the north because the selected feature is smaller (160 versus 300 m high) and has very steep relief along the edge, possibly indicating fault control on basement relief. We targeted these steep sides with little success. None of the cores was long enough to obtain more than three pore water samples. Given the problems recovering sediment from this site, we are unlikely to consider working at this site, or at the similar feature to the north, during the 2002 survey.

Gravity cores GC32-34 targeted a bathymetric high seaward of the trench (Figs. V-1 and V-15). This feature was not crossed during the original seismic and hydrosweep survey, but was mapped by hydrosweep during a transit between northern and southern edges of the field area, between heat flow station HF04 and coring station GC20. The feature rises about 160 m above the surrounding sediment, is elongate in shape, and coincides with the triple junction trace identified mainly on the basis of magnetic anomalies. We cored both ends of this feature (GC32 and GC34) and also placed a core on a ledge about half way up side (GC33). Only core GC34 recovered significant sediment, and there is no indication of a basement fluid component in the pore waters from this core. The fourth core from this coring session (GC35) was placed 7 km southwest of this feature, on the top of a small topographic high that rises about 60 m above the surrounding sediment. This feature was promising in that it is about the shape and size of the Baby Bare seamount on the west flank of Juan de Fuca Ridge. The corer landed to the northwest of the local topographical high and recovered a good sediment section, but shipboard chemical analyses are consistent with early diagenetic processes and no identifiable basement component. No additional coring in this area is justified given the results to date.

Piston cores PC36 and PC37 were located to the northwest of seismic Line 2, near where it is crossed by seismic Line 13 (Figs. V-1 and V-16). The cores were collected from one of two local topographic highs bisected by seismic Line 2. Because the core locations are off the seismic line, basement relief and sediment thickness are unknown at the coring sites, but sediment thickness is about 80 m 1-2 km to the southeast, where seismic Line 2 crosses the edge of the feature (Fig. V-16). Because the topographic high is about 40 m shallower where we cored relatively to where seismic Line 2 crosses the edge of the feature, we infer that sediment thickness

at the coring sites should be less than 80 m. Piston cores were located at the peaks of two local highs separated by about 600 m. Concentrations of chlorinity and alkalinity did not change with depth, but concentrations of Ca increased to 12.5 mmol/kg at the base of the cores (about a 22% increase). Even with this indication of an altered fluid at depth, there was no evidence for fluid seepage through the sediments at this site. Given the Ca gradient and the relatively high heat flow in the area, it seems likely that basement is fully buried in this area, and since we have no evidence for faults or other structures that may guide basement fluids, this area does not offer an attractive target for future work.

Gravity cores GC40-43 were taken on small basement high (about 200 m high) located at the base of a much larger one (1200 m high), along seismic Line 4 (Figs. V-1 and V-17). Coring targeted the bases of both features, including the area between them. Pore waters were obtained from three of the four cores and showed signs of early diagenetic reactions. There is no evidence for a basement component in the pore fluids. Additional work at this site is thus unlikely to yield pore fluids indicating conditions in basement.

Ca versus depth profiles for most cores collected during the TicoFlux expedition are plotted together in Figure V-18. Most data fall along a line that varies little with depth, indicating either very thick sediments above reacted basement or basement pore fluids that look very much like seawater. Pore fluids from GC23, PC18, PC38 and PC39 yielded profiles that indicate upward fluid seepage through sediments and a basement fluid that differs significantly from seawater.

In summary, we have located and sampled:

1. a unique, highly-altered fluid that is upwelling through the sediment and must be derived from a source other than the permeable upper 200-500 m of basaltic crust (Cores PC18, PC38, PC39; Figs V-1 and V-11);
2. pore fluids seeping through the sediment in the 'warm' crust area associated with a basement outcrop and bounding fault (Figs. V-1 and V-12);
3. sediment and pore water that provide indications that, with additional coring, we may be able to sample basement formation fluids that upwell from 'cold' basement.

Work during the 2002 expedition will include additional coring to define the composition of fluids in basement and to determine relations among geologic setting, heat flow, and fluid flow in this region.

VI. Comments and Recommendations Concerning Facilities and Personnel

The *Maurice Ewing* is an outstanding observational platform run by a skilled and dedicated crew. Nevertheless, we have a few suggestions for improvements that could help to enhance scientific operations in the future.

A. Facilities

The 10-gun array used for acquisition of seismic data provided an exceptionally clean source, the long streamer worked well, and the Syntron data acquisition system (installed on *Ewing* recently) allowed collection and storage of data with few problems. The system has numerous automated checks to make sure that the data stream is not interrupted, but it would be helpful to have a check for the acquisition of P-code GPS data. The P-code GPS antenna was upsidedown for most of the primary seismic/hydrosweep survey, but although we noted that navigation records appeared to be noisy, we did not realize that we were acquiring only rare P-code fixes until late in the survey. The hydrosweep system provided useful data in a swath having a width only slightly greater than water depth, but we understand that an upgrade to this system is being installed.

We were able to connect portable computers to the shipboard network relatively easily, but the Sunray terminals often locked up during routine operations. In addition, the system was frustratingly slow when we tried to run backups and other operations at the same time as we acquired seismic data. We recommend having two or three Sun workstations available for scientific use rather than trying to run all programs through a single workstation using Sunrays. This would allow scientific backups (seismic and other data and programs) to be run from a machine separate from that handling primary system backups, reducing bottlenecks on the network. We were also frustrated by having access to only a single-seat license for Matlab, since this software was needed for seismic, heat flow and general data analysis.

Removal of the aft-starboard crane in the last year increased the working area on the fantail, but also limited our ability to move equipment around on deck. We suggest consideration of installation of a crane capable of handling loads up to 5000 lbs for future expeditions of this kind. We were initially concerned with launch and recovery of heat flow equipment through the stern A-frame without the assistance of the fantail crane, but these operations were handled smoothly using the A-frame tugger, a snatch-block and capstan, and taglines.

Use of separate wires for running coring and heat flow operations (3/19 trawl and 0.680 wires, respectively) made switching between these operations relatively simple since we did not have to reroute or reterminate the wires. We also greatly appreciated being able to run wire operations from inside the main lab, using video displays of the drums and sheaves. However, there were intermittent problems throughout the cruise with wire depth, rate and tension readouts, both on the main gauges and on the numbers superimposed on the video screens. In addition, there were problems with the level wind system on the trawl winch and with positioning of the sheave that guides the 0.680 wire from the A-deck to the A-frame. We understand that these problems resulted, in part, from these systems being used infrequently, but these problems were frustrating and could have lead to instrument damage or loss. We estimate a total loss of about 24 hours of

science time during our expedition because of winch, sheave and gauge problems, and urge increased testing and maintenance of these important systems in the future.

B. Personnel

We were impressed with *Ewing's* crew and technical support group. These personnel were concerned with the nature and quality of scientific data being acquired by TicoFlux scientists, generous with thoughtful advice, and willing to work long hours with humor and patience. They were also extremely mindful of safety and helped us to streamline and simplify deck operations. Although many other individuals contributed to the success of the TicoFlux scientific program, the work of the following personnel is particularly noteworthy.

Captain Mark Landow ran virtually all heat-probe deployment and recovery operations on the fantail, handing these tasks with grace and skill, and also participated in numerous core recovery operations. The ship's mates (Bert Thurston, Jeff Sylvia, and Rick Thomas) demonstrated outstanding skill at station keeping during heat flow and coring operations, in many cases remaining within 100 m or less of our targets for hours at a time, dodging fishing boats and skirting rip currents. All of the officers responded positively to abrupt schedule changes and helped us to use our time more effectively. First Engineer Matt Tucke and Technician Carlos Gutierrez modified and repaired instruments and constructed adapters, contributing significantly to the success of scientific operations.

Science Officer Chris Leidhold and Technician Karl Hagel launched and recovered the seismic streamer rapidly and smoothly, tirelessly guided operation of the seismic data acquisition system, managed winch operations, trouble-shot winch and wire-gauge problems, and performed numerous other tasks that enhanced our scientific return. Technician Richard Oliver-Goodwin kept the shipboard computer network running, despite being relatively unfamiliar with some shipboard systems at the start, and assisted in troubleshooting data acquisition and storage problems throughout the expedition.

VII. TicoFlux I Scientist Contact Information

Andrew T. Fisher
UCSC, Earth Sciences Department
1156 High Street
Santa Cruz, CA 95064
831-459-5598
831-459-3074 (fax)
afisher@es.ucsc.edu

Eli Silver
UCSC, Earth Sciences Department
1156 High Street
Santa Cruz, CA 95064
831-459-2266
831-459-3074 (fax)
esilver@es.ucsc.edu

Carol Stein
Department of Earth and
Environmental Sciences (M/C 186)
University of Illinois, Chicago
845 West Taylor Street
Chicago, Illinois 60607-7059
(312) 996-9349
(312) 413-2279
cstein@uic.edu

Summer 2001 (until 20 August)
Dept. of Geological Sciences
Northwestern University
Evanston, IL 60208
847-491-5265
847-491-8060 (fax)
carol@earth.northwestern.edu

Rob Harris
Department of Geology and Geophysics
University of Utah
717 W. B. B.
SLC, UT 84112
(801) 587-9366
(801) 581-7065
rnharris@mines.utah.edu

C. Geoff Wheat
West Coast and Polar Regions
Undersea Research Center
PO Box 475
Moss Landing, Ca 95039
(shipping)
NURP/MLML Marine Operations
7700 Sandholdt Road, Bldg D
Moss Landing, Ca 95039
(831) 633-7033
(831) 633-6872 (fax)
wheat@mbari.org

Kelin Wang
Pacific Geoscience Center, GSC
9860 W. Saanich Road
Sydney, B.C. Canada V8L4B2
(250) 363-6429
(250) 363-6565 (fax)
wang@pgc.nrcan.gc.ca

Michael B. Underwood
101 Geology Building
Department of Geological Sciences
University of Missouri
Columbia, MO 65211
573-882-4685
573-882-5458 (fax)
UnderwoodM@missouri.edu

Chris Moser
Oregon State University - COAS
104 COAS Ocean. Admin. Bldg.
Corvallis, OR 97331-5503
(541) 737-5217
(541) 737-2064 (fax)
cmoser@oce.orst.edu

Abdellah Cherkaoui
UCSC, Earth Sciences Department
1156 High Street
Santa Cruz, CA 95064
831-251-667
916-314-9264 (fax)
abdul@es.ucsc.edu

Mike Hutnak
UCSC, Earth Sciences Department
1156 High Street
Santa Cruz, CA 95064
831-459-2838
831-459-3074 (fax)
mhutnak@es.ucsc.edu

Patrice Friedmann
UCSC, Earth Sciences Department
1156 High Street
Santa Cruz, CA 95064
831-459-4090
831-459-3074 (fax)
p_friedmann@hotmail.com

Raanan Bodzin
UCSC, Earth Sciences Department
1156 High Street
Santa Cruz, CA 95064
831-459-4090
831-459-3074 (fax)
raanan.bodzin@usa.net

Rob Cleary
UCSC, Earth Sciences Department
1156 High Street
Santa Cruz, CA 95064
831-459-4090
831-459-3074 (fax)
robclery@yahoo.com

Robyn Kelly
MS #22, Clark 244B
Woods Hole Oceanographin Institution
Woods Hole, MA 02543
(508) 289 3422
rkelly@whoi.edu

Marion Pfender
Fachbereich Geowissenschaften
Postfach 330 440
Universitaet Bremen
D-28334 Bremen
GERMANY
+(421) 218 4509
+(421) 218 7163 (fax)
pfender@GeophyS2.uni-bremen.de

Yvonne Stewart
Maine Maritime Academy, Box 447
Castine, ME 04420
goof@backpacker.com

Kevin ~~Stewart~~ Jones
Indiana University of Pennsylvania
1661 Pinewind Dr.
Alburtis PA 18011
(610) 336-0963
martdog@hotmail.com

Figures and Tables

Figure IV-1. TicoFlux I heat flow station locations.

Figure IV-2. Example of data collected during four penetrations with multipenetration heat flow probe. Measurement interval is 10 s. There are 11 sediment thermistors and one bottom water thermistor (value of latter remains relatively constant through penetration). Initial period of temperature rise and equilibration follows penetration of the seafloor by the probe. Heat pulse is fired after seven minutes in bottom with no change in elevation of probe. The instrument is left to equilibrate for about 7 minutes after firing heat pulse, then is removed the seafloor.

Figure IV-3. Example of processed, multipenetration probe data. A. Estimated equilibrium temperatures versus depth. All temperatures are relative to bottom water. Open symbols indicate depths for temperatures based on assumption that shallowest measurement is at seafloor. Solid symbols show apparent depths after requiring that thermal gradient pass through bottom water temperature at the seafloor. B. Sediment thermal conductivity versus depth. Solid lines indicate depth intervals over which conductivites are assumed to apply in calculating thermal resistances, half way between successive measurements, except for the shallowest value, which is assumed to apply up to the seafloor. Dashed line indicates thermal conductivity of shallow sediments required to make best-fitting straight line in part C pass through zero. This is the effective conductivity of the shallow sediment section, assuming that other conductivities and depth intervals are correct. C. Temperature versus cumulated thermal resistance (depth corrected for differences in thermal conductivity). The slope of the best-fitting straight line that passes through the data is the conductive heat flow.

Figure IV-4. Contoured hydrosweep bathymetry with HF01 measurement locations.

Figure IV-5. Contoured hydrosweep bathymetry with HF02 measurement locations.

Figure IV-6. Contoured hydrosweep bathymetry HF03, HF09 and HF10 measurement locations.

Figure IV-7. Contoured hydrosweep bathymetry with HF04 and HF11 measurement locations.

Figure IV-8. Contoured hydrosweep bathymetry with HF05 measurement locations.

Figure IV-9. Contoured hydrosweep bathymetry with HF06 measurement locations.

Figure IV-10. Contoured hydrosweep bathymetry with HF07 measurement locations.

Figure IV-11. Contoured hydrosweep bathymetry with HF08 measurement locations.

Figure IV-12. Contoured hydrosweep bathymetry with contours and HF12 measurement locations.

Figure IV-13. Contoured hydrosweep bathymetry with contours and HF13 measurement locations.

Figure IV-14. Example of data from autonomous thermistor probes strapped to core barrels from GC06.

Figure IV-15. Thermal conductivity from core PC18 collected with Bremen and UCSC (WHOI-ThermCon 96) instruments.

Table V-1. Summary of core types, locations, times and recovery.

Table I-1. Summary of TicoFlux I (EW0104) operations.

Date and Time (starting, local)		Date and Time (starting, GMT)		Event	Duration (hrs)	Duration (days)	Running (days)	Comments
4/12/01	17:00	4/12/01	22:00	Ship reaches dock	24.0	1.00	0.00	
4/13/01	17:00	4/13/01	22:00	Ship leaves for locks	10.0	0.42	0.42	
4/14/01	3:00	4/14/01	8:00	Ship arrives at anchorage	16.0	0.67	1.08	
4/14/01	19:00	4/15/01	0:00	Transit to WP-1	39.0	1.63	2.71	
4/16/01	10:00	4/16/01	15:00	TF01GC-01	3.0	0.13	2.83	Start of seismic line
4/16/01	13:00	4/16/01	18:00	Rig for seismic survey	8.5	0.35	3.19	
4/16/01	21:30	4/17/01	2:30	Start survey, seismic Line 1	25.0	1.04	4.23	seismic Line 1
4/17/01	22:30	4/18/01	3:30	End seismic Line 1	1.0	0.04	4.27	turn for seismic Line 2
4/17/01	23:30	4/18/01	4:30	Start seismic Line 2	15.5	0.65	4.92	seismic Line 2
4/18/01	15:00	4/18/01	20:00	End seismic Line 2	2.5	0.10	5.02	turn for seismic Line 3
4/18/01	17:30	4/18/01	22:30	Start seismic Line 3	18.0	0.75	5.77	seismic Line 3
4/19/01	11:30	4/19/01	16:30	End seismic Line 3	2.0	0.08	5.85	turn for seismic Line 4
4/19/01	13:30	4/19/01	18:30	Start seismic Line 4	19.0	0.79	6.65	seismic Line 4
4/20/01	8:30	4/20/01	13:30	End 4/start seismic Line 5	5.0	0.21	6.85	seismic Line 5
4/20/01	13:30	4/20/01	18:30	End 5/start seismic Line 6	15.0	0.63	7.48	seismic Line 6
4/21/01	4:30	4/21/01	9:30	End 6/start seismic Line 7	13.0	0.54	8.02	seismic Line 7
4/21/01	17:30	4/21/01	22:30	End 7/start seismic Line 8	17.0	0.71	8.73	seismic Line 8
4/22/01	10:30	4/22/01	15:30	End 8/start seismic Line 9	8.3	0.35	8.00	seismic Line 9
4/22/01	18:48	4/22/01	23:48	End 9/start seismic Line 10	4.5	0.19	8.19	seismic Line 10
4/22/01	23:18	4/23/01	4:18	End 10/start seismic Line 11	20.5	0.85	9.04	seismic Line 11
4/23/01	19:48	4/24/01	0:48	End 11/start seismic Line 12	3.0	0.13	9.17	seismic Line 12
4/23/01	22:48	4/24/01	3:48	End 12/start seismic Line 13	21.5	0.90	10.06	seismic Line 13
4/24/01	20:18	4/25/01	1:18	End seismic Line 13	2.5	0.10	10.17	turn for seismic Line 14
4/24/01	22:48	4/25/01	3:48	Start seismic Line 14	21.9	0.91	11.08	seismic Line 14
4/25/01	20:42	4/26/01	1:42	End 14, derig seismic	6.5	0.27	11.35	Pull streamer, prep for coring
4/26/01	3:12	4/26/01	8:12	Transit to TF01GC-02	5.0	0.21	11.56	transit to site
4/26/01	8:12	4/26/01	13:12	TF01GC-02, 03, 04, 05	12.5	0.52	12.08	
4/26/01	20:42	4/27/01	1:42	TF01HF-01	27.0	1.13	13.20	includes transit
4/27/01	23:42	4/28/01	4:42	TF01GC-06, 07, 08, 09	13.8	0.58	13.78	includes transit
4/28/01	13:30	4/28/01	18:30	TF01HF-02	24.0	1.00	14.78	includes transit
4/29/01	13:30	4/29/01	18:30	Transit and hydrosweep	10.0	0.42	15.20	
4/29/01	23:30	4/30/01	4:30	TF01GC-10, 11, 12, 13	12.0	0.50	15.28	includes transit

Table I-1. Summary of TicoFlux I (EW0104) operations.

Date and Time (starting, local)		Date and Time (starting, GMT)		Event	Duration (hrs)	Duration (days)	Running (days)	Comments
4/30/01	11:30	4/30/01	16:30	TF01HF-03	25.5	1.06	16.34	includes transit and probe repair
5/1/01	13:00	5/1/01	18:00	TF01GC-14, 15, 16, 17	13.5	0.56	16.90	includes transit
5/2/01	2:30	5/2/01	7:30	TF01HF-04	19.0	0.79	17.70	includes transit and probe repair
5/2/01	21:30	5/3/01	2:30	TF01PC-18, 19	13.5	0.56	18.26	includes transit
5/3/01	11:00	5/3/01	16:00	TF01HF-05	36.0	1.50	19.76	includes transit and winch repair
5/4/01	23:00	5/5/01	4:00	Transit	6.5	0.27	20.03	
5/5/01	5:30	5/5/01	10:30	TF01GC-20, 21, 22, 23	13.5	0.56	20.59	includes transit and winch repair
5/5/01	19:00	5/6/01	0:00	TF01HF-06	27.0	1.13	21.72	includes transit
5/6/01	22:00	5/7/01	3:00	TF01GC-24, 25, 26, 27	15.0	0.63	22.34	includes transit
5/7/01	13:00	5/7/01	18:00	TF01HF-07	31.0	1.29	23.63	includes transit and probe repair
5/8/01	20:00	5/9/01	1:00	TF01GC-28, 29, 30, 31	13.0	0.54	24.18	includes transit
5/9/01	9:00	5/9/01	14:00	TF01HF-08	28.5	1.19	25.36	includes transit
5/10/01	13:30	5/10/01	18:30	TF01GC-32, 33, 34, 35	15.5	0.65	26.01	includes transit
5/11/01	5:00	5/11/01	10:00	TF01HF-09	25.5	1.06	27.07	includes transit
5/12/01	6:30	5/12/01	11:30	TF01PC-36, 37	12.0	0.50	27.57	includes transit
5/12/01	18:30	5/12/01	23:30	TF01HF-10	20.5	0.85	28.43	includes transit
5/13/01	15:00	5/13/01	20:00	TF01PC-38, 39	14.0	0.58	29.01	includes transit
5/14/01	5:00	5/14/01	10:00	TF01HF-11	25.0	1.04	30.05	includes transit
5/15/01	6:00	5/15/01	11:00	TF01GC-40, 41, 42, 43	18.5	0.77	30.82	includes transit
5/16/01	0:30	5/16/01	5:30	TF01HF-12	19.0	0.79	31.61	includes transit
5/16/01	19:30	5/17/01	0:30	Transit	5.0	0.21	31.82	
5/17/01	0:30	5/17/01	5:30	TF01HF-13	8.0	0.33	32.15	
5/17/01	8:30	5/17/01	13:30	**Transit to Panama**	**46.0**	1.92	34.07	
5/19/01	6:30	5/19/01	11:30	**Arrive at anchorage**				

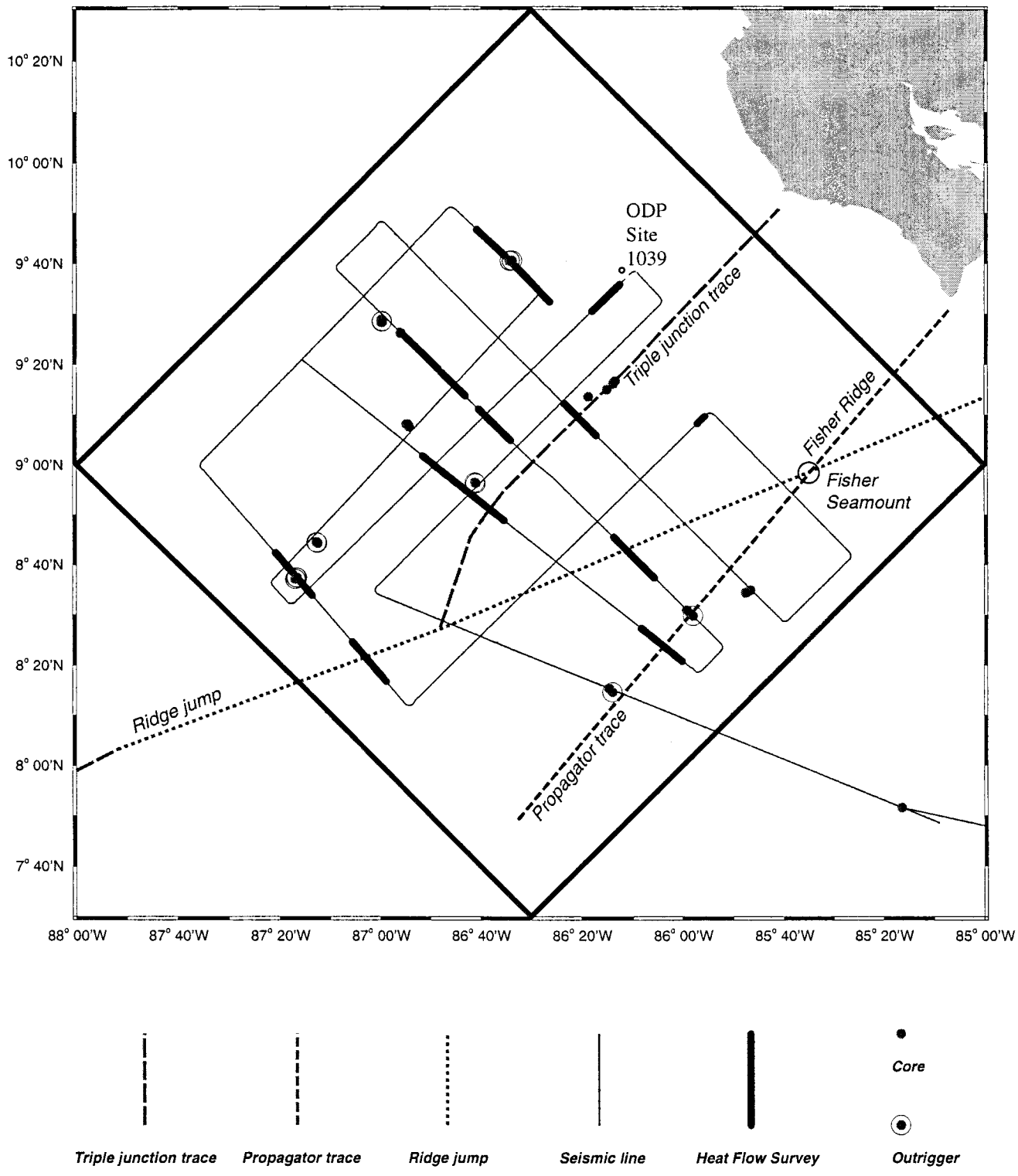
10° 20'N
10° 00'N
9° 40'N
9° 20'N
9° 00'N
8° 40'N
8° 20'N
8° 00'N
7° 40'N
88° 00'W
87° 40'W
87° 20'W
87° 00'W
86° 40'W
86° 20'W
86° 00'W
85° 40'W
85° 20'W
85° 00'W
ODP
Site
1039
Triple junction trace
Fisher Ridge
Fisher
Seamount
Ridge jump
Propagator trace
Core
Triple junction trace
Propagator trace
Ridge jump
Seismic line
Heat Flow Survey
Outrigger

Figure I-1

Table III-1. Seismic survey parameters.

Sample rate	**(ms)**	4
Streamer		
	length (m)	6000
	Number of channels	480
Record length	**(s)**	12.5
Distances	**(m)**	
Center of array from stern		39.6
Center of Ch 480 from stern		221.3
Consists of:		
	Tow leader	115.0
	Two 50m head stretches	100.0
CDP spacing		6.3
Stern to Tasmon P-code antenna		13.8
Tasmon P-code to hydrosweep		50.6
Tasmon P-code to center line		6.2
Tasmon P-code to 3.5 kHz		32.3
Source array to NT		**181.7**

Table III-2. Gun configuration.

Gun ID	Side	Gun size (in^3)	Gun size (m)	enterline distance (m)
1	Stbd	145	59	17.98
2	Stbd	850 (spare)	54	16.46
5	Stbd	850	39	11.89
7	Stbd	235	29	8.84
8	Stbd	80	24	7.32
9	Stbd	200	10	3.05
12	Port	385	10	3.05
13	Port	305	24	7.32
14	Port	120	29	8.84
16	Port	585	39	11.89
19	Port	585 (spare)	54	16.46
20	Port	145	59	17.98

Table III-3. Seismic line locations, times and backup parameters.

Line #	Start		End		Start time		End time	
	Latitude (N)	Longitude (N)	Latitude (N)	Longitude (N)	Julian day	GMT	Julian day	GMT
1	07 50.604	85 13.959	08 34.091	87 00.542	107	02:45	108	03:53
2	08 37.394	86 59.037	09 30.137	86 06.250	108	04:42	108	19:40
3	09 37.105	86 11.334	08 32.639	87 16.944	108	22:26	109	17:43
4	08 38.795	87 19.757	09 34.082	86 28.395	109	19:45	110	11:24
5	09 36.701	86 30.010	09 51.170	86 45.748	110	12:01	110	16:24
6	09 49.880	86 47.807	09 02.853	87 33.255	110	16:53	111	07:14
7	08 57.785	87 34.116	08 12.182	86 55.044	111	08:01	111	20:26
8	08 14.574	86 51.364	09 10.059	85 55.316	111	21:22	112	13:19
9	09 08.475	85 52.317	08 43.784	85 28.118	112	14:05	112	21:33
10	08 39.800	85 28.214	08 28.696	85 39.710	112	22:13	113	01:36
11	08 29.737	85 41.219	09 47.521	86 58.021	113	02:02	114	00:40
12	09 46.834	87 01.411	09 40.642	87 07.730	114	01:12	114	03:30
13	09 37.898	87 07.855	08 25.133	85 53.324	114	03:51	115	01:36
14	08 20.574	85 59.761	09 25.537	87 21.485	115	03:57	116	01:36

Line #	First Shot	Last Shot	First Trace	Last Trace	DAT #	Comments
1	2	5643	1591	34117	1,2,3	missed shots 3294, 5642
				34843	20,21	*Repeat copy and stack Line 1*
2	5660	9436	34118	57583	4,5	missed shots 7320, 7423, 7556, 7557, 7617-7621, 8519, 9408
3	9350	13870	57584	84115	6,7	
4	14000	17699	84116?	107173	7,8	missed shots 14159, 14389, 14708, 14888, 16992
5	17700	18746	107174	113461	8,9	
6	18749	22114	113462	133561	9,10	missed shots 19949, 19957-19980, 20143, 20144, 21286-21289
7	22200	25147	133562	171849	11	
8	25151	29020	151850	174985	12,13	missed shots 25468, 25707, 27227
9	29050	30789	174986	187701	13	
10	30800	31581	187702	190471	14	
11	31590	37013	190472	223015	14,15,16	
12	37020	37538	223016	226213	16	
13	37550	42748	226214	257287	16,17,18	missed shots 40575, 41734; last trace is bad
14	42750	47878	257288	287587	18,19	missed shot 43201; Shots 45960-46105 copied before 45813-45959

Seismic line locations and dates

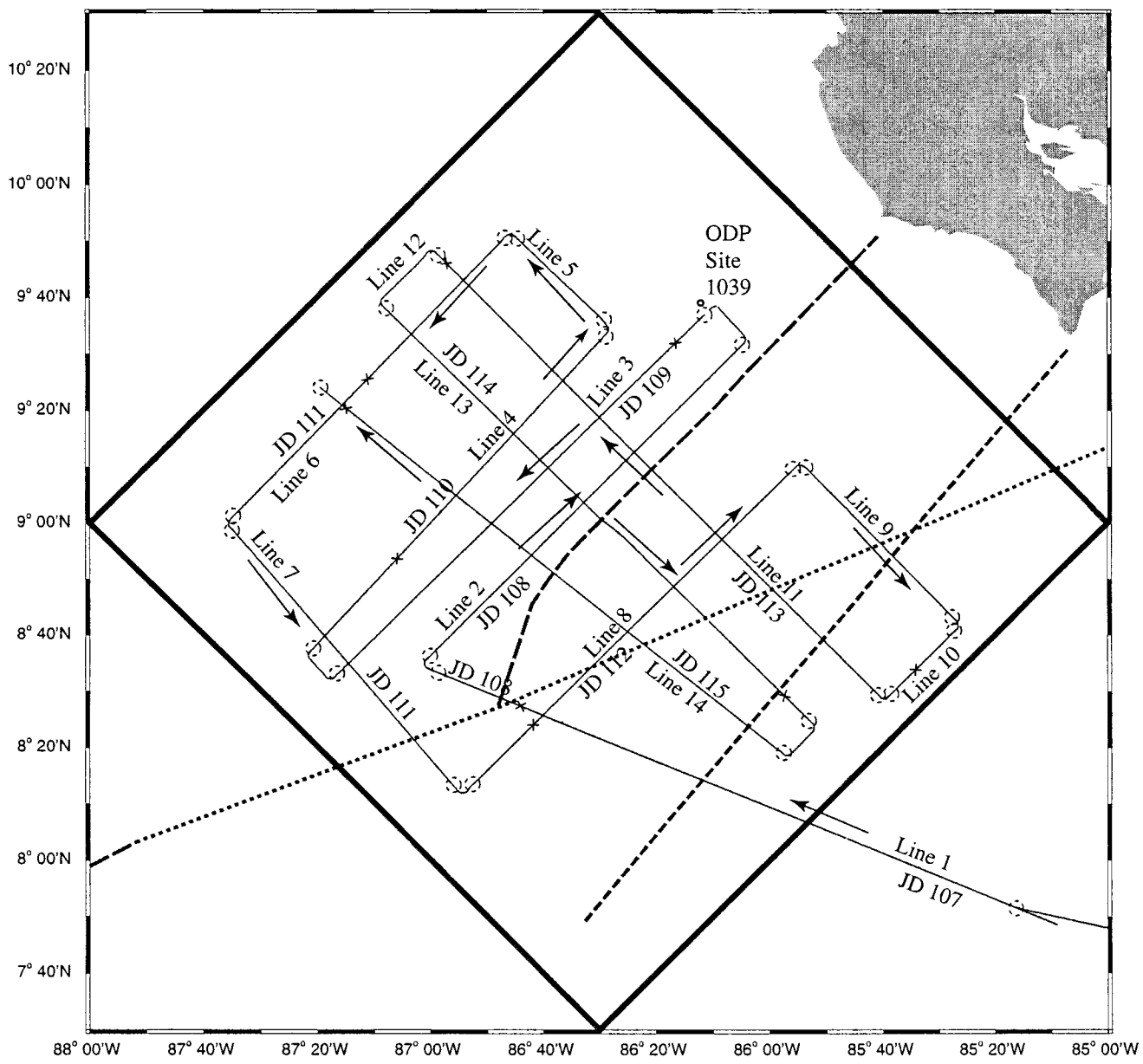

Figure III-1

Seismic Line 7, HF01

SE

NW

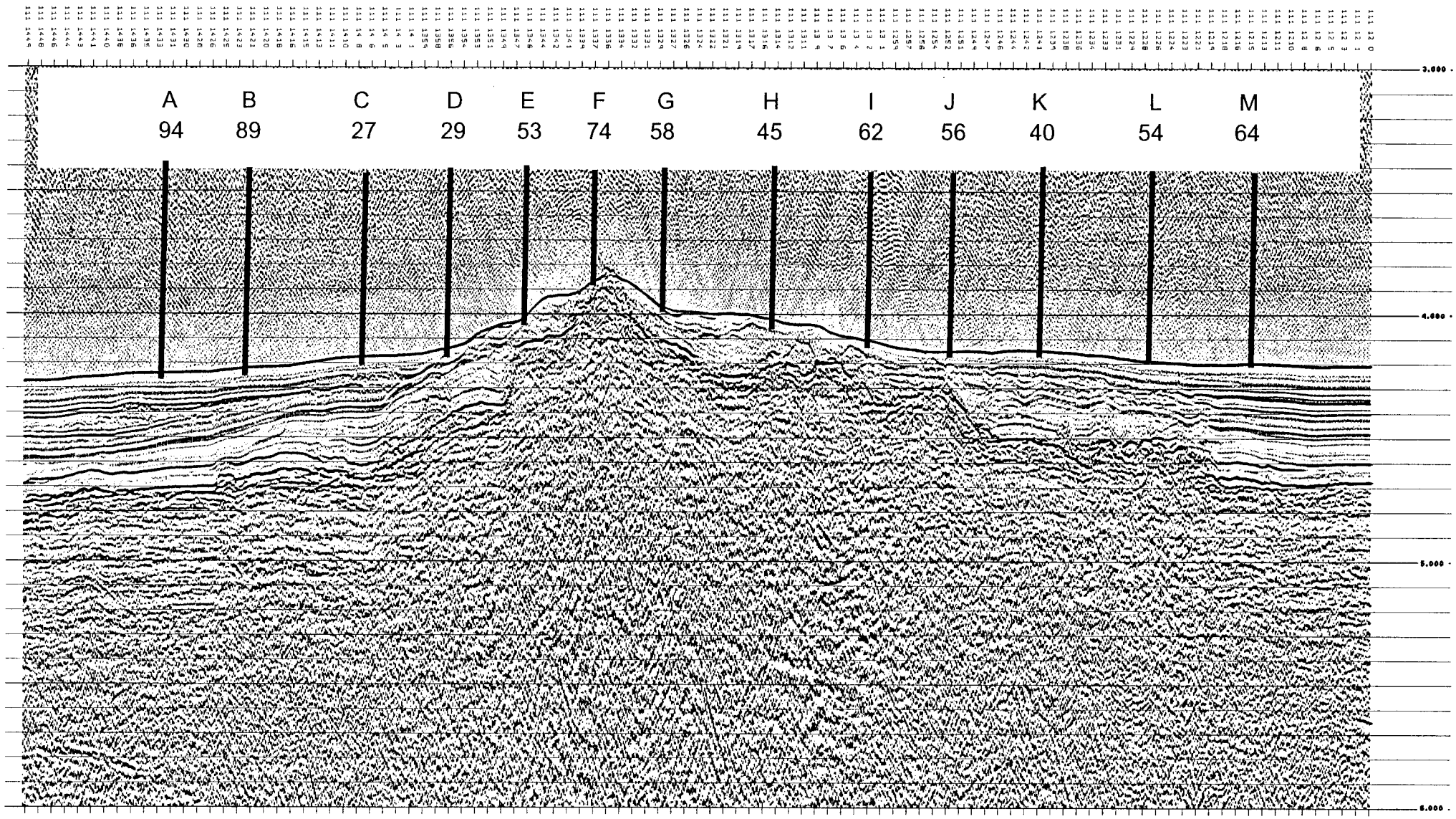

Figure III-2

NW

Seismic Line 7, HF02

SE

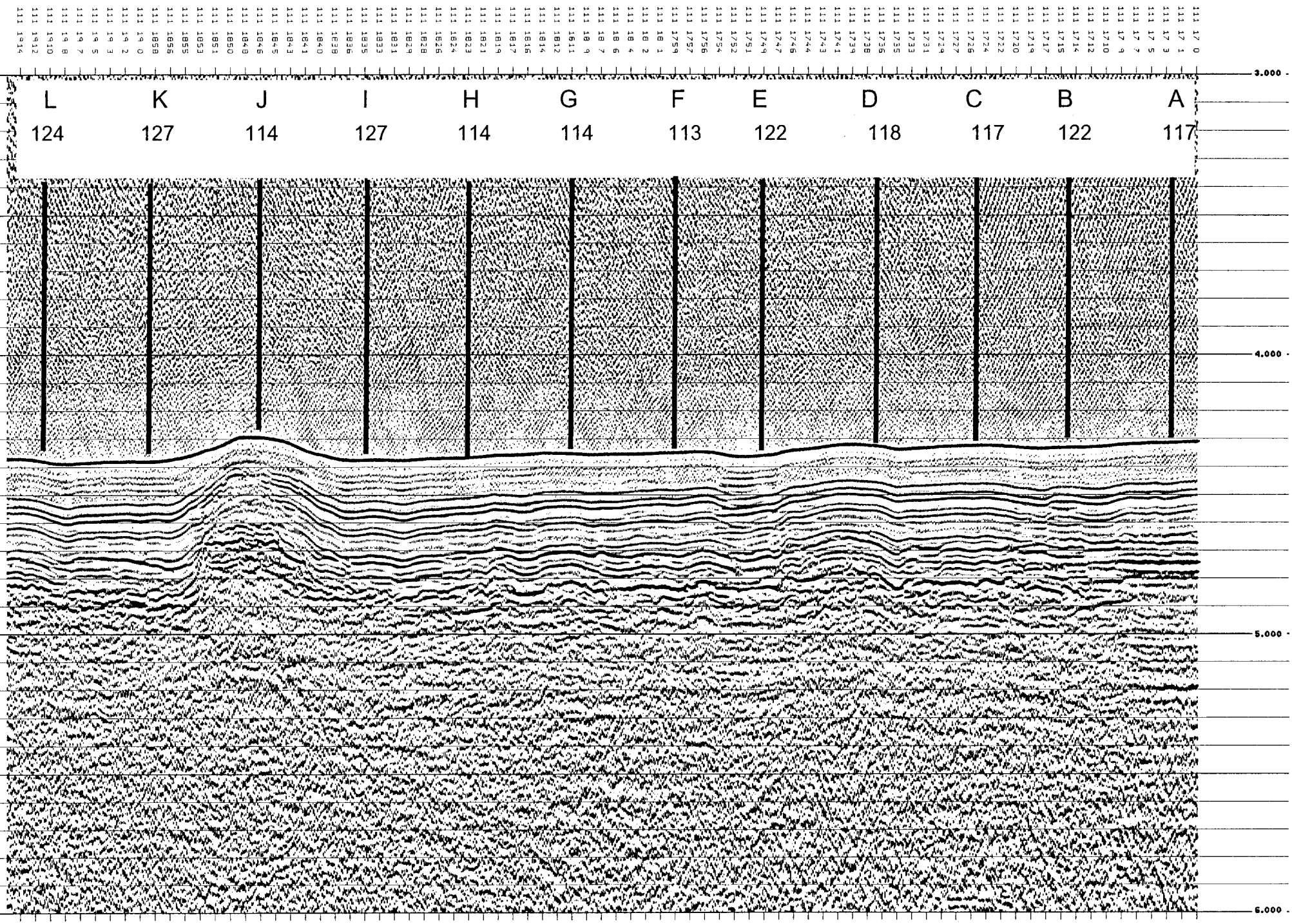

Figure III-2

Seismic Line 13, HF03

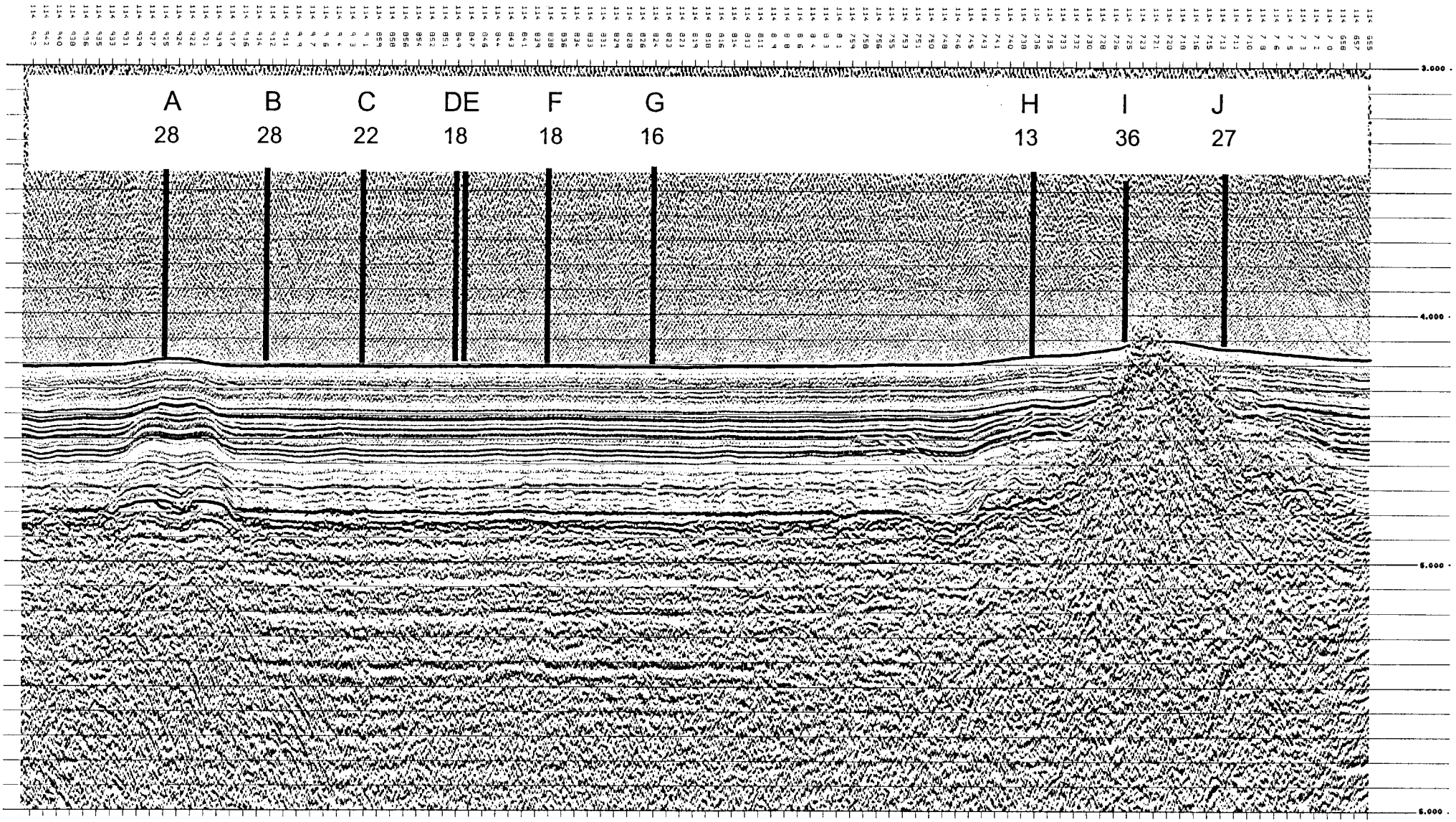

Figure III-4

Seismic Line 5, HF04

NW SE

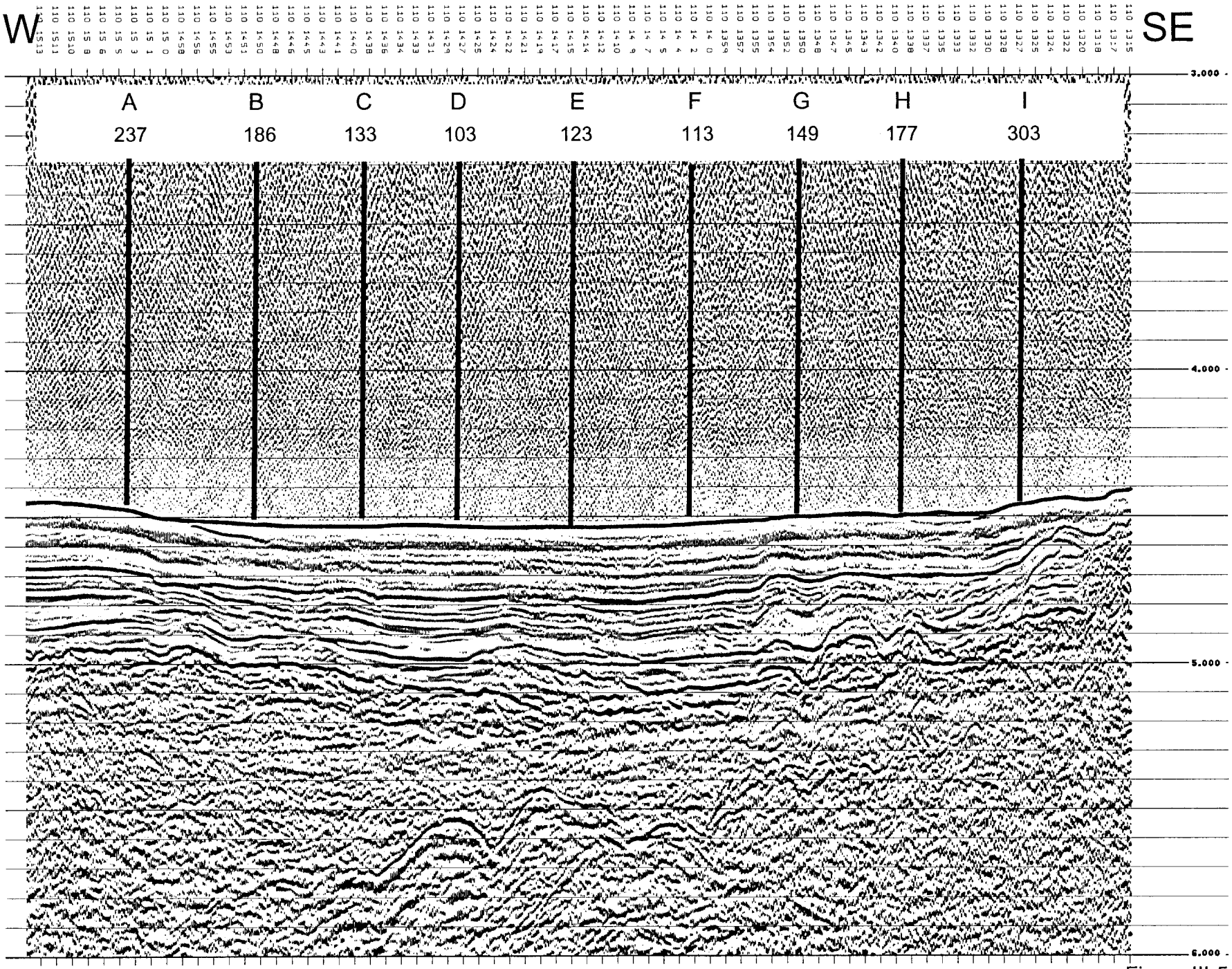

Figure III-5

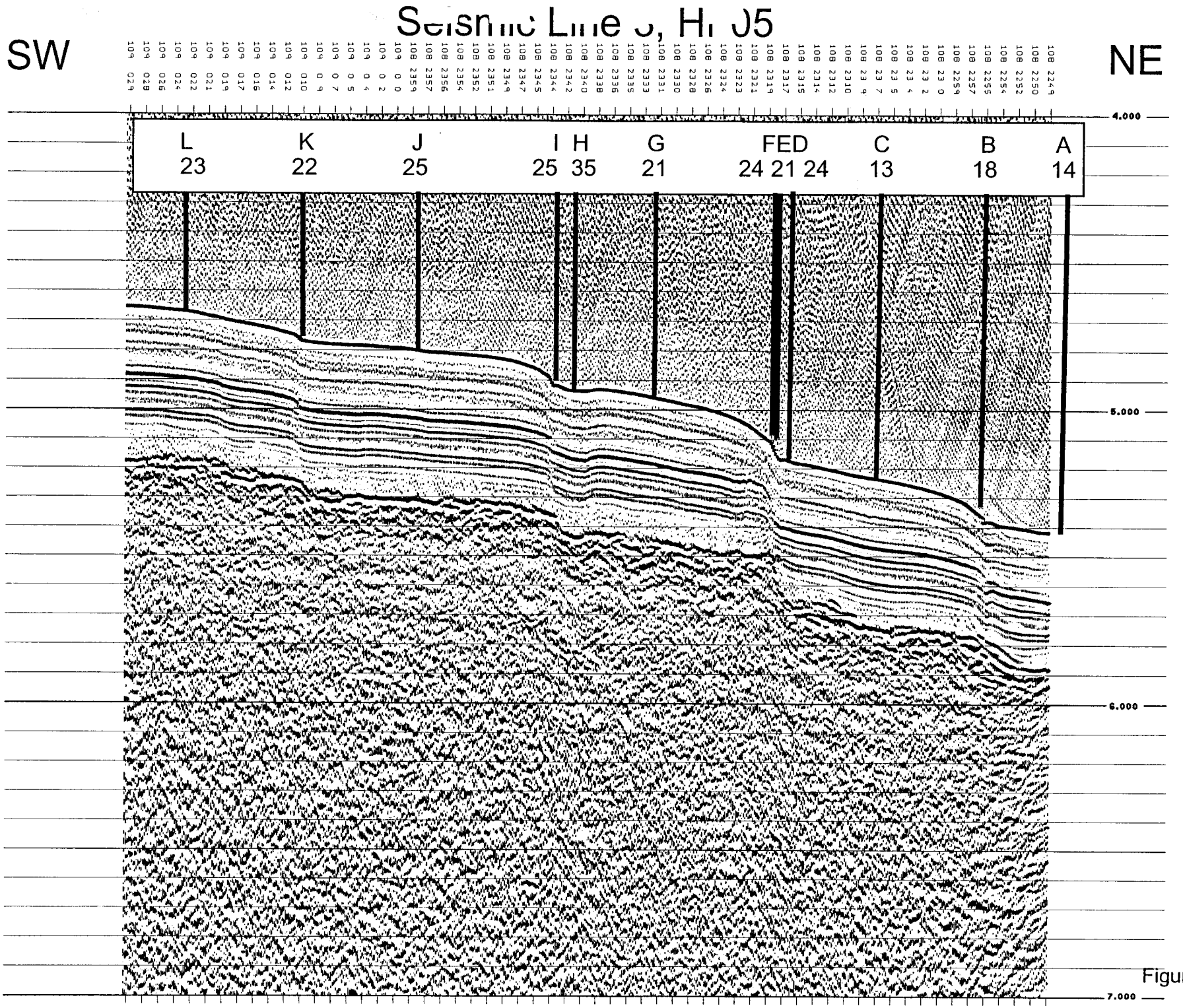
Seismic Line 3, HR 05
SW
NE
L 23
K 22
J 25
I 25
H 35
G 21
FED 24 21 24
C 13
B 18
A 14
4.000
5.000
6.000
7.000

Figure III-6

Seismic Line 14, HF06

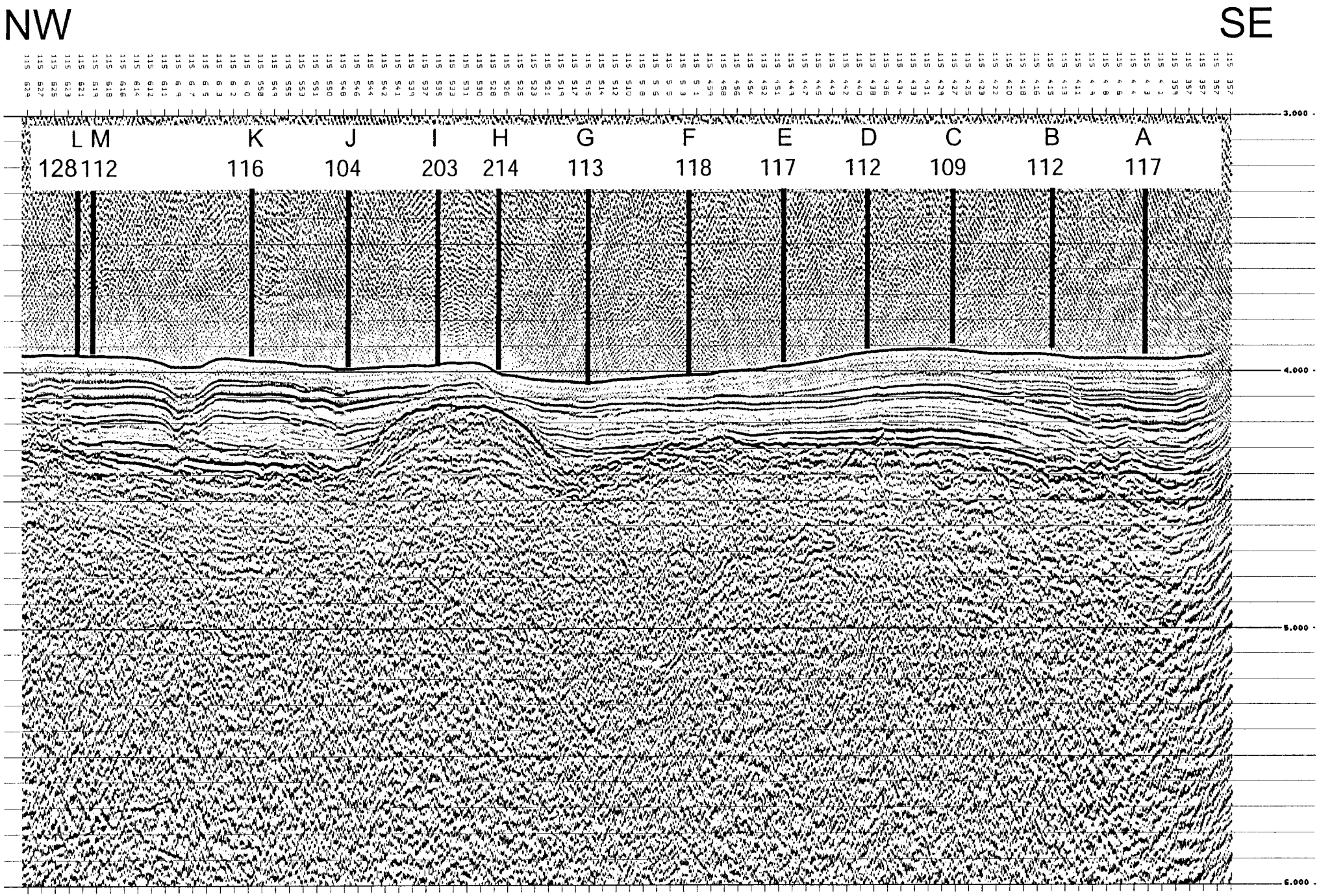

Figure III-7

Seismic Line 13, HF07

SE

NW

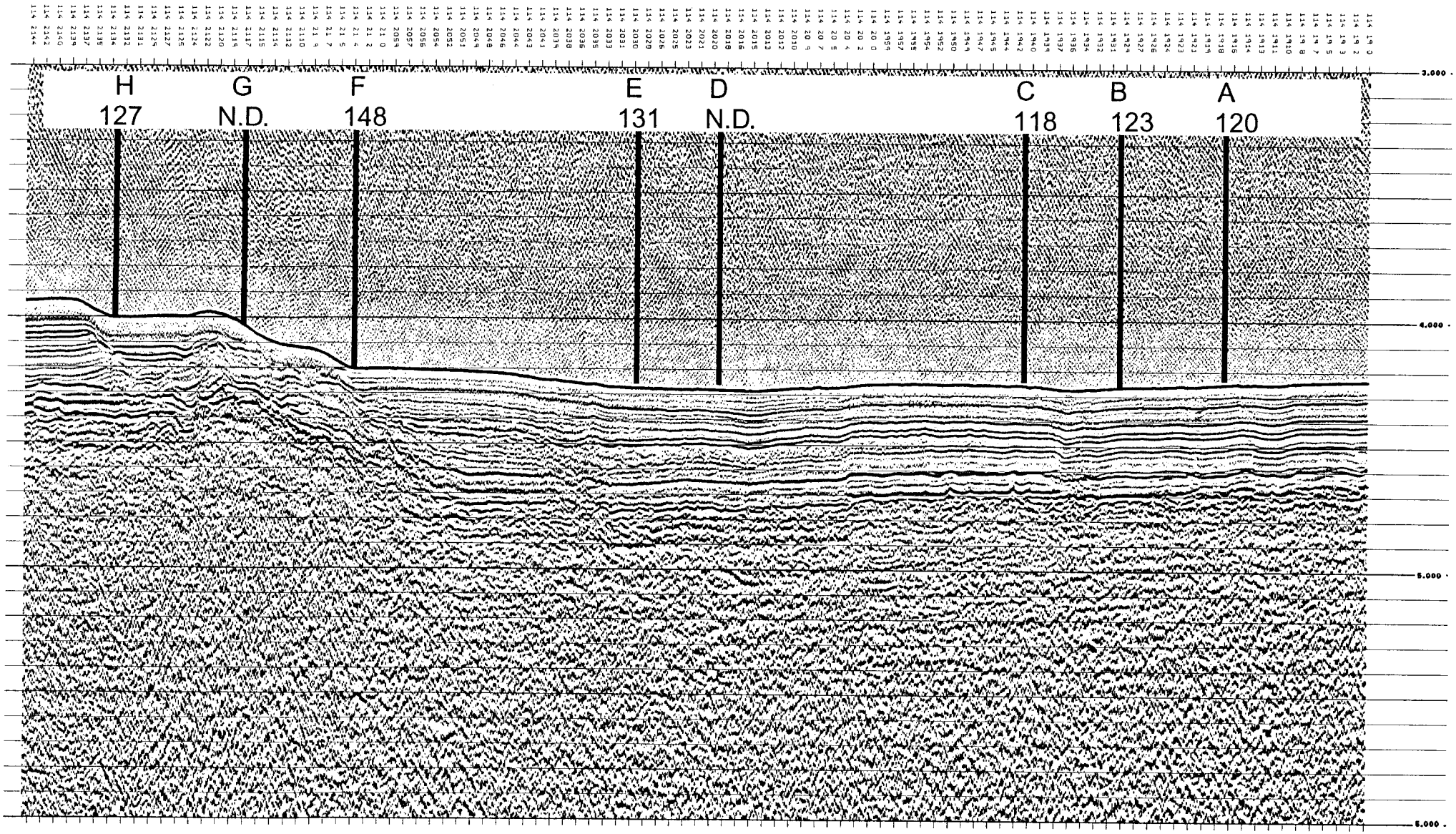

Figure III-8

Seismic Line 11, HF08

NW

SE

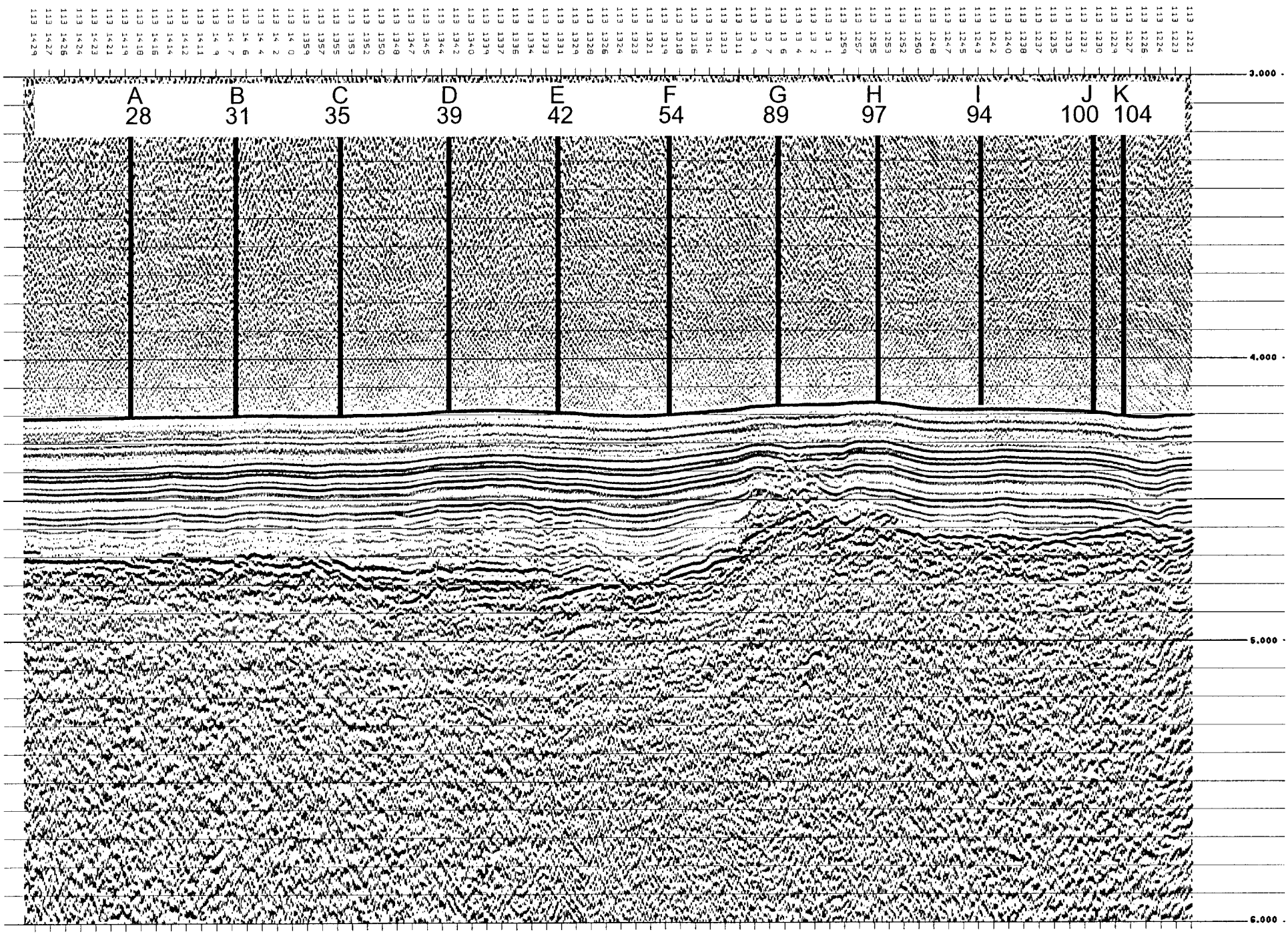

Figure III-9

HF09 Seismic Line 13

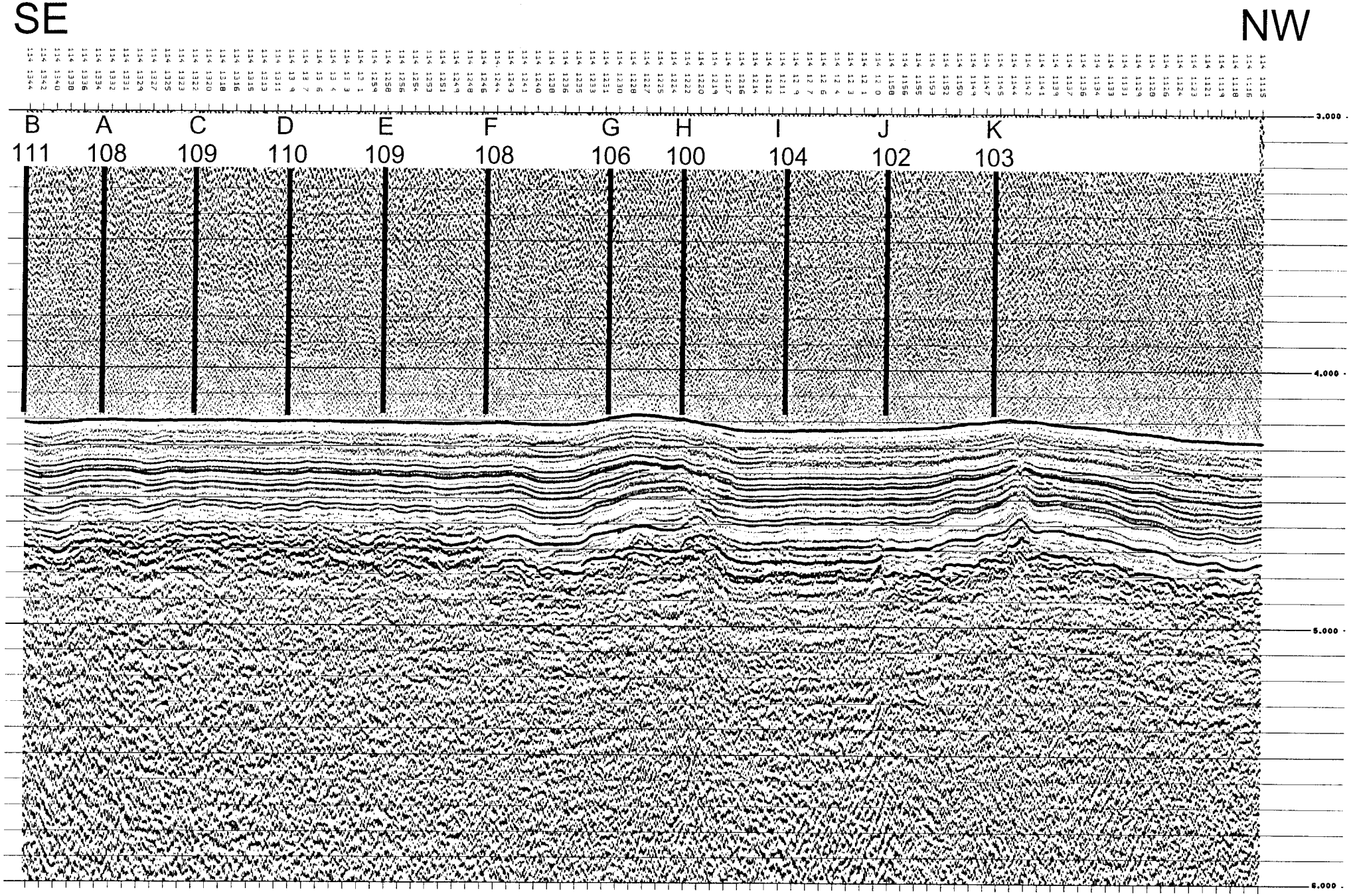

Figure III-10

Seismic Line 13, HF10

SE NW

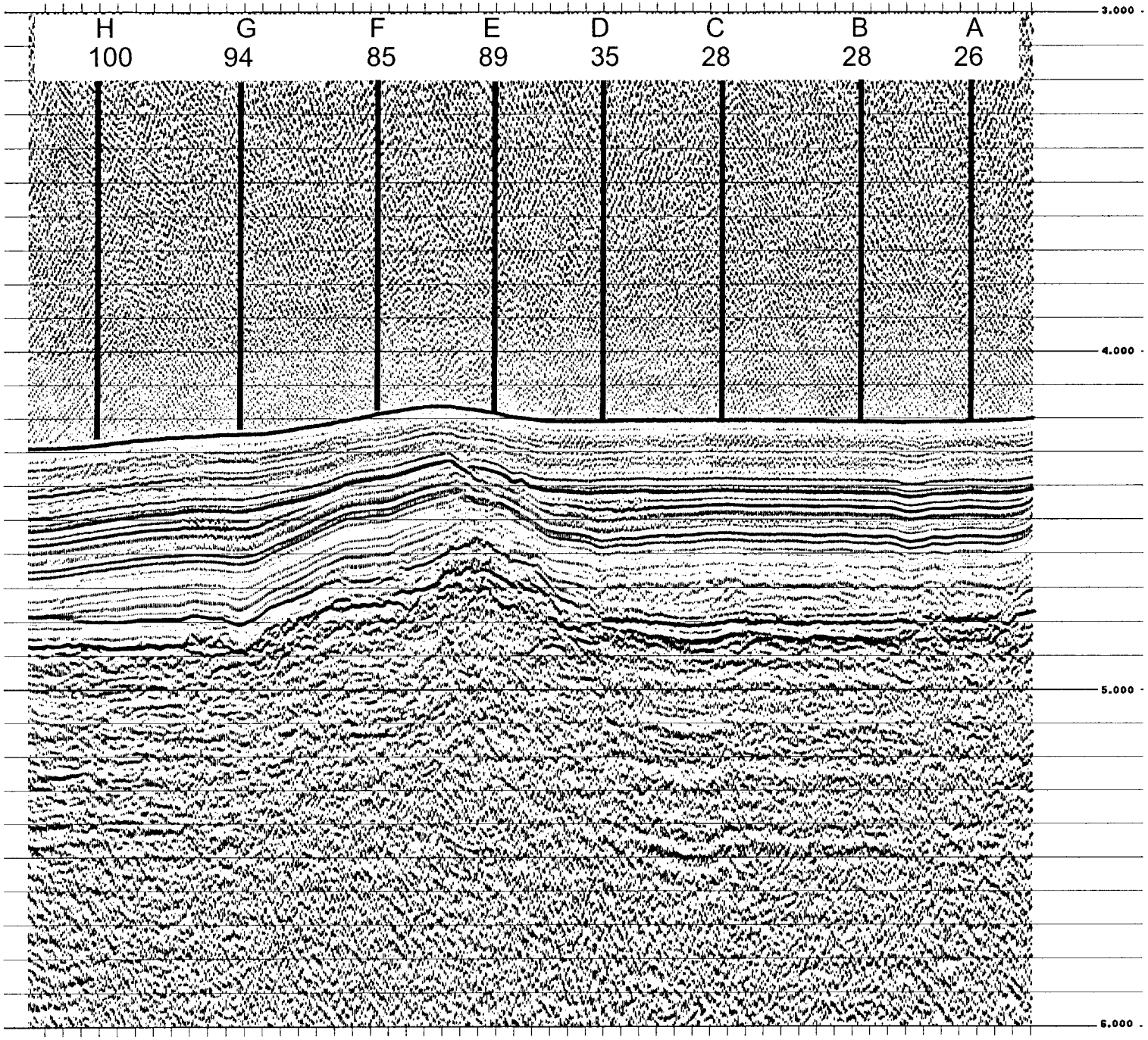

Figure III-11

Seismic Line 5, HF11

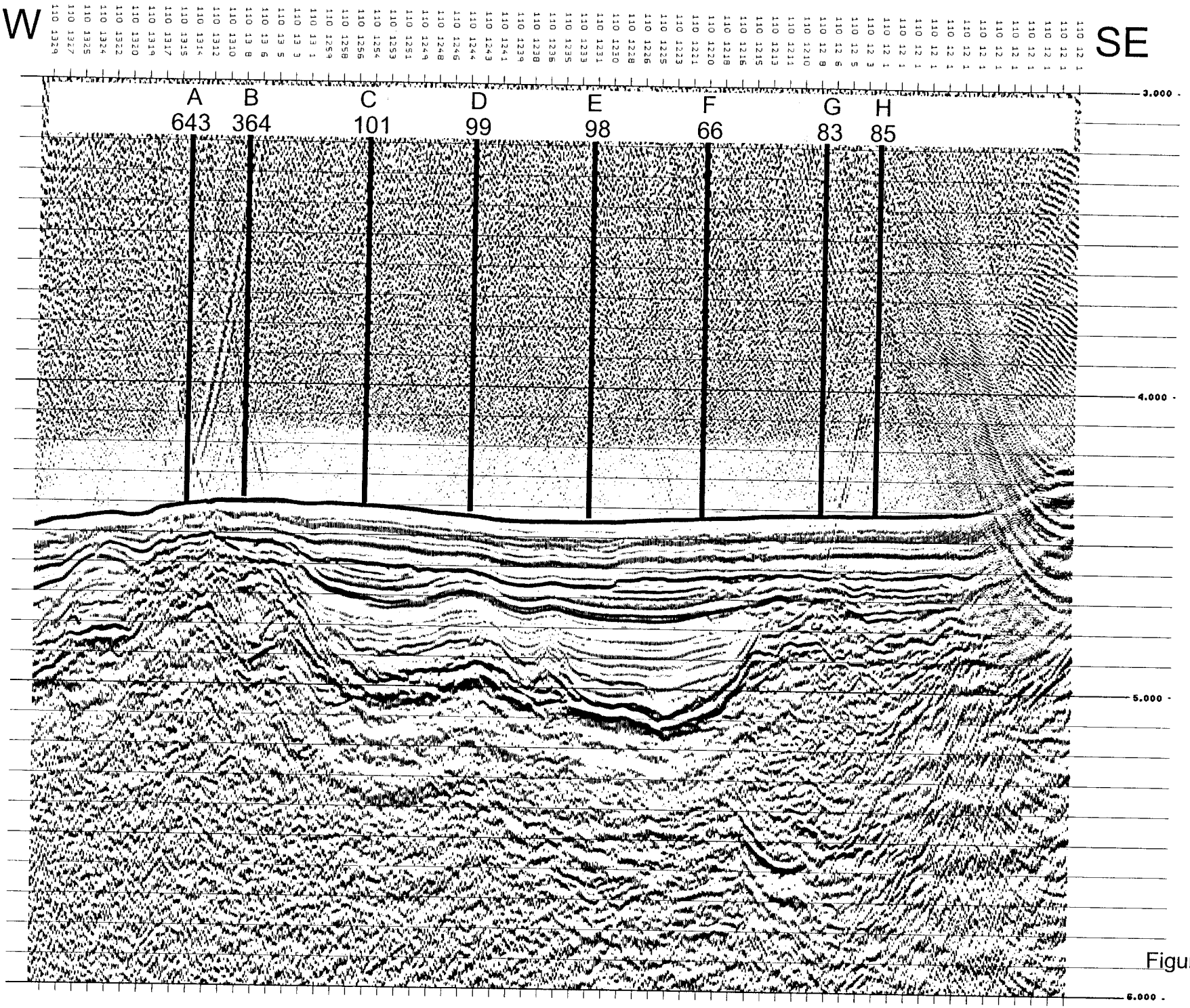

Figure III-12

Seismic Line 14, HF12

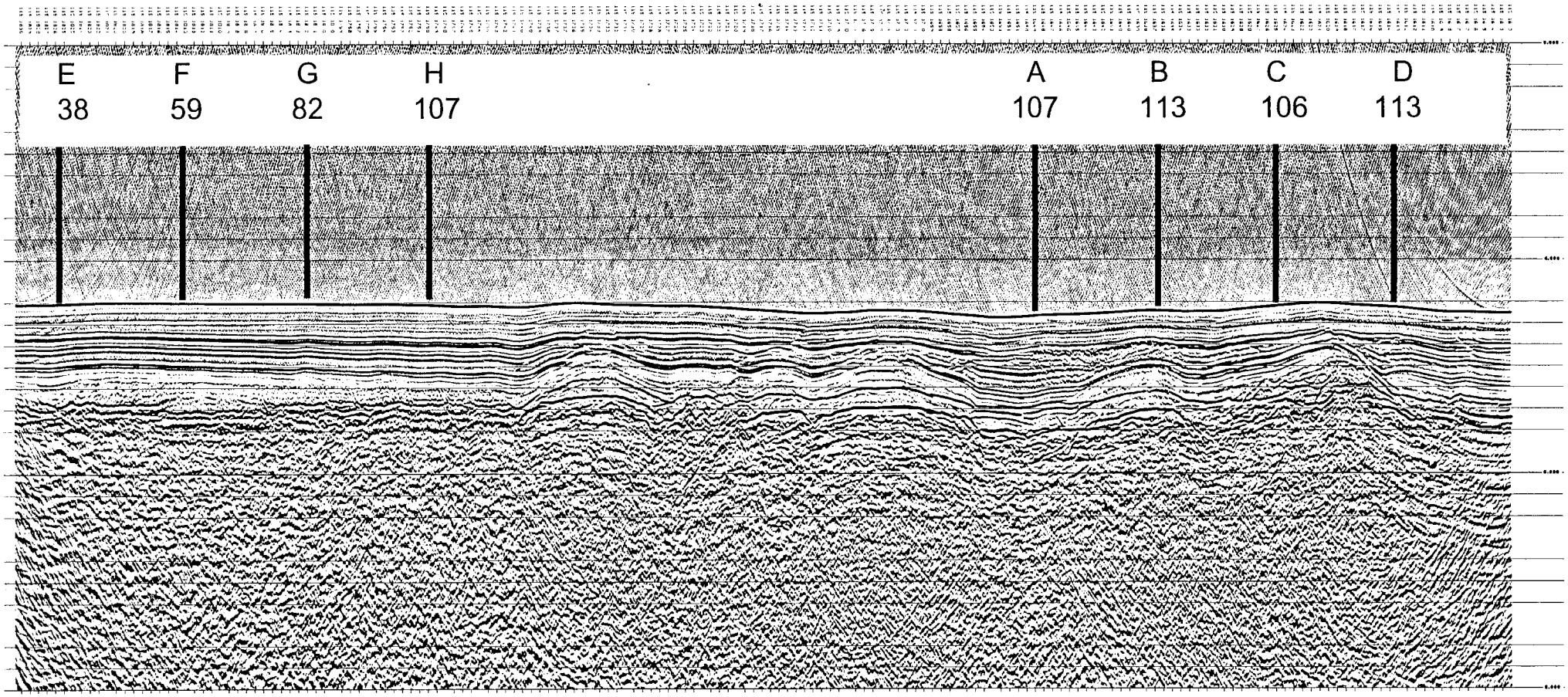

Figure III-13

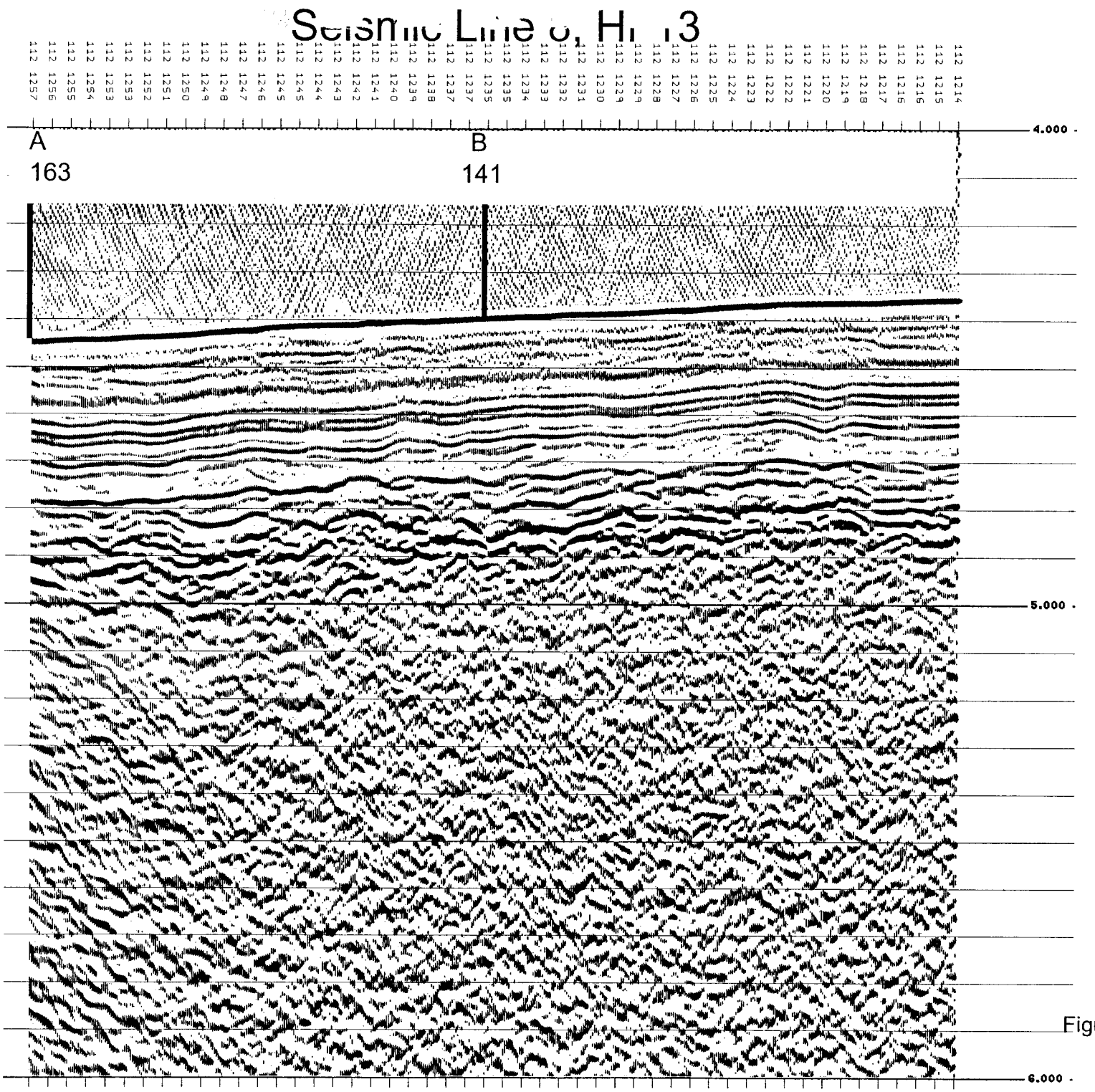

Figure III-14

Line 11, Northern Part

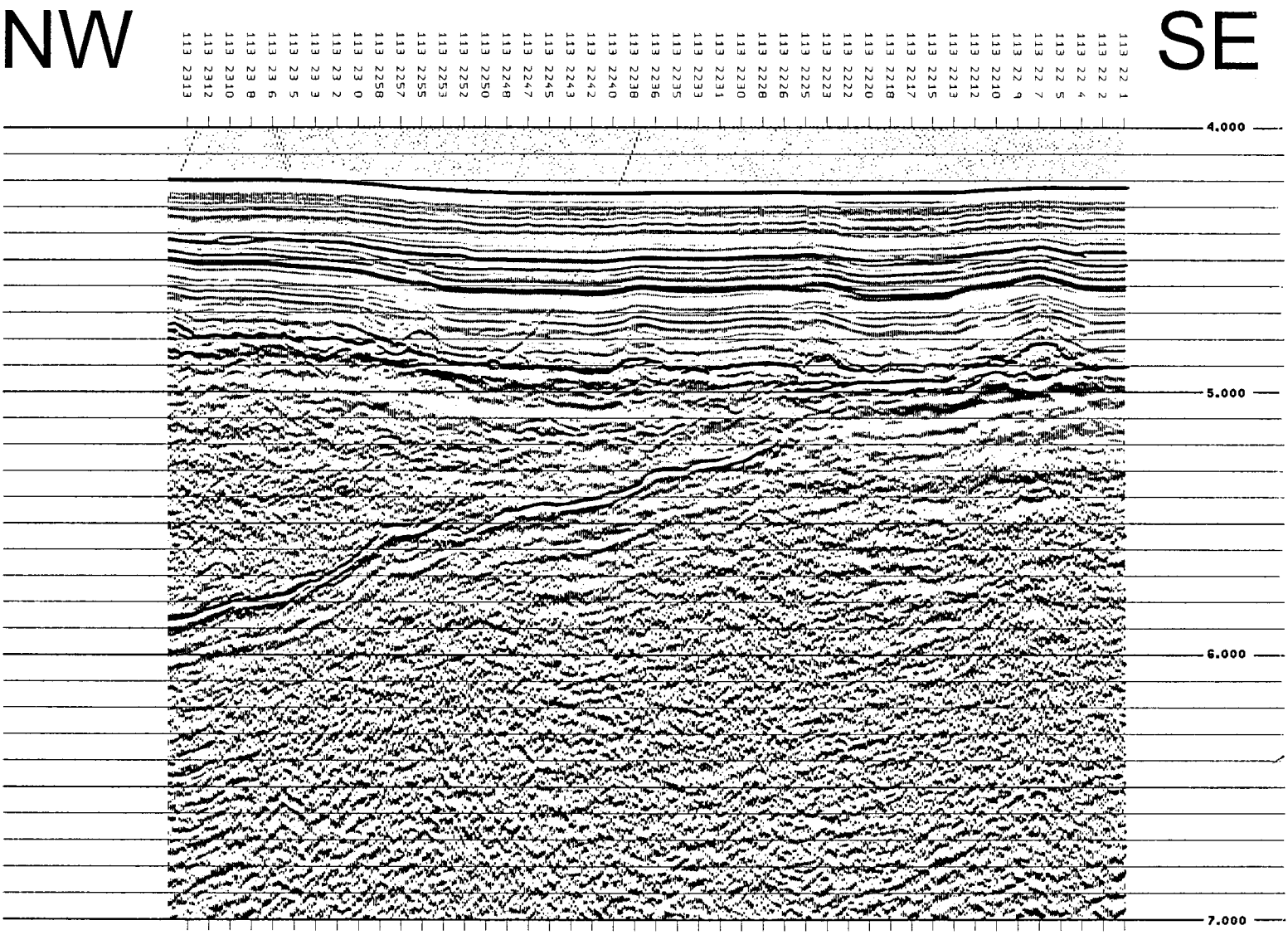

Figure III-15

Line 13: Northern Part

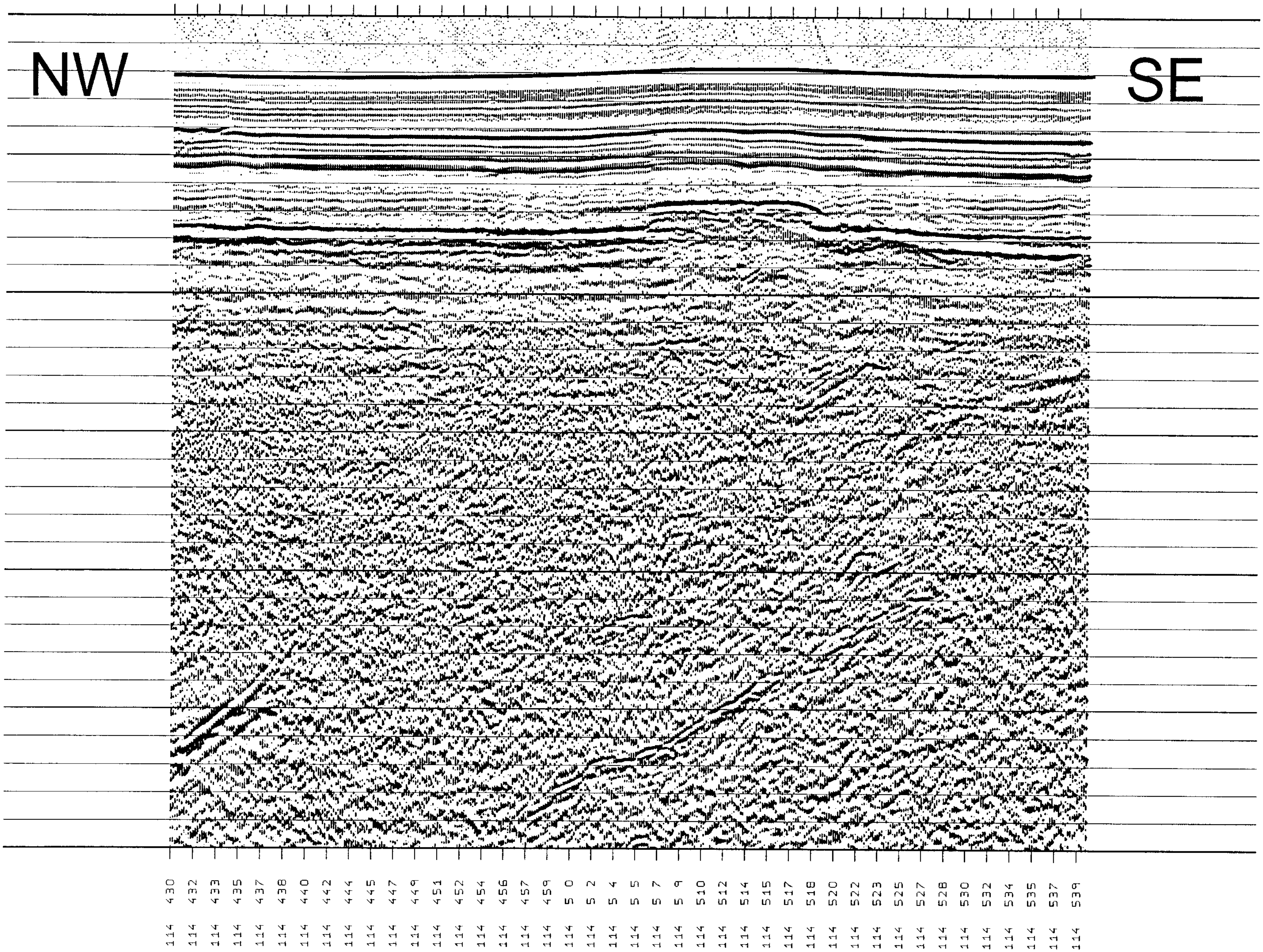

Figure III-16

Line 13, Sill Intrusion

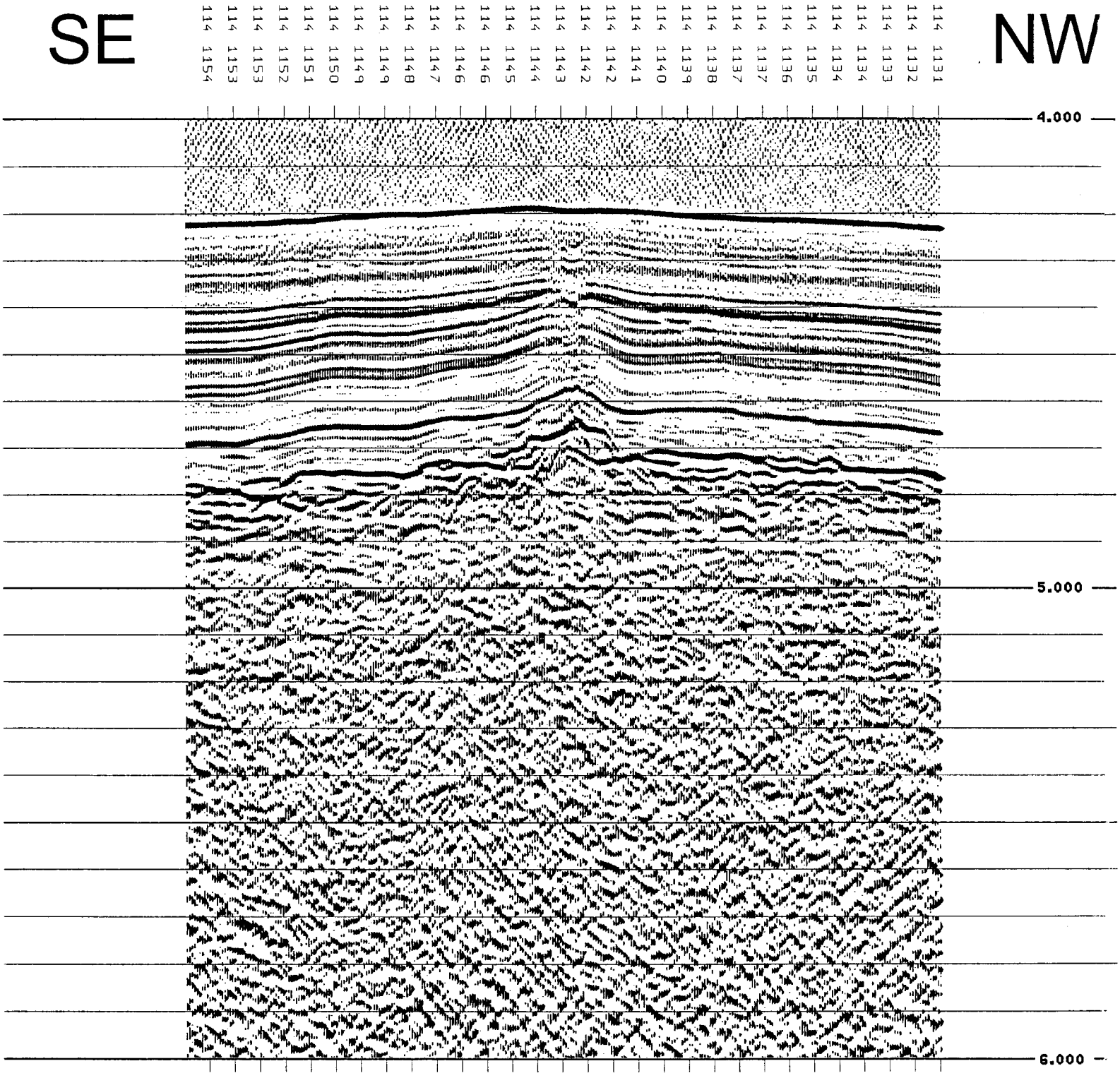

FigIII-17

Table IV-1. Summary of PGC heat flow positions, values, and nearest seismic shot points.

Station	Heat Flow Data										Closest seismic shot								
	Date (GMT)	Time	Latitude (°N)	Latitude (min)	Longitude (°W)	Longitude (min)	Heat Flow (mW/m²)	Tilt (°)	Depth (m)	Spacing (km)	Seismic Line	J - Day	Time (GMT)	Latitude (°N)	Latitude (min)	Longitude (°W)	Longitude (min)	Shot	Distance (m)
TF01HF01A	04/27/01	7:33	8	33.860	87	13.639	94	2.9	3280	0.000	7	111	14:32:48	87	13.632	8	33.871	23746	26
TF01HF01B	04/27/01	9:46	8	34.582	87	14.262	89	4.6	3265	1.758	7	111	14:21:18	87	14.245	8	34.580	23700	27
TF01HF01C	04/27/01	11:44	8	35.426	87	14.974	27	4.4	3233	2.035	7	111	14:07:38	87	14.979	8	35.429	23645	16
TF01HF01D	04/27/01	13.27	8	36.079	87	15.542	29	4.1	3210	1.595	7	111	13:56:46	87	15.551	8	36.067	23603	32
TF01HF01E	04/27/01	14:58	8	36.730	87	16.083	53	3.8	3112	1.560	7	111	13:46:02	87	16.086	8	36.734	23561	14
TF01HF01F	04/27/01	16:17	8	37.201	87	16.591	74	15.2	3033	1.275	7	111	13:37:35	87	16.535	8	37.262	23527	154
TF01HF01G	04/27/01	17:55	8	37.851	87	17.045	58	13.3	3058	1.463	7	111	13:28:03	87	17.036	8	37.853	23489	26
TF01HF01H	04/27/01	19:41	8	38.683	87	17.791	45	9.5	3109	2.059	7	111	13:14:24	87	17.765	8	38.706	23434	67
TF01HF01I	04/27/01	21:38	8	39.439	87	18.303	62	4.1	3165	1.685	7	111	13:03:19	87	18.335	8	39.398	23390	100
TF01HF01J	04/27/01	23:00	8	40.105	87	18.951	56	≥45.0	3211	1.711	7	111	12:51:54	87	18.962	8	40.095	23344	35
TF01HF01K	04/28/01	0:31	8	40.859	87	19.573	40	13.9	3209	1.802	7	111	12:40:00	87	19.596	8	40.841	23296	59
TF01HF01L	04/28/01	2:09	8	41.610	87	20.249	54	12.9	3235	1.862	7	111	12:27:41	87	20.256	8	41.618	23246	19
TF01HF01M	04/28/01	3:44	8	42.390	87	20.901	64	6.4	3252	1.874	7	111	12:15:49	87	20.903	8	42.378	23197	23
TF01HF02A	04/28/01	22:40	8	24.569	87	5.688	117	1.3	3339	0.000	7	111	17:02:09	87	5.681	8	24.580	24346	24
TF01HF02B	04/29/01	0:40	8	23.832	87	5.065	122	10.3	3350	1.779	7	111	17:14:38	87	5.071	8	23.842	24393	22
TF01HF02C	04/29/01	2:20	8	23.146	87	4.498	117	6.7	3346	1.641	7	111	17:25:53	87	4.474	8	23.172	24437	62
TF01HF02D	04/29/01	4:01	8	22.452	87	3.882	118	7.5	3349	1.711	7	111	17:37:44	87	3.867	8	22.457	24483	27
TF01HF02E	04/29/01	6:10	8	21.668	87	3.217	122	7.9	3374	1.896	7	111	17:49:48	87	3.204	8	21.683	24533	37
TF01HF02F	04/29/01	7:47	8	21.019	87	2.746	113	5.4	3369	1.480	7	111	17:59:24	87	2.694	8	21.073	24572	143
TF01HF02G	04/29/01	9:24	8	20.360	87	2.056	114	7.7	3369	1.757	7	111	18:11:07	87	2.065	8	20.351	24619	19
TF01HF02H	04/29/01	10:58	8	19.608	87	1.424	114	8.5	3377	1.811	7	111	18:23:17	87	1.431	8	19.606	24667	21
TF01HF02I	04/29/01	12:25	8	18.863	87	0.825	127	10.6	3385	1.763	7	111	18:35:29	87	0.792	8	18.861	24715	70
TF01HF02J	04/29/01	13:56	8	18.155	87	0.191	114	6.9	3326	1.752	7	111	18:46:42	87	0.203	8	18.162	24760	24
TF01HF02K	04/29/01	15:34	8	17.422	86	59.561	127	12.6	3387	1.782	7	111	18:59:03	86	59.573	8	17.414	24808	27
TF01HF02L	04/29/01	17:32	8	16.678	86	58.917	124	9.6	3391	1.814	7	111	19:11:18	86	58.932	8	16.676	24856	23
TF01HF03A	04/30/01	19:42	9	19.036	86	48.374	28	3.6	3230	0.000	12	114	9:25:13	86	48.452	9	18.967	38878	203
TF01HF03B	04/30/01	21:35	9	19.658	86	49.125	28	8.8	3255	1.792	12	114	9:13:20	86	49.158	9	19.645	38830	59
TF01HF03C	04/30/01	23:07	9	20.304	86	49.888	22	9.0	3255	1.837	12	114	9:01:33	86	49.853	9	20.336	38782	95
TF01HF03D	05/01/01	0:36	9	21.070	86	50.616	Nan	Nan	3167	1.945	12	114	8:48:30	86	50.616	9	21.073	38730	10
TF01HF03E	05/01/01	6:14	9	21.333	86	50.471	18	2.9	3254	0.554	12	114	8:47:29	86	50.673	9	21.133	38726	523
TF01HF03F	05/01/01	7:44	9	21.693	86	51.209	18	2.6	3252	1.504	12	114	8:38:06	86	51.226	9	21.678	38688	37
TF01HF03G	05/01/01	9:22	9	22.382	86	51.964	16	2.1	3254	1.879	12	114	8:25:32	86	51.961	9	22.385	38638	9
TF01HF03H	05/01/01	12:52	9	25.085	86	54.891	13	2.5	3219	7.325	12	114	7:37:27	86	54.814	9	25.160	38443	191
TF01HF03I	05/01/01	14:35	9	25.851	86	55.494	36	0.4	3198	1.796	12	114	7:25:33	86	55.499	9	25.834	38396	35
TF01HF03J	05/01/01	16:12	9	26.564	86	56.197	27	0.8	3193	1.842	12	114	7:13:15	86	56.217	9	26.530	38347	64
TF01HF04A	05/02/01	12:10	9	46.818	86	40.732	237	1.7	3464	0.000	5	110	15:03:42	86	40.732	9	46.818	18421	5
TF01HF04B	05/02/01	14:06	9	46.089	86	39.963	186	2.1	3503	1.947	5	110	14:50:46	86	39.959	9	46.089	18369	3
TF01HF04C	05/02/01	15:51	9	45.379	86	39.297	133	0.8	3511	1.791	5	110	14:38:43	86	39.263	9	45.428	18322	112
TF01HF04D	05/02/01	17:24	9	44.784	86	38.628	103	1.8	3511	1.645	5	110	14:27:24	86	38.612	9	44.810	18278	65
TF01HF04E	05/02/01	19:00	9	44.134	86	37.875	123	4.2	3513	1.827	5	110	14:14:55	86	37.875	9	44.131	18229	9
TF01HF04F	05/02/01	20:27	9	43.454	86	37.149	113	13.4	3510	1.828	5	110	14:02:21	86	37.157	9	43.433	18180	34
TF01HF04G	05/02/01	21:57	9	42.777	86	36.460	149	7.0	3495	1.776	5	110	13:50:23	86	36.454	9	42.778	18133	12
TF01HF04H	05/02/01	23:21	9	42.143	86	35.763	177	5.4	3477	1.731	5	110	13:38:53	86	35.780	9	42.124	18087	48
TF01HF04I	05/03/01	0:57	9	41.474	86	35.044	303	15.0	3487	1.805	5	110	13:26:57	86	35.050	9	41.469	18039	18
TF01HF05A	05/03/01	21:14	9	35.901	86	12.509	14	2.8	4218	0.000	3	108	22:47:38	86	12.530	9	35.917	9432	49

Table IV-1. Summary of PGC heat flow positions, values, and nearest seismic shot points.

Station	Heat Flow Data										Closest seismic shot								
	Date (GMT)	Time	Latitude (°N)	Latitude (min)	Longitude (°W)	Longitude (min)	Heat Flow (mW/m²)	Tilt (°)	Depth (m)	Spacing (km)	Seismic Line	J - Day	Time (GMT)	Latitude (°N)	Latitude (min)	Longitude (°W)	Longitude (min)	Shot	Distance (m)
TF01HF05B	05/04/01	2:37	9	35.511	86	12.998	18	3.0	4187	1.149	3	108	22:55:15	86	12.972	9	35.492	9462	62
TF01HF05C	05/04/01	5:18	9	34.843	86	13.610	13	4.3	4067	1.667	3	108	23:06:33	86	13.616	9	34.836	9507	13
TF01HF05D	05/04/01	7:24	9	34.295	86	14.194	24	4.6	4014	1.472	3	108	23:16:10	86	14.186	9	34.310	9545	20
TF01HF05E	05/04/01	8:27	9	34.224	86	14.318	21	3.7	3965	0.262	3	108	23:18:13	86	14.306	9	34.199	9553	47
TF01HF05F	05/04/01	9:30	9	34.184	86	14.318	24	3.4	3954	0.074	3	108	23:18:27	86	14.321	9	34.184	9554	8
TF01HF05G	05/04/01	16:00	9	33.487	86	15.035	21	3.8	3846	1.839	3	108	23:31:28	86	15.027	9	33.476	9603	35
TF01HF05H	05/04/01	18:03	9	32.926	86	15.568	35	4.2	3823	1.424	3	108	23:41:29	86	15.576	9	32.927	9641	13
TF01HF05I	05/04/01	19:18	9	32.847	86	15.646	25	3.7	3719	0.204	3	108	23:42:50	86	15.651	9	32.858	9646	15
TF01HF05J	05/04/01	21:47	9	32.010	86	16.520	25	3.7	3719	2.225	3	108	23:57:47	86	16.521	9	32.024	9705	25
TF01HF05K	05/05/01	0:08	9	31.280	86	17.242	22	4.5	3681	1.889	3	109	0:10:22	86	17.260	9	31.290	9756	42
TF01HF05L	05/05/01	2:32	9	30.548	86	17.936	23	6.6	3619	1.856	3	109	0:22:59	86	17.963	9	30.579	9805	68
TF01HF06A	05/06/01	2:38	8	20.820	86	0.164	117	1.4	3053	0.000	13	115	4:03:14	86	0.137	8	20.856	42773	79
TF01HF06B	05/06/01	4:38	8	21.430	86	0.855	112	3.8	3041	1.697	13	115	4:14:50	86	0.846	8	21.438	42818	29
TF01HF06C	05/06/01	6:48	8	22.089	86	1.561	109	3.1	3028	1.778	13	115	4:27:28	86	1.596	8	22.036	42865	119
TF01HF06D	05/06/01	8:39	8	22.526	86	2.288	112	4.3	3038	1.559	13	115	4:38:59	86	2.265	8	22.566	42907	81
TF01HF06E	05/06/01	10:33	8	23.091	86	2.980	117	2.7	3082	1.644	13	115	4:50:29	86	2.951	8	23.117	42950	73
TF01HF06F	05/06/01	12:41	8	23.631	86	3.707	118	3.9	3101	1.666	13	115	5:02:20	86	3.672	8	23.685	42995	124
TF01HF06G	05/06/01	14:35	8	24.290	86	4.409	113	4.9	3125	1.773	13	115	5:15:10	86	4.415	8	24.282	43042	17
TF01HF06H	05/06/01	16:43	8	24.853	86	5.151	214	2.5	3087	1.713	13	115	5:26:58	86	5.138	8	24.858	43087	26
TF01HF06I	05/06/01	18:26	8	25.253	86	5.650	203	3.6	3075	1.177	13	115	5:35:31	86	5.653	8	25.257	43119	15
TF01HF06J	05/06/01	20:19	8	25.863	86	6.397	104	5.8	3085	1.775	13	115	5:47:51	86	6.400	8	25.860	43166	1
TF01HF06K	05/06/01	22:06	8	26.399	86	7.106	116	2.9	3056	1.635	13	115	5:59:29	86	7.103	8	26.416	43210	32
TF01HF06L	05/06/01	23:37	8	26.749	86	7.533	128	3.4	3076	1.016	13	115	6:06:35	86	7.532	8	26.762	43237	22
TF01HF06M	05/07/01	1:36	8	27.348	86	8.256	112	3.3	3041	1.728	13	115	6:19:00	86	8.268	8	27.352	43284	15
TF01HF07A	05/07/01	22:52	8	45.518	86	13.714	120	6.6	3290	0.000	12	114	19:17:23	86	13.727	8	45.509	41241	38
TF01HF07B	05/08/01	1:01	8	44.767	86	13.019	123	2.5	3299	1.885	12	114	19:29:34	86	13.010	8	44.784	41291	31
TF01HF07C	05/08/01	3:08	8	44.049	86	12.287	118	2.7	3292	1.888	12	114	19:41:41	86	12.297	8	44.055	41341	16
TF01HF07D	05/08/01	12:34	8	41.882	86	10.119	Nan	Nan	3313	5.644	12	114	20:18:11	86	10.104	8	41.890	41492	36
TF01HF07E	05/08/01	14:51	8	41.156	86	9.394	131	3.4	3301	1.889	12	114	20:30:00	86	9.392	8	41.164	41542	8
TF01HF07F	05/08/01	18:57	8	39.137	86	7.394	148	3.5	3238	5.234	12	114	21:03:50	86	7.385	8	39.160	41681	38
TF01HF07G	05/08/01	21:11	8	38.319	86	6.584	Nan	Nan	3093	2.120	12	114	21:17:46	86	6.559	8	38.343	41738	58
TF01HF07H	05/08/01	23:35	8	37.432	86	5.715	127	8.5	3093	2.287	12	114	21:33:16	86	5.683	8	37.459	41799	88
TF01HF08A	05/09/01	20:39	9	12.239	86	23.461	28	3.5	3257	0.000	11	113	14:18:47	86	23.467	9	12.241	34527	12
TF01HF08B	05/09/01	23:15	9	11.558	86	22.770	31	3.8	3254	1.785	11	113	14:06:38	86	22.785	9	11.539	34479	45
TF01HF08C	05/10/01	1:05	9	10.870	86	22.145	35	4.4	3252	1.711	11	113	13:54:49	86	22.142	9	10.884	34434	27
TF01HF08D	05/10/01	3:11	9	10.168	86	21.431	39	4.2	3239	1.842	11	113	13:42:54	86	21.431	9	10.179	34385	21
TF01HF08E	05/10/01	5:14	9	9.459	86	20.725	42	4.2	3241	1.841	11	113	13:31:17	86	20.731	9	9.462	34336	12
TF01HF08F	05/10/01	7:43	9	8.741	86	20.003	54	3.7	3250	1.874	11	113	13:18:43	86	20.006	9	8.747	34286	12
TF01HF08G	05/10/01	9:48	9	8.029	86	19.335	89	4.4	3224	1.797	11	113	13:06:24	86	19.313	9	8.055	34238	64
TF01HF08H	05/10/01	11:35	9	7.395	86	18.650	97	3.7	3215	1.717	11	113	12:54:19	86	18.657	9	7.383	34192	26
TF01HF08I	05/10/01	13:38	9	6.740	86	18.026	94	4.2	3236	1.665	11	113	12:43:03	86	18.026	9	6.744	34148	8
TF01HF08J	05/10/01	15:46	9	5.997	86	17.288	100	3.6	3241	1.927	11	113	12:30:55	86	17.288	9	6.011	34097	26
TF01HF08K	05/10/01	16:45	9	5.828	86	17.126	104	6.2	3246	0.431	11	113	12:28:08	86	17.118	9	5.835	34085	19
TF01HF09A	05/11/01	13:15	9	4.843	86	33.998	108	3.0	3252	0.000	12	114	13:33:56	86	33.995	9	4.849	39868	12
TF01HF09B	05/11/01	15:04	9	4.250	86	33.413	111	4.1	3252	1.533	12	114	13:45:52	86	33.407	9	4.255	39909	15

Table IV-1. Summary of PGC heat flow positions, values, and nearest seismic shot points.

Station	Heat Flow Data										Closest seismic shot								
	Date (GMT)	Time	Latitude (°N)	Latitude (min)	Longitude (°W)	Longitude (min)	Heat Flow (mW/m^2)	Tilt (°)	Depth (m)	Spacing (km)	Seismic Line	J - Day	Time (GMT)	Latitude (°N)	Latitude (min)	Longitude (°W)	Longitude (min)	Shot	Distance (m)
TF01HF09C	05/11/01	17:54	9	5.471	86	34.630	109	4.0	3251	3.173	12	114	13:22:04	86	34.638	9	5.477	39824	17
TF01HF09D	05/11/01	19:44	9	6.173	86	35.334	110	6.2	3253	1.830	12	114	13:09:28	86	35.346	9	6.149	39776	50
TF01HF09E	05/11/01	21:35	9	6.805	86	36.007	109	6.1	3255	1.698	12	114	12:58:22	86	35.996	9	6.802	39731	21
TF01HF09F	05/11/01	23:34	9	7.503	86	36.732	108	4.7	3258	1.852	12	114	12:45:51	86	36.723	9	7.519	39681	33
TF01HF09G	05/12/01	1:57	9	8.428	86	37.670	106	3.3	3245	2.424	12	114	12:30:32	86	37.661	9	8.429	39617	17
TF01HF09H	05/12/01	3:29	9	9.058	86	38.019	100	4.8	3238	1.330	12	114	12:22:19	86	38.151	9	8.919	39583	355
TF01HF09I	05/12/01	5:24	9	9.637	86	38.890	104	6.0	3275	1.920	12	114	12:10:13	86	38.890	9	9.622	39533	27
TF01HF09J	05/12/01	7:30	9	10.327	86	39.661	102	3.6	3269	1.903	12	114	11:58:11	86	39.637	9	10.347	39482	58
TF01HF09K	05/12/01	9:36	9	11.059	86	40.422	103	3.9	3249	1.943	12	114	11:45:57	86	40.404	9	11.081	39430	53
TF01HF10A	05/13/01	3:54	9	18.386	86	47.862	26	3.4	3254	0.000	12	114	9:36:06	86	47.852	9	18.383	38919	19
TF01HF10B	05/13/01	6:39	9	17.820	86	47.216	28	4.9	3255	1.579	12	114	9:47:18	86	47.257	9	17.787	38960	97
TF01HF10C	05/13/01	8:26	9	17.102	86	46.411	28	7.1	3251	1.983	12	114	10:01:33	86	46.483	9	17.038	39013	178
TF01HF10D	05/13/01	10:16	9	16.477	86	45.911	35	4.2	3254	1.475	12	114	10:11:53	86	45.918	9	16.478	39052	13
TF01HF10E	05/13/01	12:24	9	15.783	86	45.214	89	3.6	3228	1.810	12	114	10:24:22	86	45.213	9	15.797	39100	25
TF01HF10F	05/13/01	14:23	9	15.135	86	44.562	85	4.1	3248	1.691	12	114	10:35:54	86	44.565	9	15.146	39145	21
TF01HF10G	05/13/01	16:23	9	14.470	86	43.861	94	4.0	3285	1.777	12	114	10:47:54	86	43.852	9	14.473	39193	17
TF01HF10H	05/13/01	18:36	9	13.742	86	43.074	100	4.4	3310	1.972	12	114	11:00:40	86	43.096	9	13.729	39245	47
TF01HF11A	05/14/01	11:25	9	40.798	86	34.308	643	2.6	3418	0.000	5	110	13:14:35	86	34.327	9	40.777	17990	53
TF01HF11B	05/14/01	12:51	9	40.411	86	33.952	364	3.2	3421	0.968	5	110	13:07:42	86	33.949	9	40.404	17964	15
TF01HF11C	05/14/01	14:45	9	39.680	86	33.218	101	5.7	3406	1.905	5	110	12:54:44	86	33.219	9	39.690	17914	18
TF01HF11D	05/14/01	16:31	9	39.078	86	32.533	99	5.7	3430	1.675	5	110	12:43:42	86	32.529	9	39.081	17869	10
TF01HF11E	05/14/01	18:10	9	38.410	86	31.816	98	9.0	3447	1.801	5	110	12:31:54	86	31.822	9	38.401	17821	20
TF01HF11F	05/14/01	19:52	9	37.753	86	31.135	66	6.7	3432	1.740	5	110	12:20:17	86	31.142	9	37.754	17775	13
TF01HF11G	05/14/01	21:43	9	37.083	86	30.333	83	5.6	3423	1.919	5	110	12:07:42	86	30.361	9	37.062	17724	65
TF01HF11H	05/14/01	23:30	9	36.364	86	29.670	85	7.4	3419	1.800	5	110	12:01:43	86	30.015	9	36.716	17700	913
TF01HF11I	05/15/01	1:11	9	35.595	86	29.036	83	6.8	3427	1.835	5	110	12:01:43	86	30.015	9	36.716	17700	2757
TF01HF11J	05/15/01	3:15	9	34.708	86	28.431	61	4.1	3454	1.980	5	110	11:24:19	86	28.407	9	34.069	17699	1185
TF01HF11K	05/15/01	5:40	9	33.871	86	27.719	50	2.9	3468	2.023	5	110	11:24:19	86	28.407	9	34.069	17699	1327
TF01HF11L	05/15/01	7:20	9	33.173	86	27.022	46	5.0	3476	1.814	5	110	11:23:20	86	28.437	9	33.985	17695	3023
TF01HF11M	05/15/01	9:17	9	32.456	86	26.317	48	3.8	3481	1.850	5	110	11:21:38	86	28.512	9	33.860	17688	4829
TF01HF12A	05/16/01	7:17	8	58.752	86	47.729	107	2.6	3303	0.000	13	115	16:49:41	86	47.721	8	58.747	45754	18
TF01HF12B	05/16/01	9:23	8	58.136	86	46.970	113	3.4	3281	1.797	13	115	16:37:20	86	46.971	8	58.118	45706	33
TF01HF12C	05/16/01	11:14	8	57.544	86	46.227	106	2.6	3269	1.746	13	115	16:25:51	86	46.221	8	57.549	45660	14
TF01HF12D	05/16/01	13:16	8	56.948	86	45.484	113	2.7	3266	1.751	13	115	16:13:53	86	45.475	8	56.947	45613	17
TF01HF12E	05/16/01	18:29	9	3.521	86	53.840	38	3.6	3255	19.538	13	115	18:25:53	86	53.817	9	3.547	46134	64
TF01HF12F	05/16/01	20:13	9	2.953	86	53.081	59	7.3	3249	1.742	13	115	18:14:08	86	53.071	9	2.975	46088	44
TF01HF12G	05/16/01	23:17	9	2.344	86	52.266	82	2.1	3252	1.869	13	115	18:01:54	86	52.262	9	2.351	46038	15
TF01HF12H	05/17/01	1:19	9	1.714	86	51.579	107	3.6	3256	1.715	13	115	17:49:47	86	51.546	9	1.743	45992	81
TF01HF13A	05/17/01	9:26	9	8.891	85	56.582	163	4.5	3447	0.000	8	112	12:57:34	85	56.546	9	8.864	28937	84
TF01HF13B	05/17/01	11:40	9	7.697	85	57.784	141	7.3	3409	3.118	8	112	12:35:25	85	57.758	9	7.682	28854	55

Table IV-2. Summary of autonomous temperature logger deployments and results.

Core	Date (GMT)	Time	Position Latitude (°N)	Longitude (°W)	Core recovery (m)	ID	Distance @ deployment (m)	Distance @ recovery (m)	Sensor penetration	Tilt (°)	Gradient (°C/m)	Conductivity (W/m/°C)	Heat Flow (mW/m_2)	Remarks
GC02	04/26/01	15:03	08 37.424	087 16.621	3.1m	none	1.33	1.33	yes	<5	none	0.74	none	first test: empty logger attachment sent down
GC03	04/26/01	18:44	08 37.136	087 16.837	<0.01 m	9	1.33	none	no	~90	none	0.74	none	Logger 9 hit corer stand during deployment. Logger 5 bent during recovery
						5	2.96	2.89	yes					
GC04	04/26/01	21:57	08 37.149	087 16.984	none	9	1.58	1.58	no	<5	none	0.74	none	Loggers arranged in different angles
						20	2.82	2.82	yes					
GC05	04/27/01	0:52	08 37.441	087 16.800	1.22	9	1.58	1.58	yes	<5	0.18	0.74	132	
						20	2.82	2.82	yes					
GC06	04/28/01	7:39	08 44.485	087 12.797	none	3	1.58	1.58	yes	<5	0.15	0.74	112	Loggers arranged with angles of 60 ° for all follov
						7	2.25	2.25	yes					
						9	2.88	2.88	yes					stations
GC07	04/28/01	10:36	08 44.345	087 12.641	none	3	1.58	1.58	no	<5	0.15	0.74	111	
						7	2.25	2.25	yes					
						9	2.88	2.88	yes					
GC16	05/01/01	3:16	09 28.443	086 59.752	3.20	3	1.58	1.58	yes		0.04	0.75	33	
						7	2.25	2.25	yes					
						9	2.88	2.88	yes					
GC17	05/01/01	6:18	09 28.555	086 59.621	2.48	3	1.58	1.58	yes		0.05	0.75	35	Attachment of bottom log-
						7	2.25	2.25	yes					ger had cracks in welding
						9	2.88	2.88	yes					points - replaced
PC18	05/03/01	6:52	09 40.573	086 34.124	8.91	3	1.53	1.57	yes	<5	0.84	0.72	605	Loggers concentrated at to
						7	2.83	2.82	yes					one attachment empty on
						9	4.92	4.92	yes					bottom
						none	7.65	7.65	yes					
PC19	05/03/01	14:14	09 40.608	086 33.676	5.58	3	1.57	1.57	yes	<5	0.25	0.72	176	Loggers distributed about core length
						7	2.82	2.82	yes					
						9	4.92	4.92	yes					Core taken for phys props
						6	6.64	crashed	yes					
						11	7.65	lost						Tip of logger 8 bent on rec
						8	8.69	crashed	yes					
GC23	05/05/01	22:34	08 29.797	085 58.022	3.17	3	1.58	1.58	yes	<5	0.19	0.73	136	
						6	2.25	2.25	yes					
						9	2.88	2.88	yes					
GC26	05/07/01	14:05	08 14.575	086 13.930	3.47	3	1.58	1.58	yes	<5	0.11	0.73	77	Middle attachment loosend
						6	2.25	2.25	yes					tightened again. Logger 6
						9	2.88	2.88	yes					bent. Replaced by no. 7.
GC27	05/07/01	17:17	08 14.599	086 13.938	2.74	3	1.58	1.58	yes	<5	0.12	0.72	84	
						7	2.25	2.25	yes					
						9	2.88	2.88	yes					

Table IV-2. Summary of autonomous temperature logger deployments and results.

Core	Date (GMT)	Time	Position Latitude (°N)	Longitude (°W)	Core recovery (m)	ID	Distance @ deployment (m)	Distance @ recovery (m)	Sensor penetration	Tilt (°)	Gradient (°C/m)	Conductivity (W/m/°C)	Heat Flow (mW/m_2)	Remarks
PC36	05/12/01	15:01	08 56.250	086 40.953	6.41	3	1.57	1.57	no (?)	<5	0.15	0.72	109	Upper two attachments
						7	2.83	2.83	yes					still mounted from last
						9	4.73	4.73	yes					deployment, bottom one
														replaced and fixed with
														additional banding
PC37	05/12/01	21:12	08 56.453	086 41.110	7.74	3	1.57	1.57	yes (?)	<5	0.11	0.72	77	Gradient for all sensors rep
						7	2.83	2.83	yes (?)					When calculated for only
						9	4.73	4.73	yes					lower two sensors, gradien
														will be 0.147
PC38	05/14/01	0:56	09 40.588	086 34.132		3	1.57	1.57	yes	<5	0.79	0.72	570	Attachments of no. 3 and 9
						7	2.83	2.83	yes					had to be tightened again,
						9	4.73	4.73	yes					but did not move along the
						20	6.61	6.61	yes					core barrel
														Logger no. 7 slightly bent.
PC39	05/14/01	7:19	09 40.571	086 34.154		3	1.57	1.57	yes	<5	0.83	0.72	597	no problems
						7	2.83	2.83	yes					
						9	4.73	4.73	yes					
						20	6.61	6.61	yes					

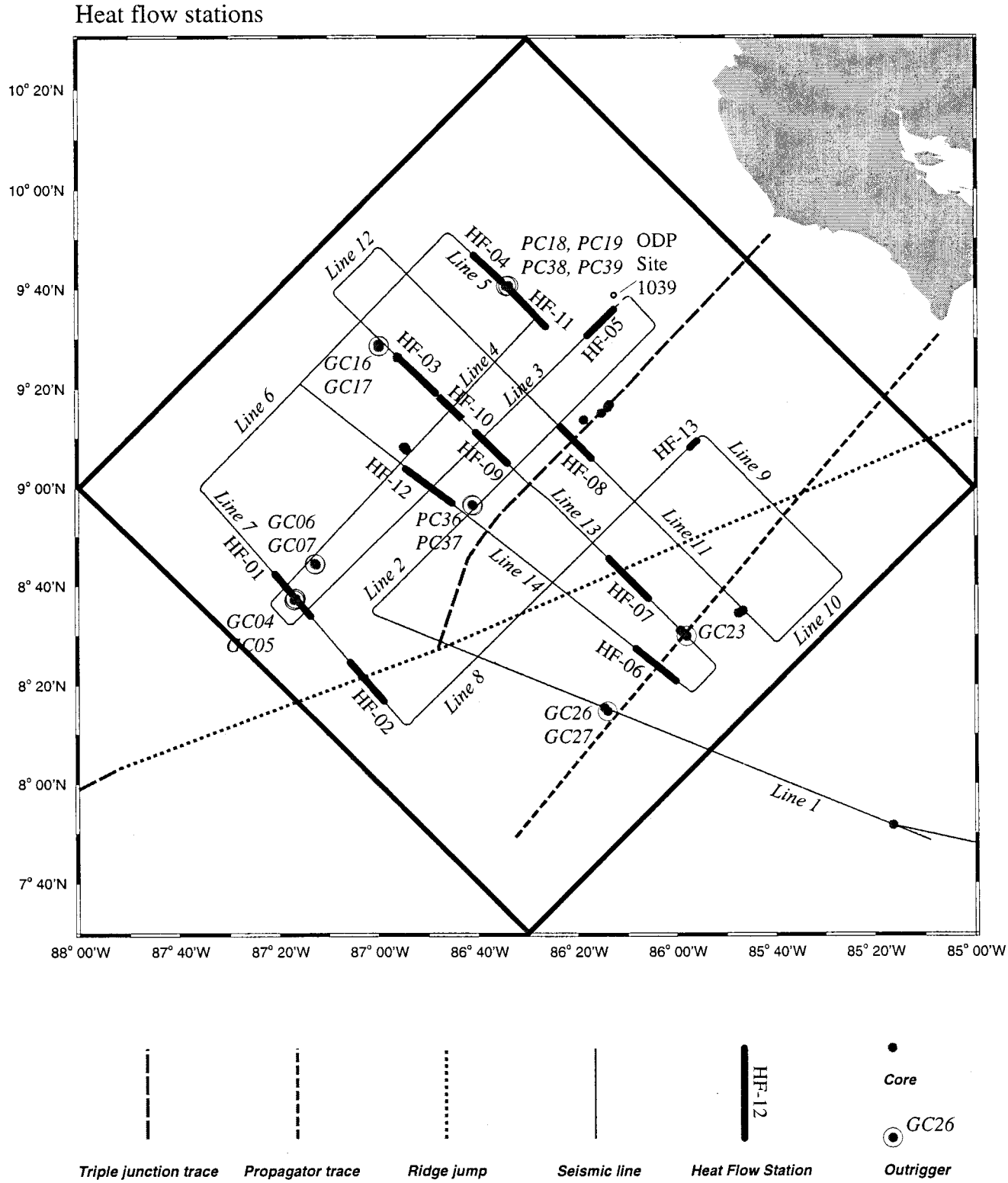
Heat flow stations
10° 20'N
10° 00'N
9° 40'N
9° 20'N
9° 00'N
8° 40'N
8° 20'N
8° 00'N
7° 40'N
88° 00'W
87° 40'W
87° 20'W
87° 00'W
86° 40'W
86° 20'W
86° 00'W
85° 40'W
85° 20'W
85° 00'W
Line 12
HF-04
PC18, PC19 ODP
PC38, PC39 Site
1039
Line 5
HF-11
HF-05
HF-03
GC16
GC17
Line 4
Line 3
Line 6
HF-10
HF-09
HF-08
HF-13
Line 9
HF-12
PC36
PC37
Line 13
Line 11
Line 7
GC06
GC07
HF-01
Line 2
Line 14
HF-07
GC23
Line 10
GC04
GC05
HF-06
HF-02
Line 8
GC26
GC27
Line 1
Triple junction trace
Propagator trace
Ridge jump
Seismic line
HF-12
Heat Flow Station
Core
GC26
Outrigger

Figure IV-1

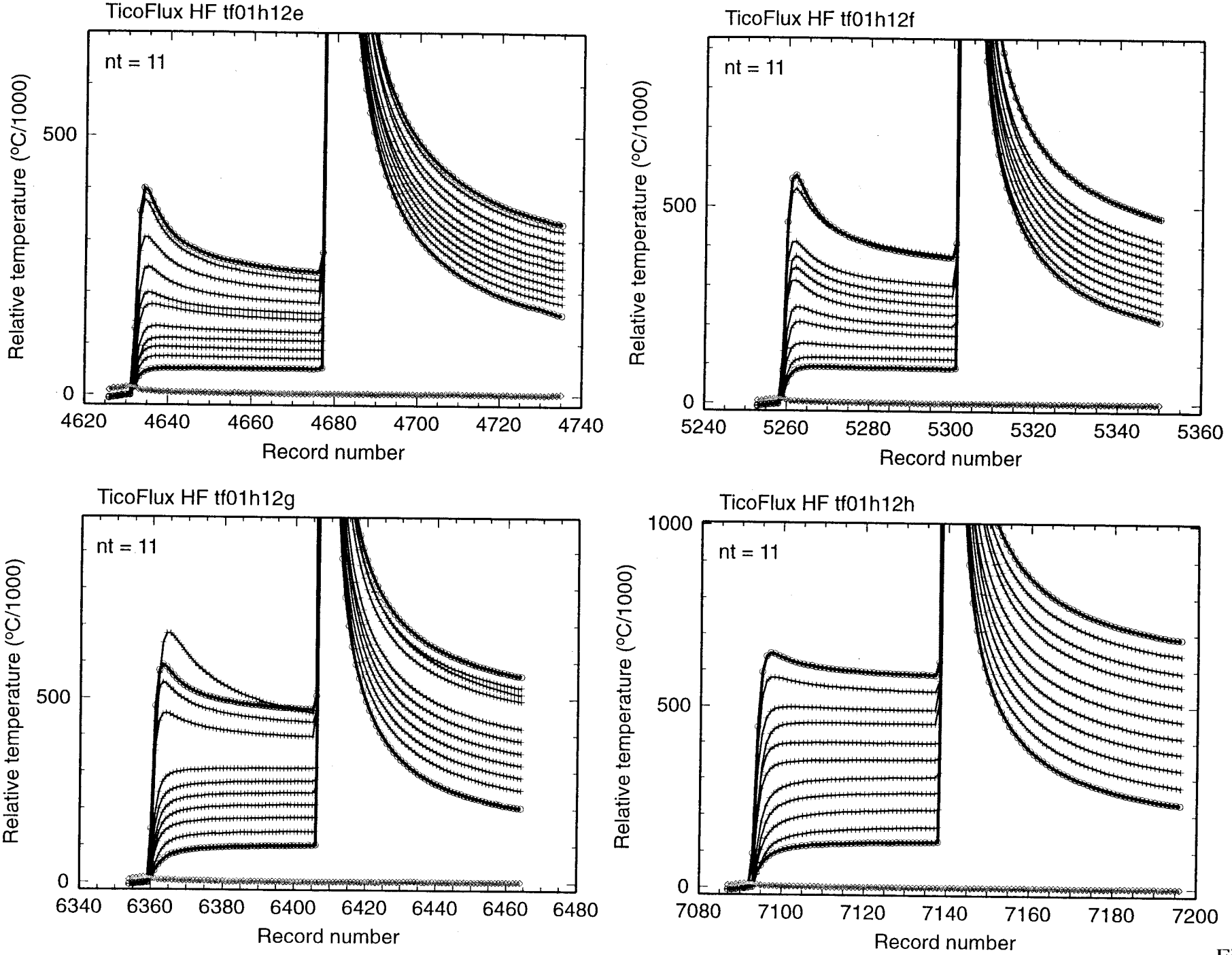
TicoFlux HF tf01h12e
nt = 11
Relative temperature (°C/1000)
500
0
4620
4640
4660
4680
4700
4720
4740
Record number
TicoFlux HF tf01h12f
nt = 11
Relative temperature (°C/1000)
500
0
5240
5260
5280
5300
5320
5340
5360
Record number
TicoFlux HF tf01h12g
nt = 11
Relative temperature (°C/1000)
500
0
6340
6360
6380
6400
6420
6440
6460
6480
Record number
TicoFlux HF tf01h12h
nt = 11
Relative temperature (°C/1000)
1000
500
0
7080
7100
7120
7140
7160
7180
7200
Record number

Figure IV-2

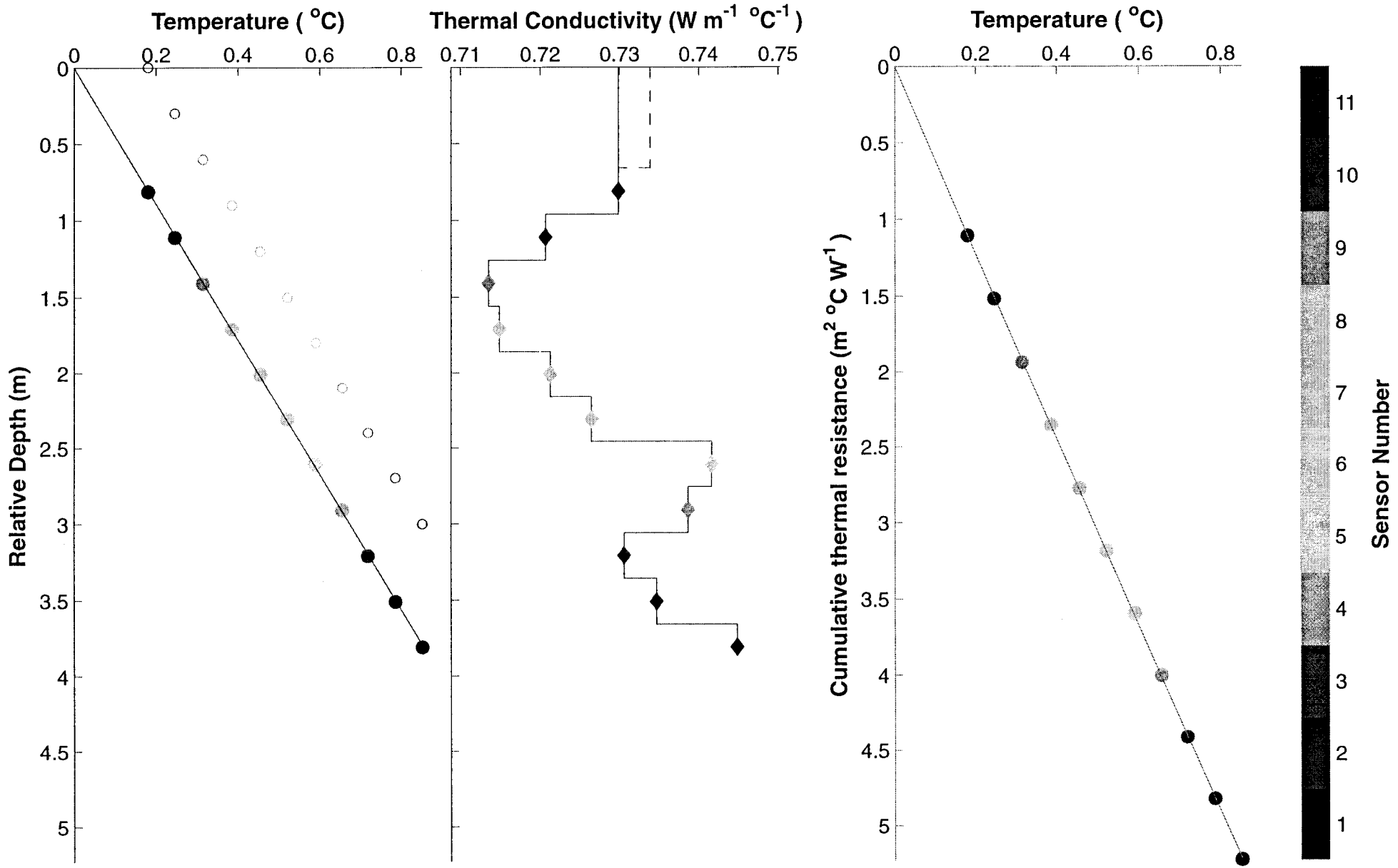
Temperature (°C)
Thermal Conductivity (W m-1 °C-1)
Relative Depth (m)
Gradient: 0.225 °C m-1
Depth of top sensor: 0.810 m
A
B
Temperature (°C)
Cumulative thermal resistance (m2 °C W-1)
Heat Flow: 0.163 W m-2
Shift: -0.006 m 2 °C W-1
C
Sensor Number
Trial: 1 - Iteration: 5
Processed: 18 May 2001 - 23:51
tf01h13a
Results: /home/afisher/ticoflux/pgc/pen/tf01h13a.res
Penetration: /home/afisher/ticoflux/pgc/pen/tf01h13a.pen

Figure IV-3

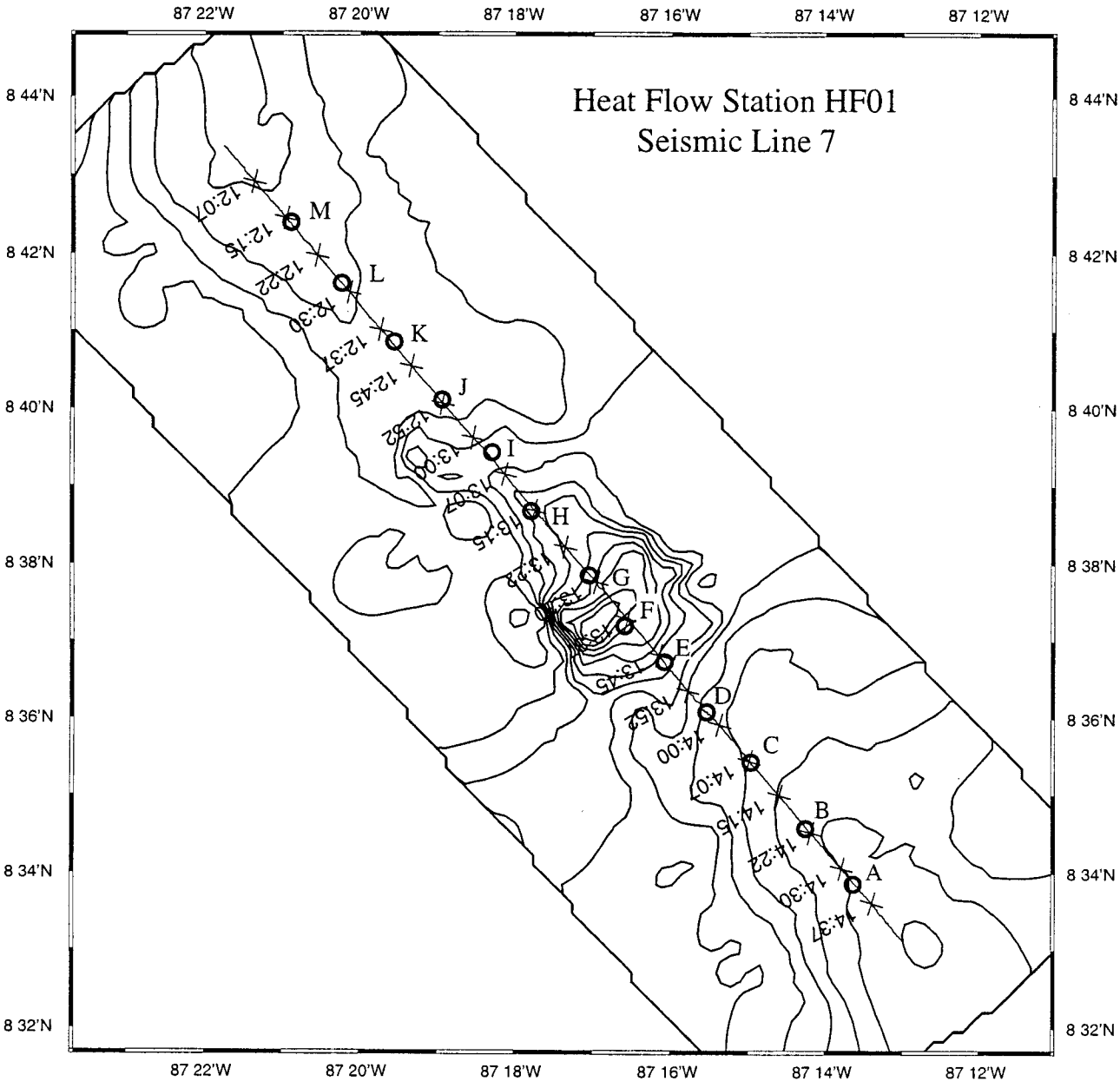
Heat Flow Station HF01
Seismic Line 7
87 22'W
87 20'W
87 18'W
87 16'W
87 14'W
87 12'W
8 44'N
8 42'N
8 40'N
8 38'N
8 36'N
8 34'N
8 32'N
M
L
K
J
I
H
G
F
E
D
C
B
A
12:07
12:15
12:22
12:30
12:37
12:45
12:52
13:00
13:07
13:15
13:22
13:30
13:37
13:45
13:52
14:00
14:07
14:15
14:22
14:30
14:37

Fig. IV-4

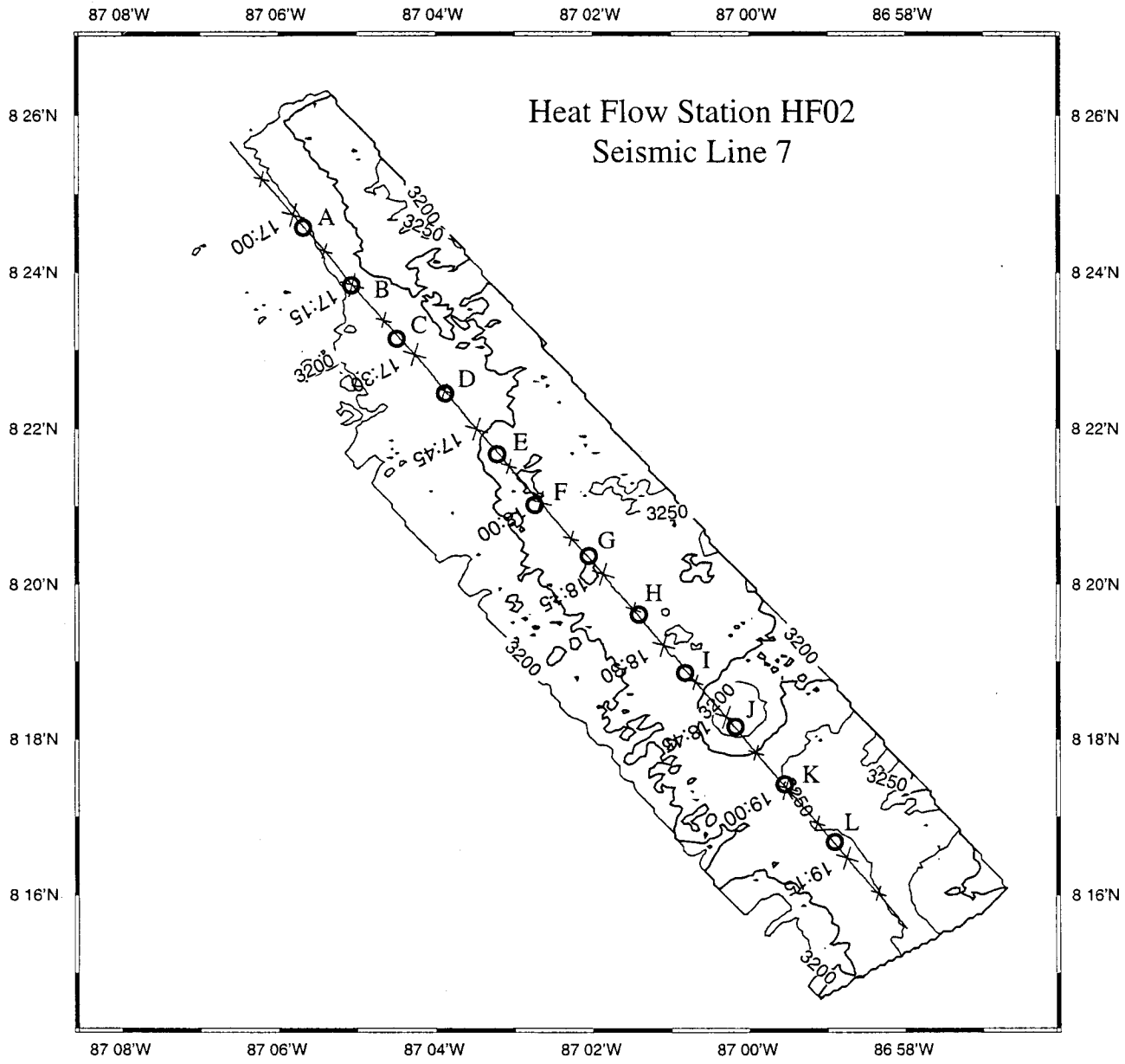
Heat Flow Station HF02
Seismic Line 7
87 08'W
87 06'W
87 04'W
87 02'W
87 00'W
86 58'W
8 26'N
8 24'N
8 22'N
8 20'N
8 18'N
8 16'N
A
B
C
D
E
F
G
H
I
J
K
L
17:00
17:15
17:30
17:45
18:00
18:15
18:30
18:45
19:00
19:15
3200
3250
3300

Fig. IV-5

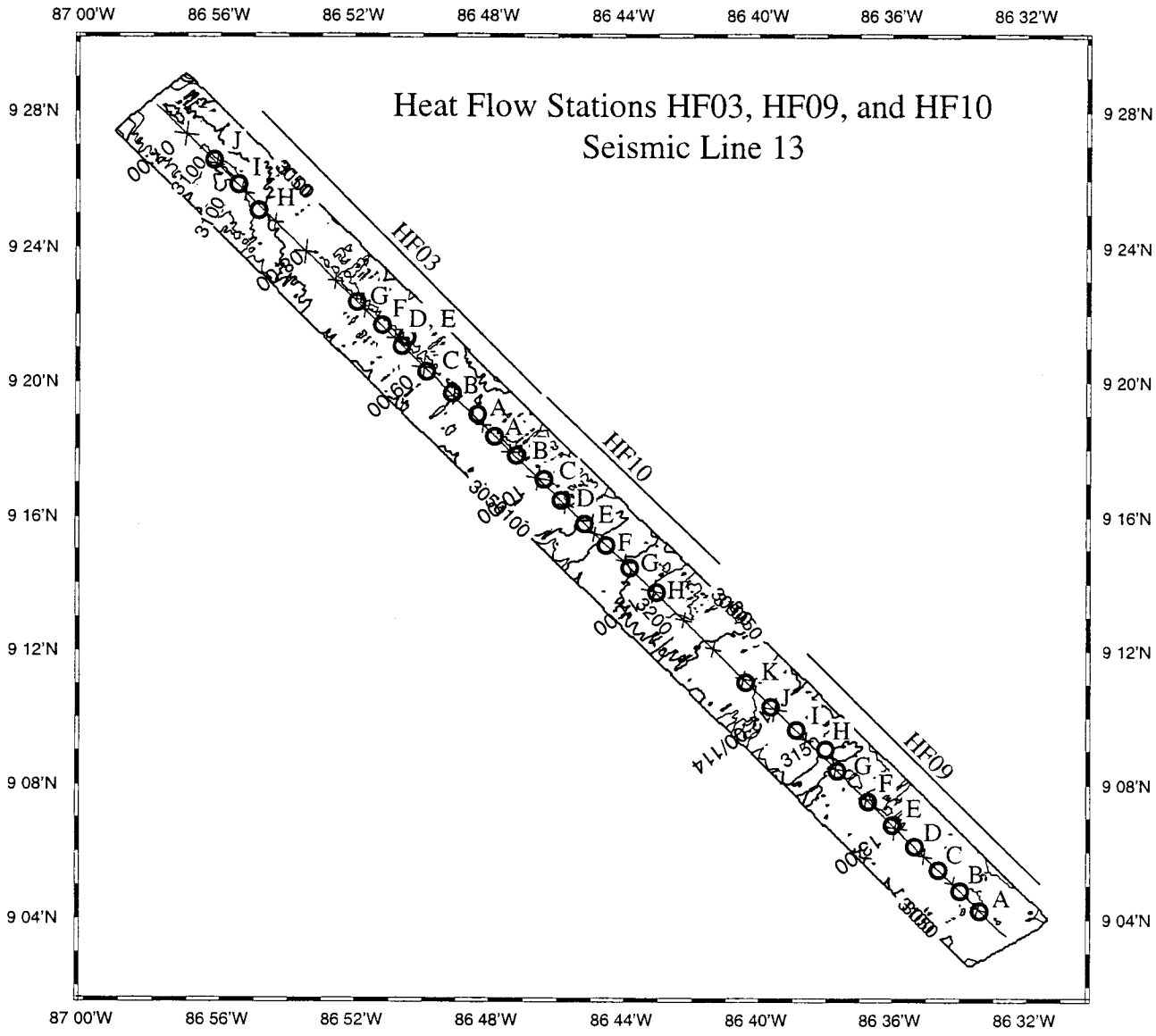
Heat Flow Stations HF03, HF09, and HF10
Seismic Line 13
HF03
HF10
HF09
87 00'W
86 56'W
86 52'W
86 48'W
86 44'W
86 40'W
86 36'W
86 32'W
9 28'N
9 24'N
9 20'N
9 16'N
9 12'N
9 08'N
9 04'N

Fig. IV-6

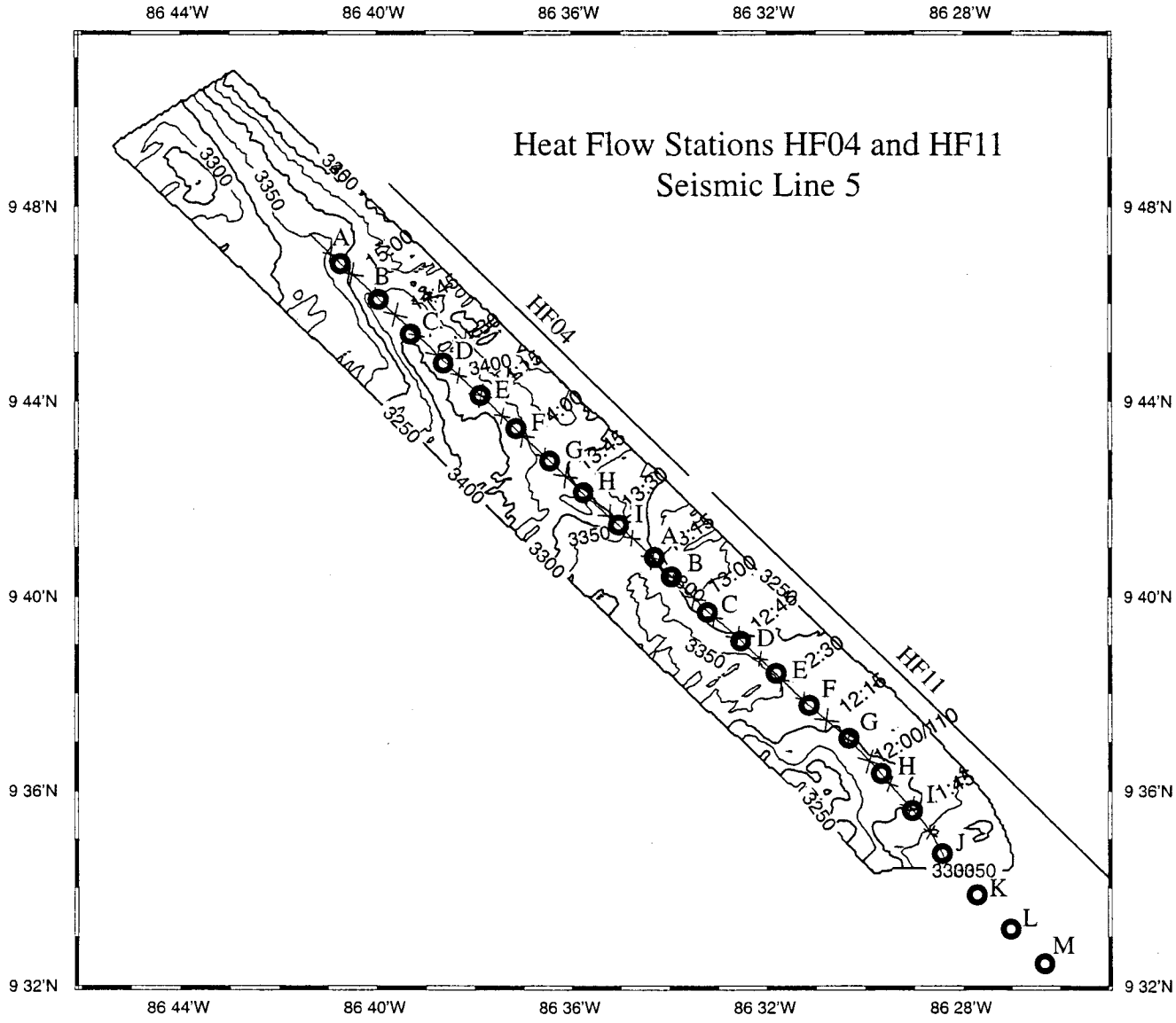
Heat Flow Stations HF04 and HF11
Seismic Line 5
86 44'W
86 40'W
86 36'W
86 32'W
86 28'W
9 48'N
9 44'N
9 40'N
9 36'N
9 32'N
HF04
HF11
A
B
C
D
E
F
G
H
I
J
K
L
M
3300
3350
3400
3250

Fig. IV-7

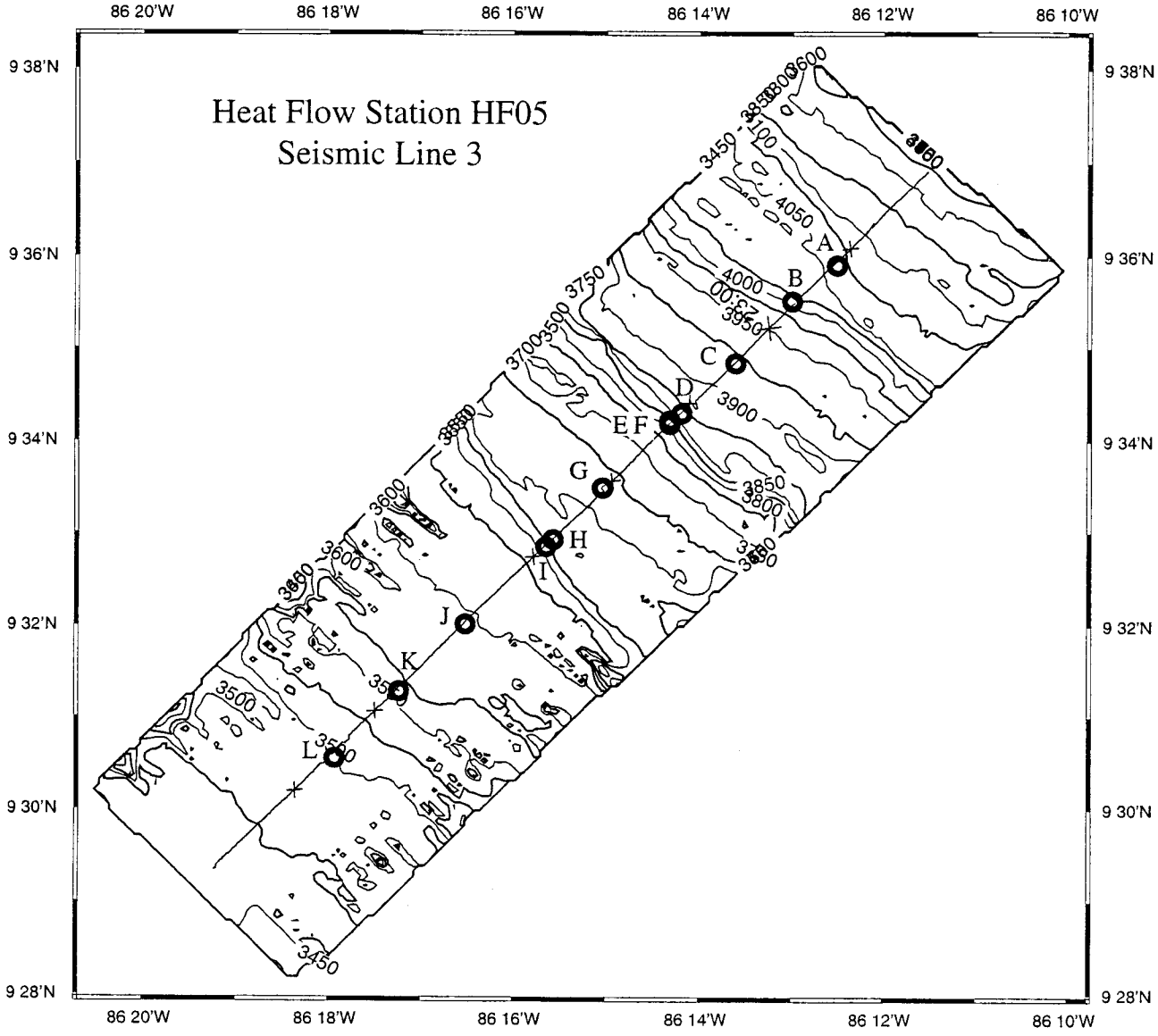
Heat Flow Station HF05
Seismic Line 3
86 20'W
86 18'W
86 16'W
86 14'W
86 12'W
86 10'W
9 38'N
9 36'N
9 34'N
9 32'N
9 30'N
9 28'N
A
B
C
D
E F
G
H
I
J
K
L
3450
3500
3550
3600
3650
3700
3750
3800
3850
3900
3950
4000
4050
4100

Fig. IV-8

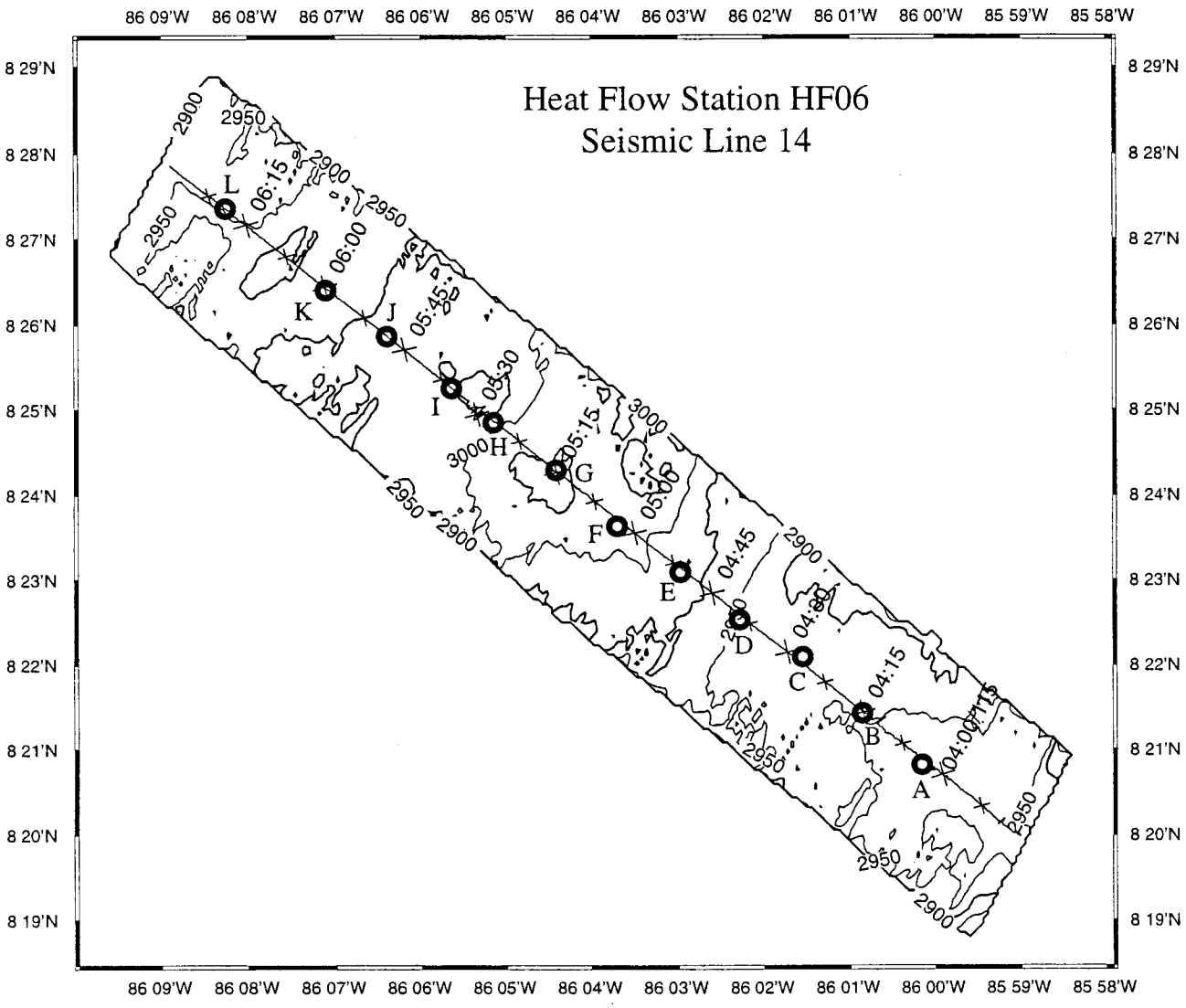
Heat Flow Station HF06
Seismic Line 14
86 09'W
86 08'W
86 07'W
86 06'W
86 05'W
86 04'W
86 03'W
86 02'W
86 01'W
86 00'W
85 59'W
85 58'W
8 29'N
8 28'N
8 27'N
8 26'N
8 25'N
8 24'N
8 23'N
8 22'N
8 21'N
8 20'N
8 19'N
L
K
J
I
H
G
F
E
D
C
B
A
06:15
06:00
05:45
05:30
05:15
05:00
04:45
04:30
04:15
04:00
2900
2950
3000

Fig. IV-9

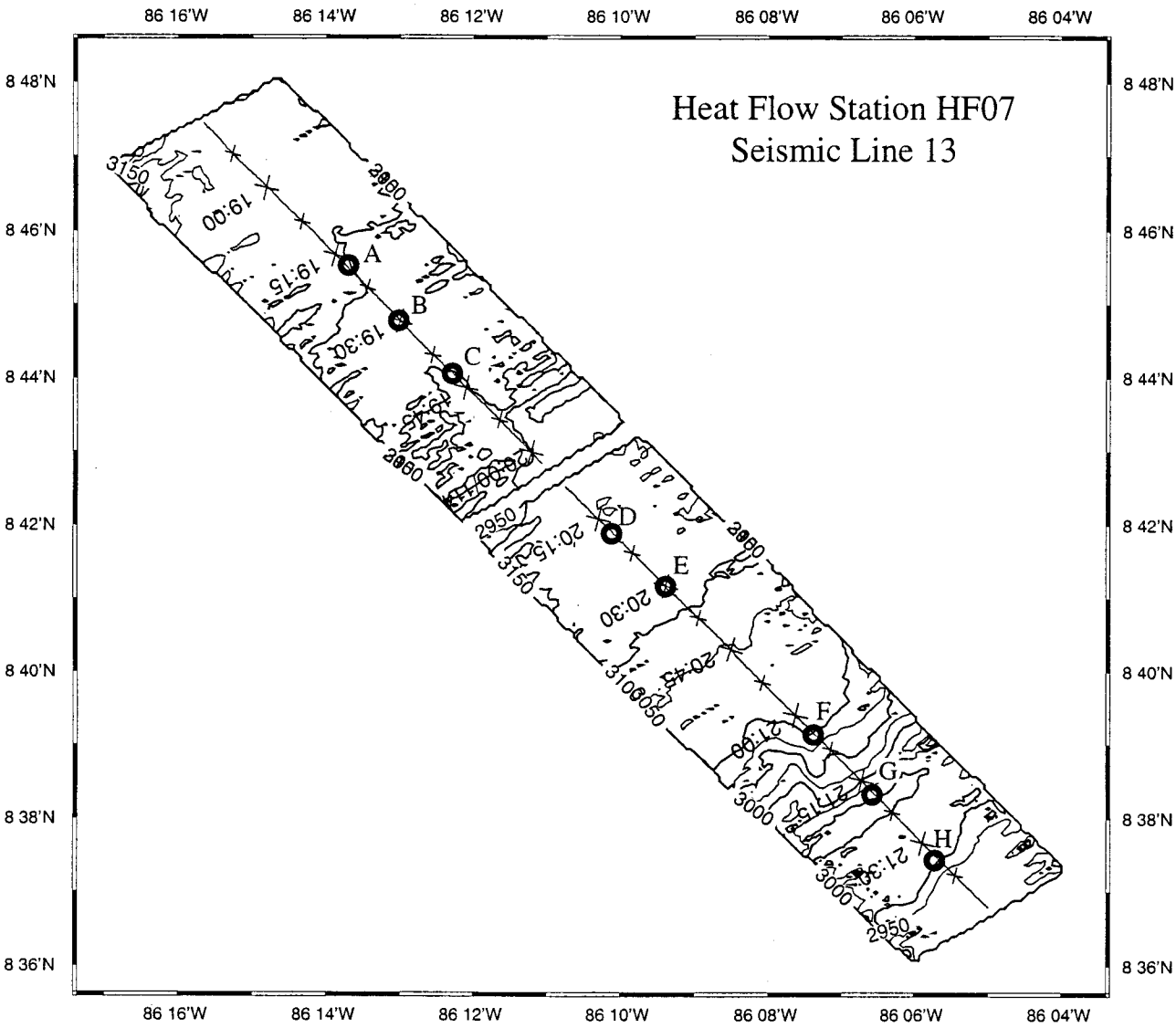
Heat Flow Station HF07
Seismic Line 13
86 16'W
86 14'W
86 12'W
86 10'W
86 08'W
86 06'W
86 04'W
8 48'N
8 46'N
8 44'N
8 42'N
8 40'N
8 38'N
8 36'N
A
B
C
D
E
F
G
H
19:00
19:15
19:30
20:15
20:30
20:45
21:00
21:15
21:30
2950
2980
3000
3050
3100
3150

Fig. IV-10

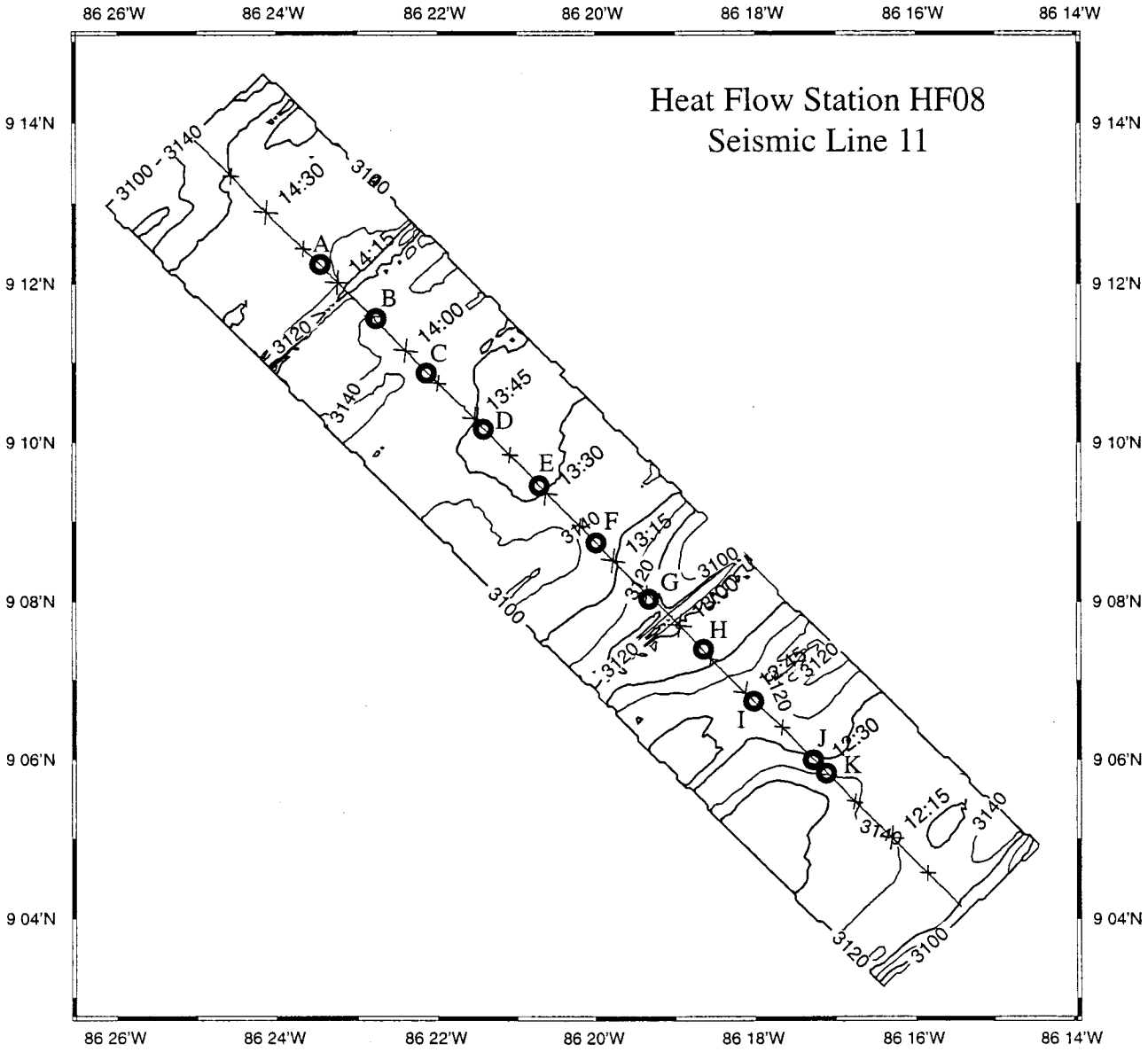
Heat Flow Station HF08
Seismic Line 11
86 26'W
86 24'W
86 22'W
86 20'W
86 18'W
86 16'W
86 14'W
9 14'N
9 12'N
9 10'N
9 08'N
9 06'N
9 04'N
A
B
C
D
E
F
G
H
I
J
K
14:30
14:15
14:00
13:45
13:30
13:15
12:30
12:15
3100
3120
3140

Fig. IV-11

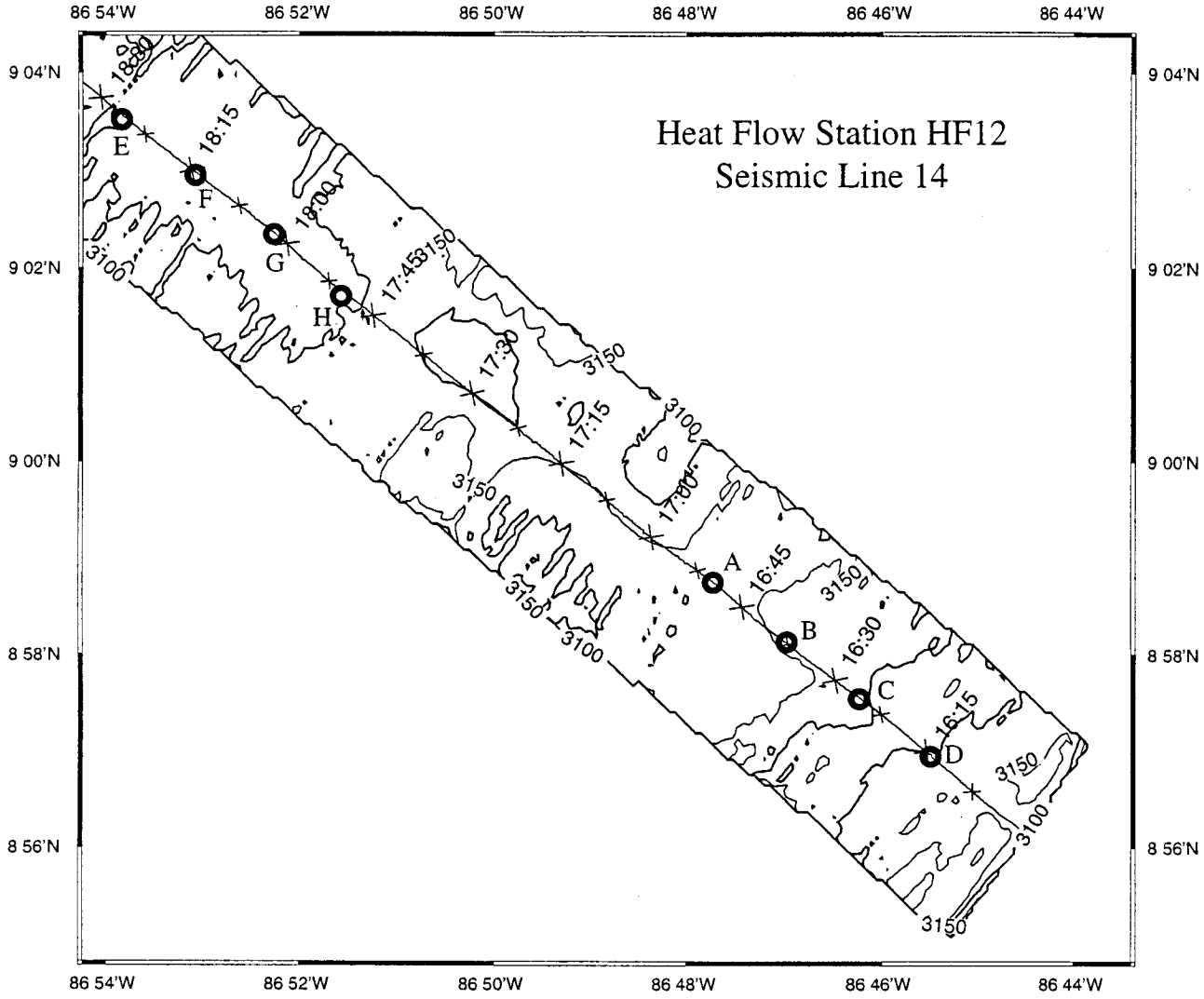
Heat Flow Station HF12
Seismic Line 14
86 54'W
86 52'W
86 50'W
86 48'W
86 46'W
86 44'W
9 04'N
9 02'N
9 00'N
8 58'N
8 56'N
E
F
G
H
A
B
C
D
18:15
18:00
17:45
17:30
17:15
17:00
16:45
16:30
16:15
3100
3150

Fig. IV-12

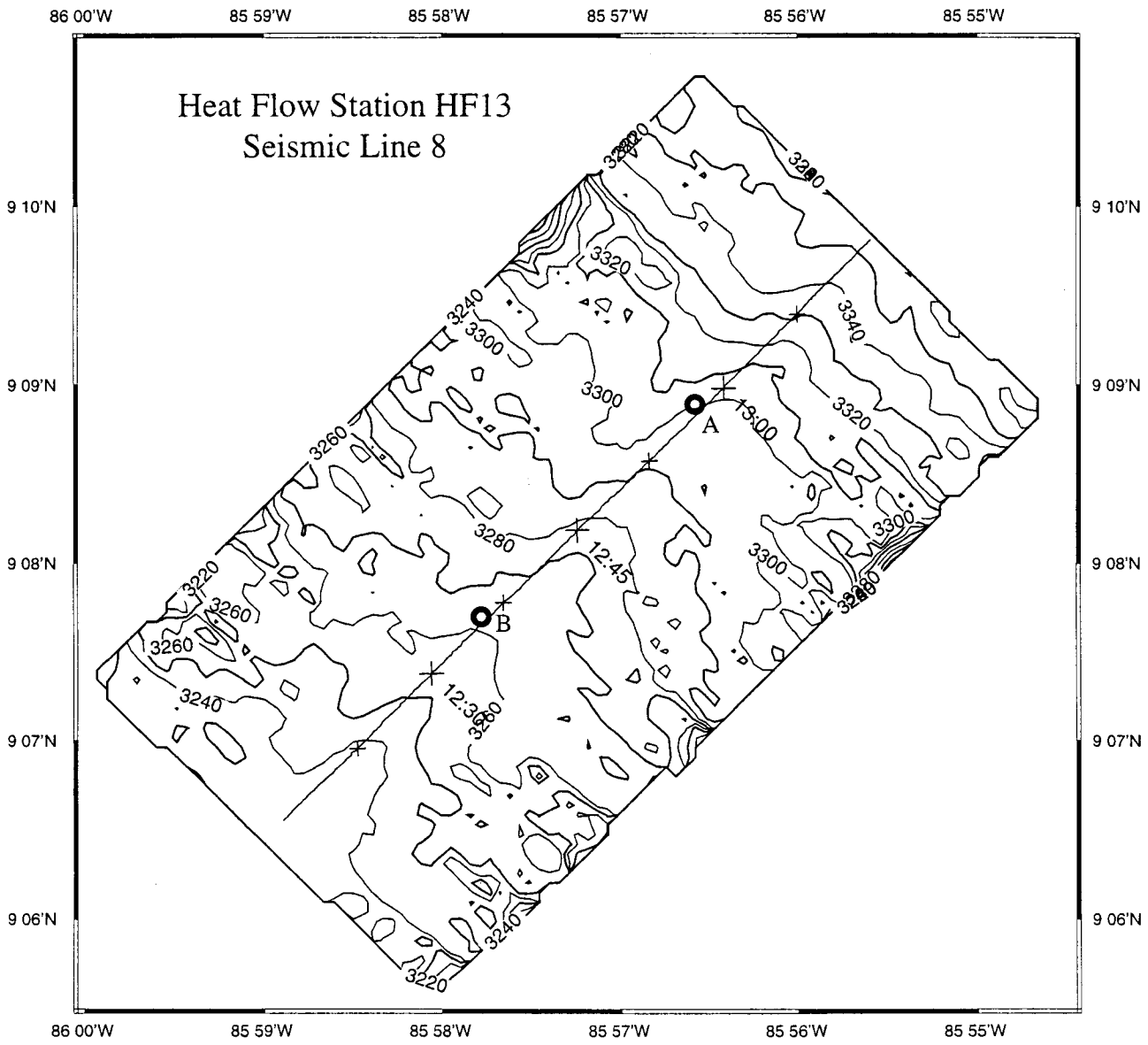
Heat Flow Station HF13
Seismic Line 8
86 00'W
85 59'W
85 58'W
85 57'W
85 56'W
85 55'W
9 10'N
9 09'N
9 08'N
9 07'N
9 06'N
A
B
12:45
3:00
12:30
3220
3240
3260
3280
3300
3320
3340

Fig. IV-13

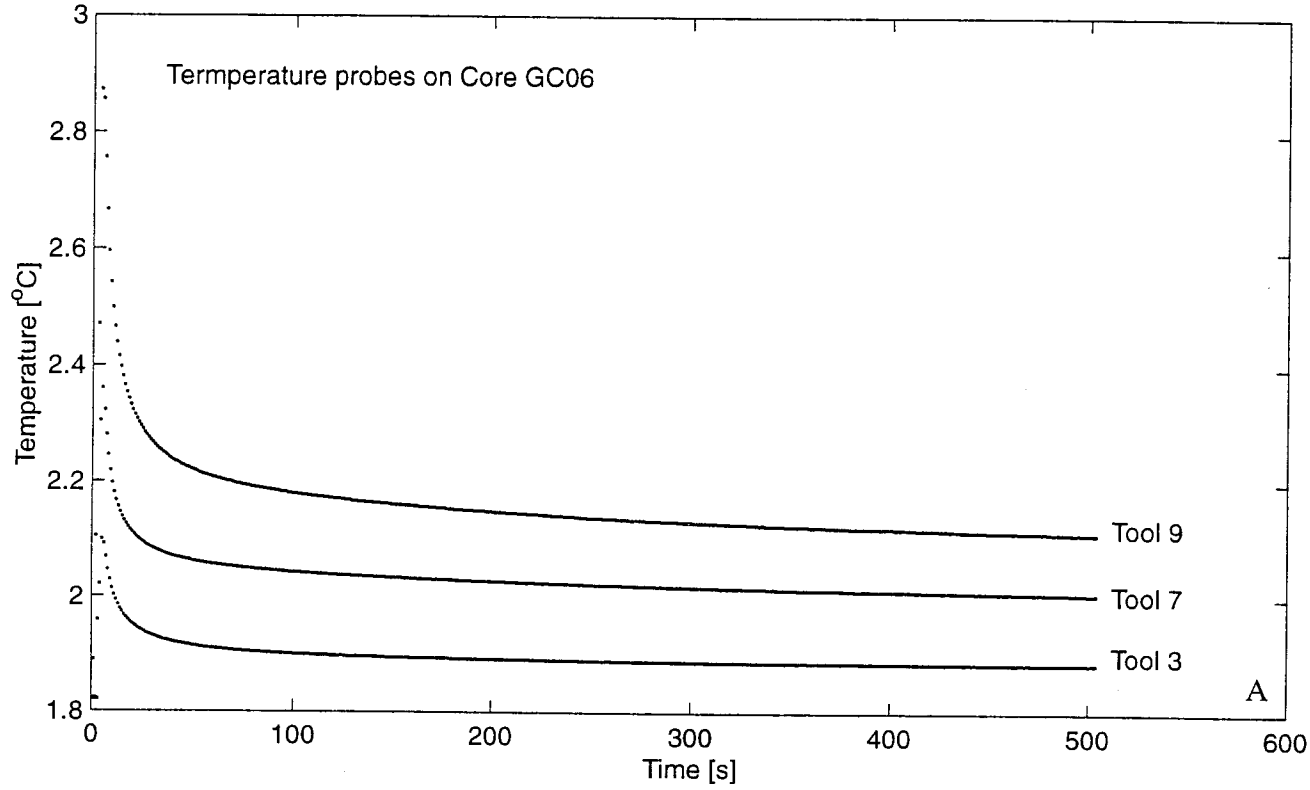
Termperature probes on Core GC06
Temperature [°C]
Time [s]
Tool 9
Tool 7
Tool 3
A
3
2.8
2.6
2.4
2.2
2
1.8
0
100
200
300
400
500
600

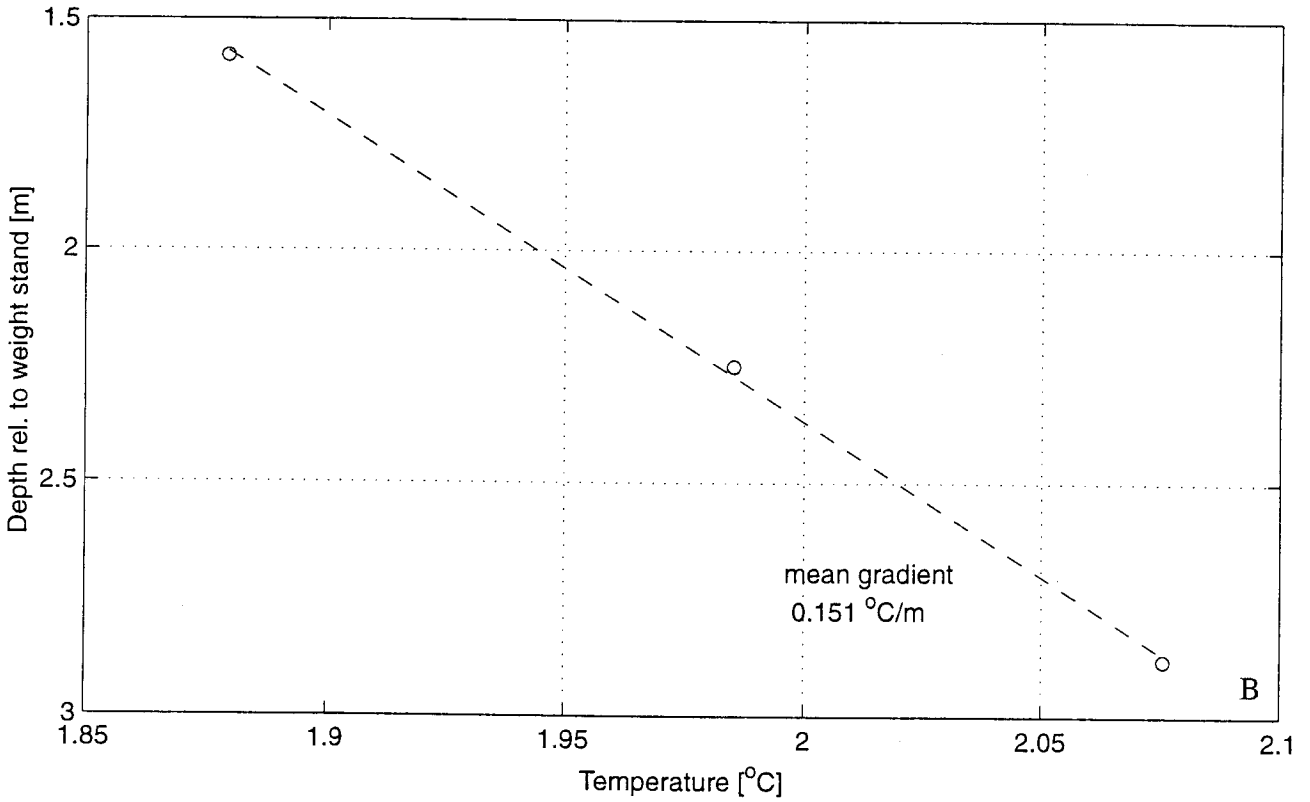
Depth rel. to weight stand [m]
Temperature [°C]
mean gradient
0.151 °C/m
B
1.5
2
2.5
3
1.85
1.9
1.95
2
2.05
2.1

Figure IV-14

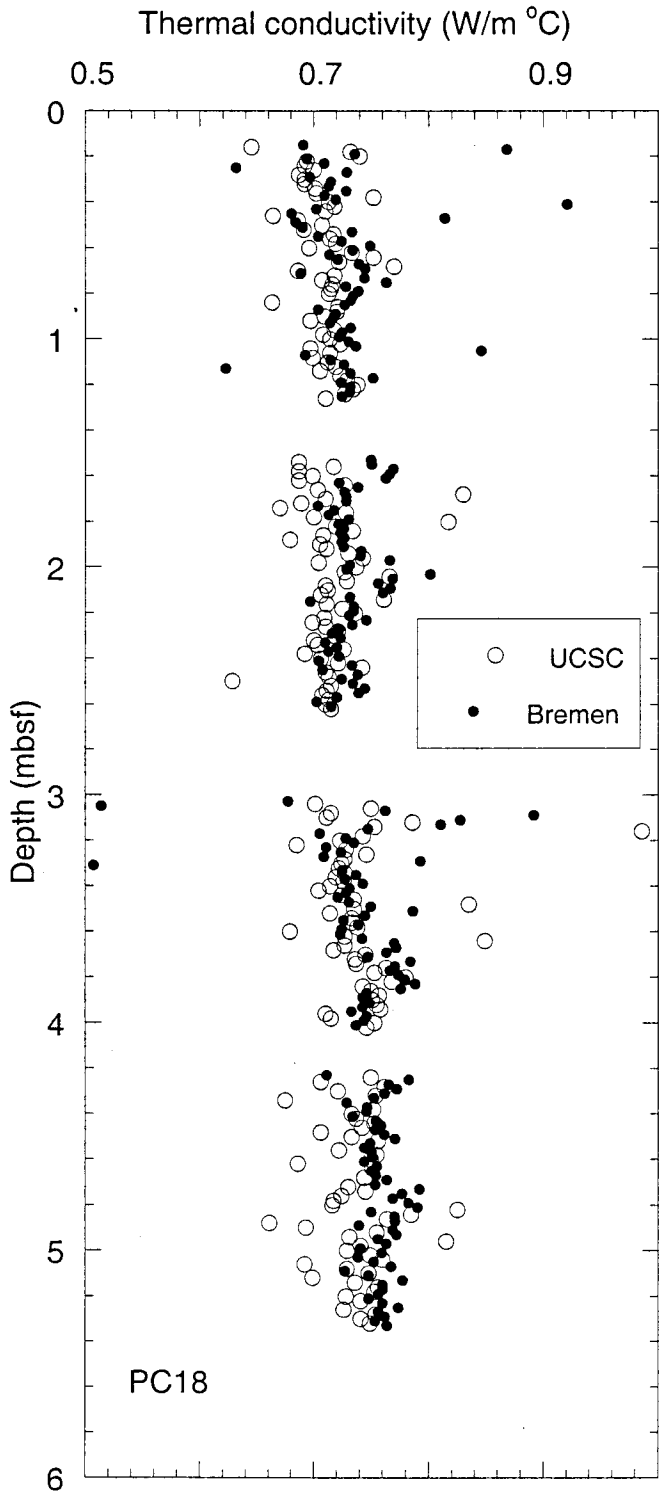
Thermal conductivity (W/m °C)
0.5
0.7
0.9
0
1
2
3
4
5
6
Depth (mbsf)
UCSC
Bremen
PC18

Figure IV-15

Table V-1. Summary of core types, locations, times and recovery.

Core ID Core	Sizeand type	ime in botto		Recovered	Number of	Porewater	Latitude (N)		Longitude (W)	
	Type	J. Day	GMT Time	length (cm)	sections	samples	Degrees	Minutes	Degrees	Minutes
EW0104-01GC	2.5" Gravity	106	1605	231	2	10	7	51.603	85	16.390
EW0104-O2GC	2.5" Gravity	116	1503	310	2	12	8	37.424	87	16.621
EW0104-03GC	2.5" Gravity	116	1844	<1	0	0	8	37.136	87	16.837
EW0104-04GC	2.5" Gravity	116	2157	0	0	0	8	37.149	87	16.984
EW0104-05GC	2.5" Gravity	117	0052	122	1	6	8	37.441	87	16.800
EW0104-06GC	2.5" Gravity	118	0739	0	0	0	8	44.485	87	12.797
EW0104-07GC	2.5" Gravity	118	1036	0	0	0	8	44.345	87	12.641
EW0104-08GC	4" Gravity	118	1345	16	1	2	8	44.245	87	12.484
EW0104-09GC	2.5" Gravity	118	1714	297	2	13	8	44.519	87	12.820
EW0104-10GC	2.5" Gravity	119	0459	293	2	12	9	26.184	86	55.921
EW0104-11GC	2.5" Gravity	119	0800	317	2	10	9	26.147	86	55.990
EW0104-12GC	2.5" Gravity	119	3038	285	2	10	9	28.847	86	59.797
EW0104-13GC	2.5" Gravity	119	1329	300	2	10	9	28.873	86	59.781
EW0104-14GC	2.5" Gravity	121	2106	305	2	10	9	28.278	86	59.673
EW0104-15GC	2.5" Gravity	122	0000	322	2	10	9	28.259	86	59.847
EW0104-16GC	2.5" Gravity	122	0316	320	2	10	9	28.443	86	59.752
EW0104-17GC	2.5" Gravity	122	0618	248	2	8	9	28.555	86	59.621
EW0104-18PC	4" Piston	123	0652	891	7	17	9	40.573	86	34.124
EW0104-18GC	4" Gravity	123	0652	212	2	8	9	40.573	86	34.124
EW0104-19PC	4" Piston	123	1414	558	4	4	9	40.608	86	33.676
EW0104-19GC	4" Gravity	123	1414	190	2	9	9	40.608	86	33.676
EW0104-20GC	2.5" Gravity	125	1337	275	2	8	8	30.935	85	59.199
EW0104-21GC	2.5" Gravity	125	1639	258	2	8	8	30.360	85	58.587
EW0104-22GC	2.5" Gravity	125	1944	185	2	8	8	30.086	85	58.308
EW0104-23GC	2.5" Gravity	125	2234	317	2	8	8	29.797	85	58.022
EW0104-24GC	2.5" Gravity	127	0814	187	2	8	8	15.323	86	14.589
EW0104-25GC	2.5" Gravity	127	1106	52	1	2	8	15.319	86	14.553
EW0104-26GC	2.5" Gravity	127	1405	347	3	10	8	14.575	86	13.930
EW0104-27GC	2.5" Gravity	127	1717	274	2	8	8	14.599	86	13.938
EW0104-28GC	2.5" Gravity	129	0415	55	1	3	8	34.821	85	46.675
EW0104-29GC	2.5" Gravity	129	0654	50	1	1	8	34.876	85	46.653
EW0104-30GC	2.5" Gravity	129	1027	40	1	2	8	34.369	85	47.478
EW0104-31GC	2.5" Gravity	129	1257	10	1	0	8	34.479	85	47.554
EW0104-32GC	2.5" Gravity	130	2213	0	0	0	9	16.655	86	13.390
EW0104-33GC	2.5" Gravity	131	0148	59	1	3	9	16.107	86	13.821
EW0104-34GC	2.5" Gravity	131	0451	218	2	8	9	15.008	86	15.019
EW0104-35GC	2.5" Gravity	131	0834	304	2	8	9	13.555	86	18.699
EW0104-36PC	4" Piston	132	1501	641	5	16	8	56.250	86	40.953
EW0104-36GC	4" Gravity	132	1501	98	1	6	8	56.250	86	40.953
EW0104-37PC	4" Piston	132	2112	774	6	19	8	56.453	86	41.110
EW0104-37GC	4" Gravity	132	2112	27	1	2	8	56.453	86	41.110
EW0104-38PC	4" Piston	134	0056	798	6	19	9	40.588	86	34.132
EW0104-38GC	4" Gravity	134	0000	208	2	7	9	40.588	86	34.132
EW0104-39PC	4" Piston	134	0719	788	6	19	9	40.571	86	34.154
EW0104-39GC	4" Gravity	134	0719	243	2	6	9	40.571	86	34.154
EW0104-40GC	2.5" Gravity	135	1808	237	2	8	9	8.103	86	54.591
EW0104-41GC	2.5" Gravity	135	2049	133	1	6	9	7.784	86	54.376
EW0104-42GC	2.5" Gravity	136	0000	14	1	0	9	7.521	86	54.286
EW0104-43GC	2.5" Gravity	136	0305	302	2	8	9	8.144	86	54.845

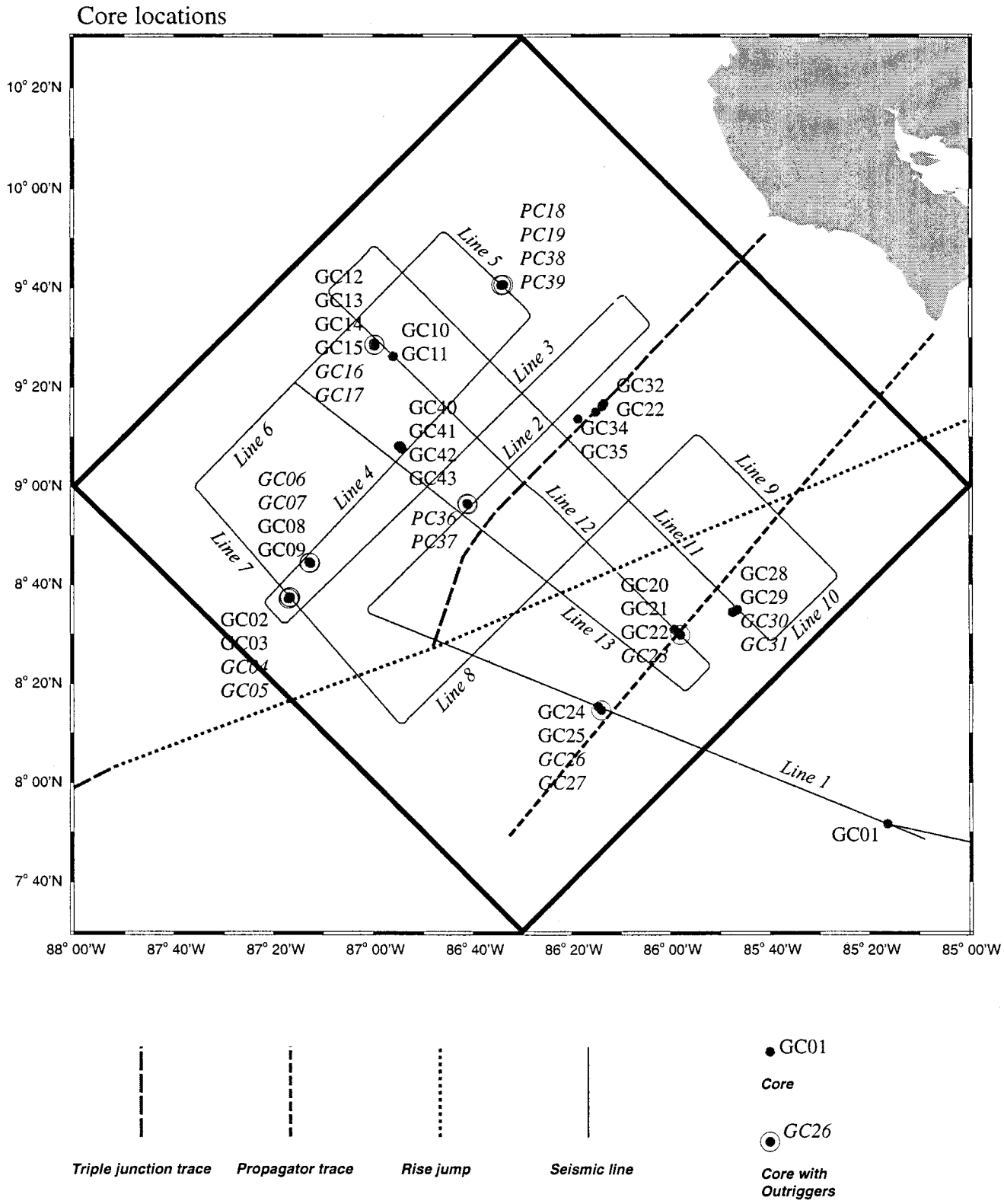
Core locations
10° 20'N
10° 00'N
9° 40'N
9° 20'N
9° 00'N
8° 40'N
8° 20'N
8° 00'N
7° 40'N
88° 00'W
87° 40'W
87° 20'W
87° 00'W
86° 40'W
86° 20'W
86° 00'W
85° 40'W
85° 20'W
85° 00'W
PC18
PC19
PC38
PC39
Line 5
GC12
GC13
GC14
GC15
GC16
GC17
GC10
GC11
Line 3
GC32
GC22
GC34
GC35
Line 6
Line 4
Line 2
GC40
GC41
GC42
GC43
GC06
GC07
GC08
GC09
Line 7
PC36
PC37
Line 12
Line 9
Line 11
GC20
GC21
GC22
GC23
GC28
GC29
GC30
GC31
Line 10
Line 13
GC02
GC03
GC04
GC05
Line 8
GC24
GC25
GC26
GC27
Line 1
GC01
Triple junction trace
Propagator trace
Rise jump
Seismic line
GC01
Core
GC26
Core with Outriggers

Figure V-1

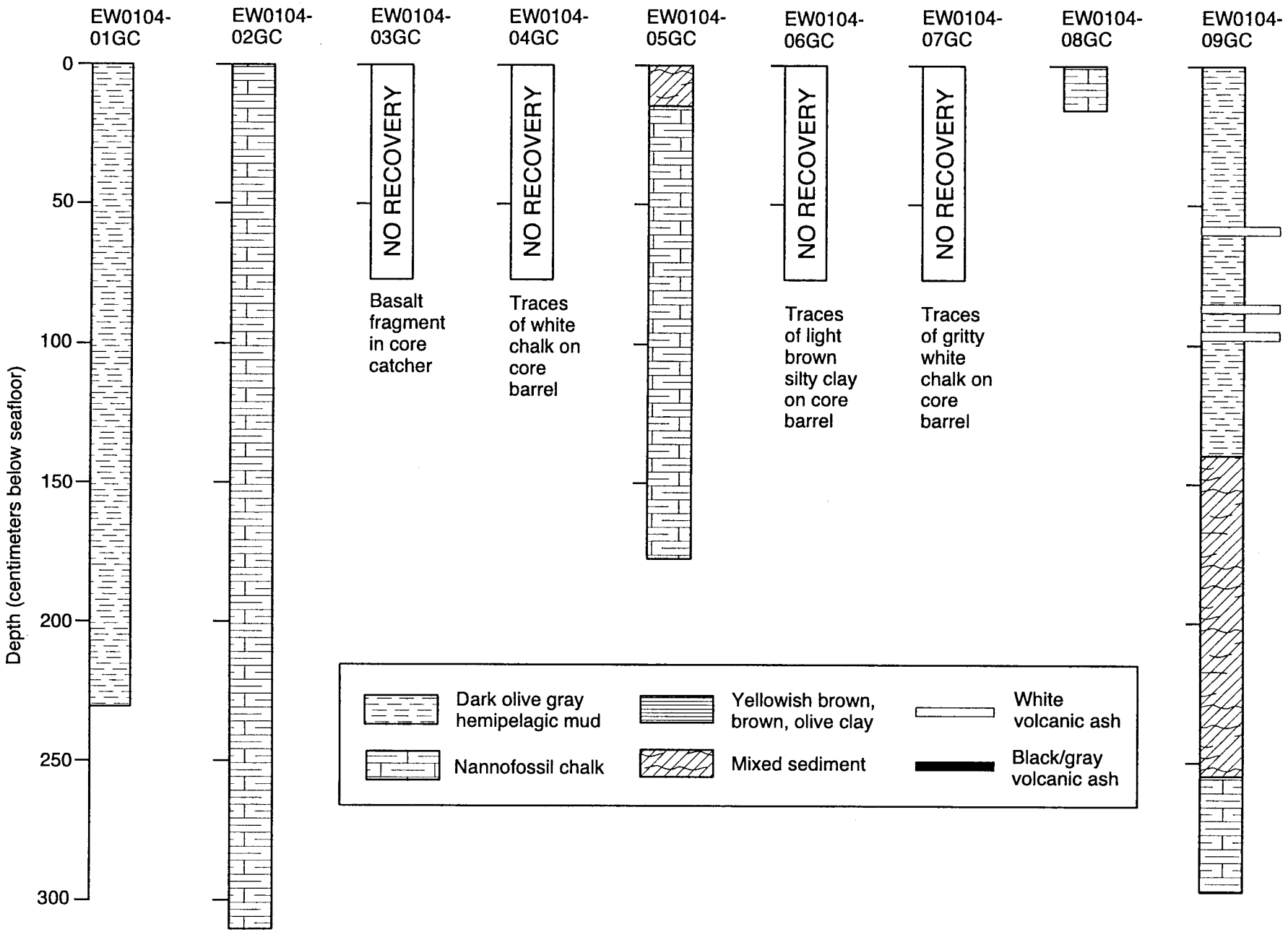
EW0104-01GC
EW0104-02GC
EW0104-03GC
EW0104-04GC
EW0104-05GC
EW0104-06GC
EW0104-07GC
EW0104-08GC
EW0104-09GC
Depth (centimeters below seafloor)
0
50
100
150
200
250
300
NO RECOVERY
NO RECOVERY
NO RECOVERY
Basalt fragment in core catcher
Traces of white chalk on core barrel
Traces of light brown silty clay on core barrel
Traces of gritty white chalk on core barrel
Dark olive gray hemipelagic mud
Nannofossil chalk
Yellowish brown, brown, olive clay
Mixed sediment
White volcanic ash
Black/gray volcanic ash

Figure V-2

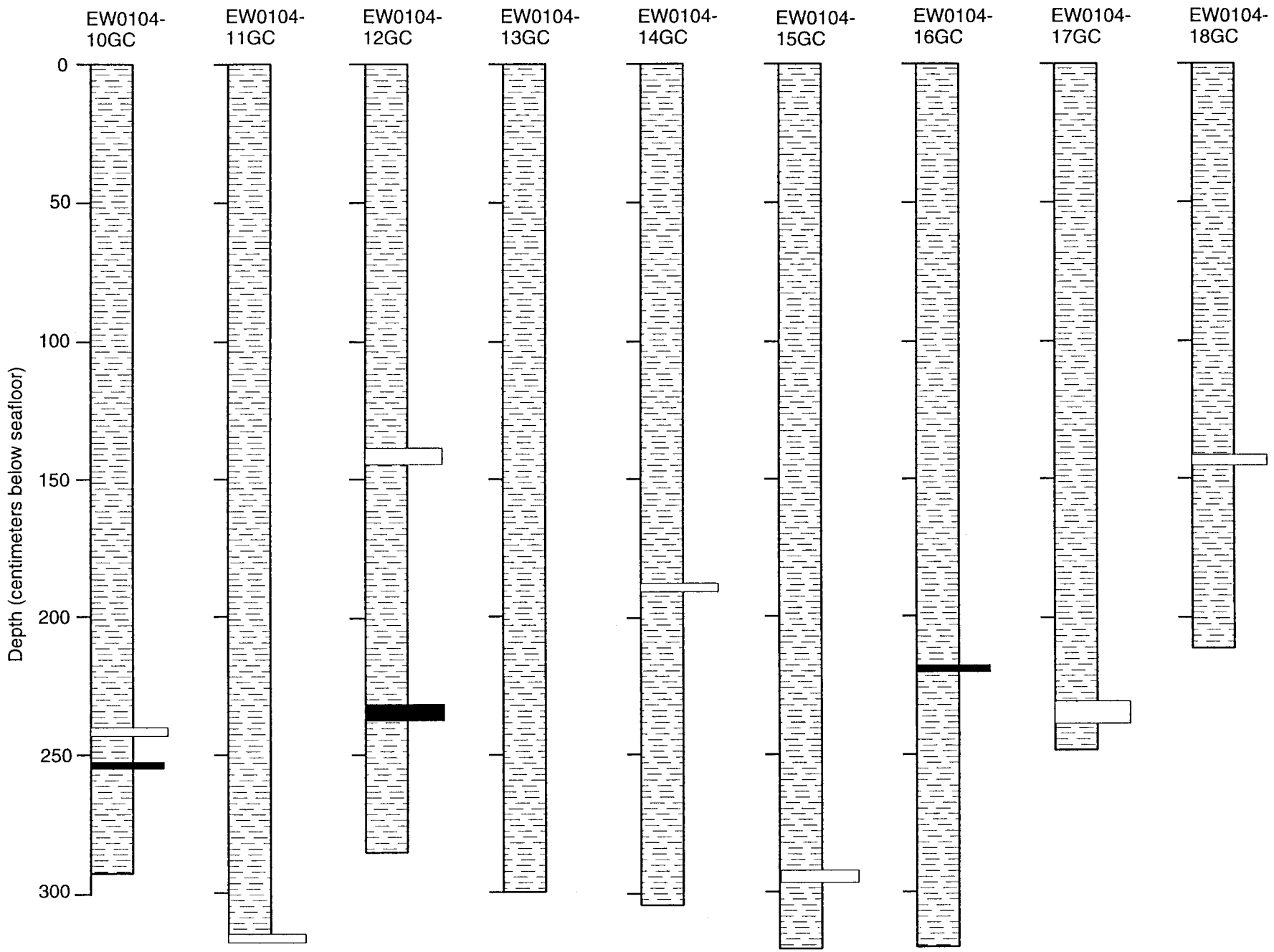
EW0104-10GC
EW0104-11GC
EW0104-12GC
EW0104-13GC
EW0104-14GC
EW0104-15GC
EW0104-16GC
EW0104-17GC
EW0104-18GC
Depth (centimeters below seafloor)
0
50
100
150
200
250
300

Figure V-3

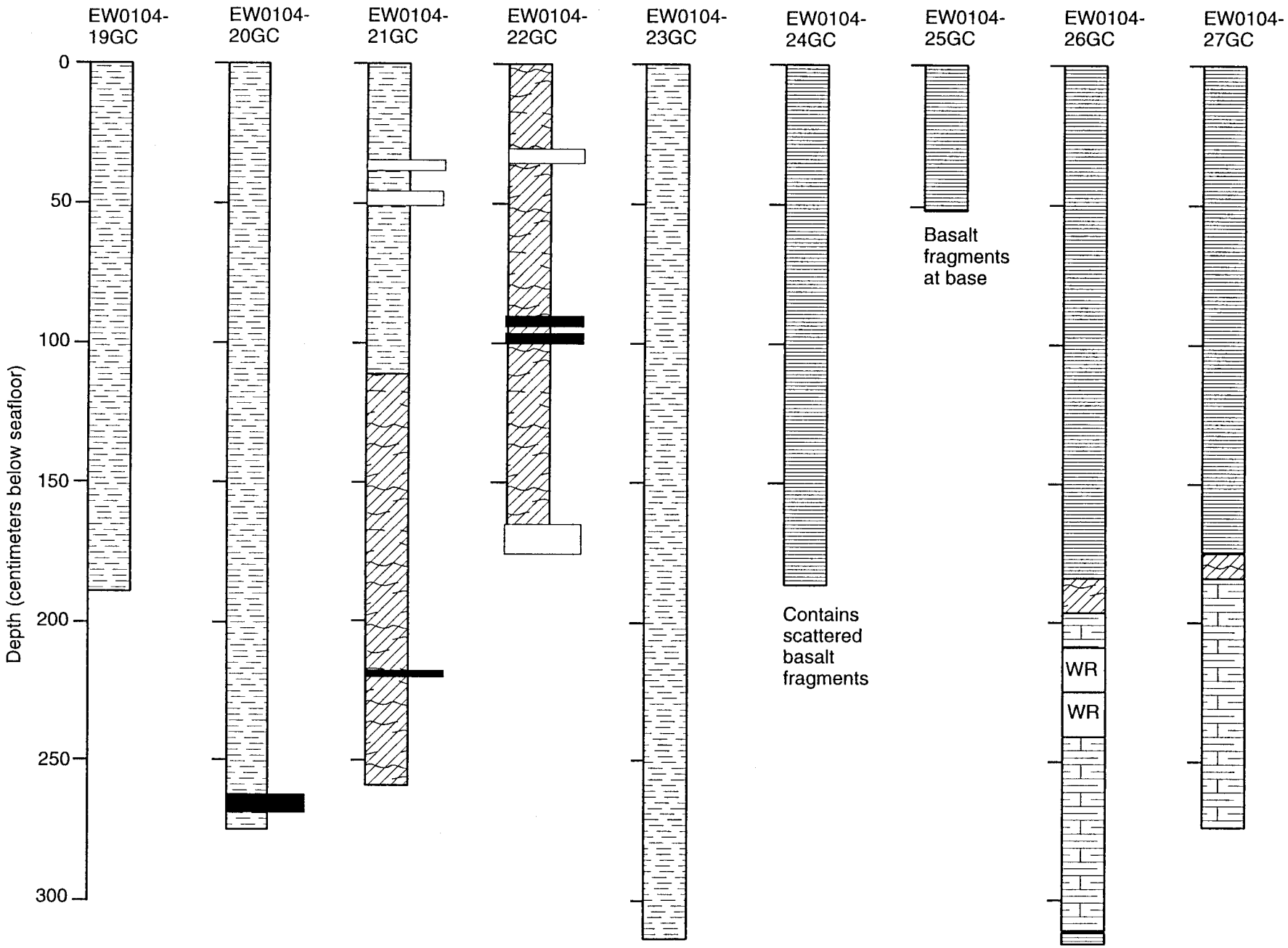
EW0104-19GC
EW0104-20GC
EW0104-21GC
EW0104-22GC
EW0104-23GC
EW0104-24GC
EW0104-25GC
EW0104-26GC
EW0104-27GC
Depth (centimeters below seafloor)
0
50
100
150
200
250
300
Basalt fragments at base
Contains scattered basalt fragments
WR
WR

Figure V-4

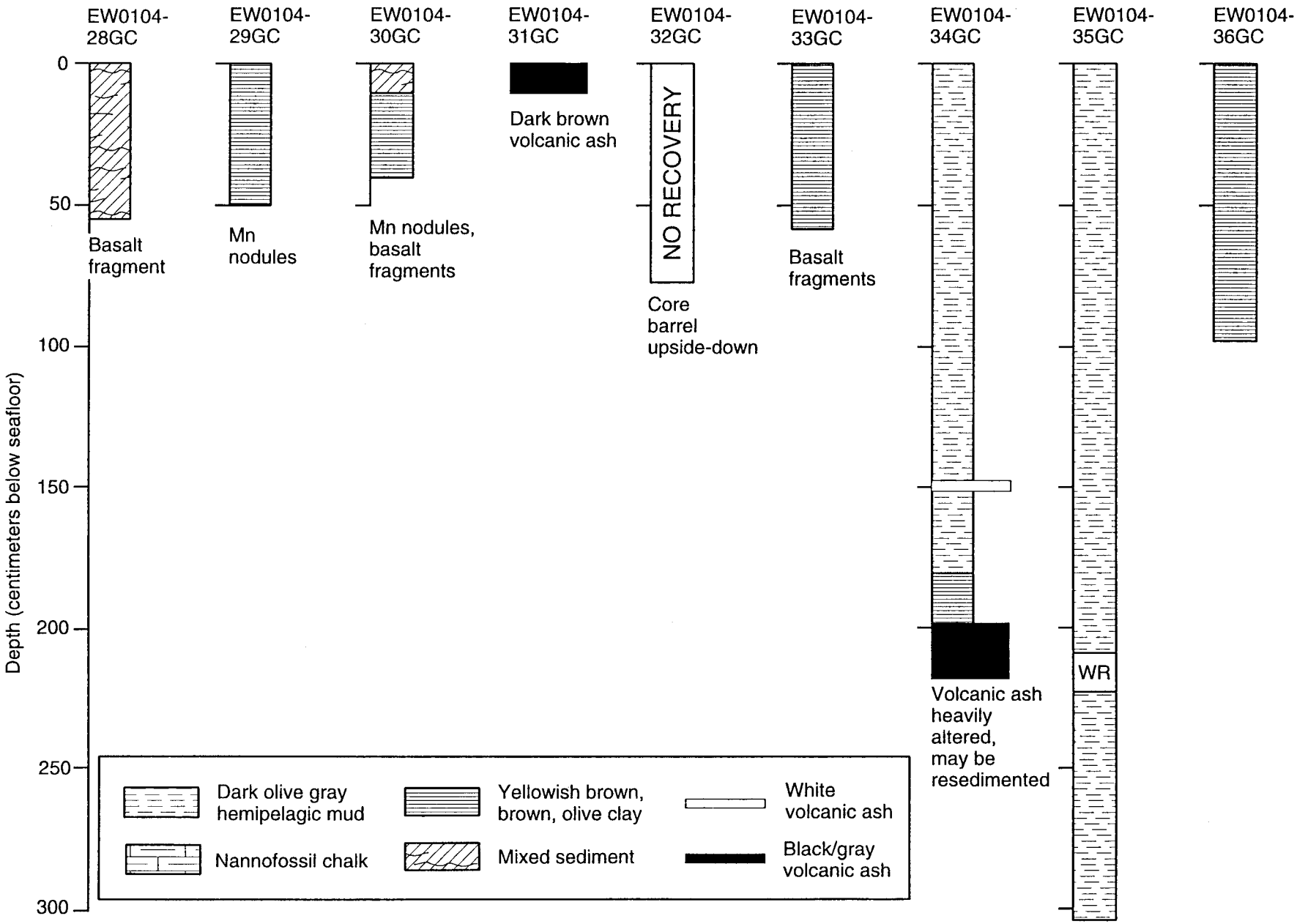
EW0104-28GC
EW0104-29GC
EW0104-30GC
EW0104-31GC
EW0104-32GC
EW0104-33GC
EW0104-34GC
EW0104-35GC
EW0104-36GC
Depth (centimeters below seafloor)
0
50
100
150
200
250
300
Basalt fragment
Mn nodules
Mn nodules, basalt fragments
Dark brown volcanic ash
NO RECOVERY
Core barrel upside-down
Basalt fragments
Volcanic ash heavily altered, may be resedimented
WR
Dark olive gray hemipelagic mud
Nannofossil chalk
Yellowish brown, brown, olive clay
Mixed sediment
White volcanic ash
Black/gray volcanic ash

Figure V-5

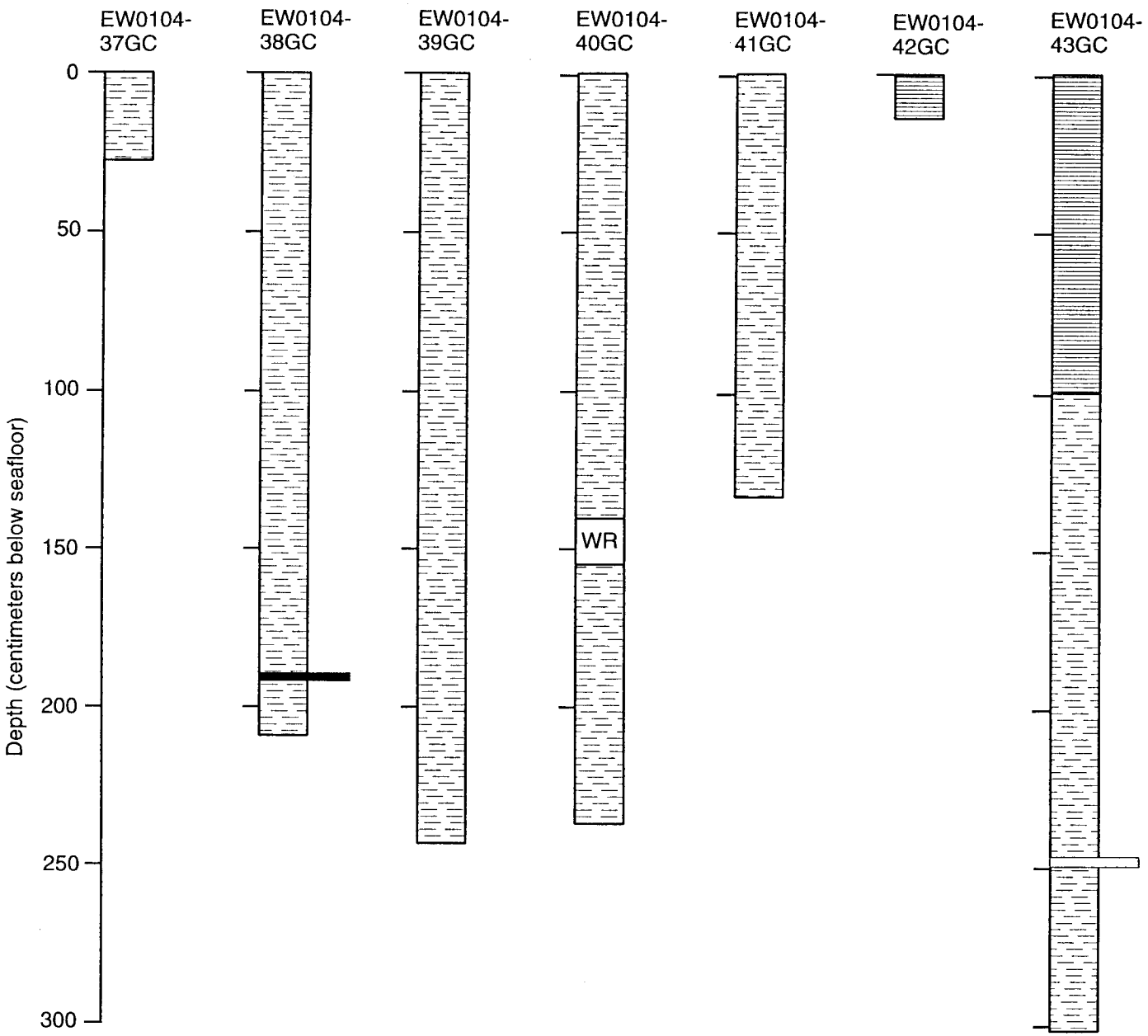
EW0104-37GC
EW0104-38GC
EW0104-39GC
EW0104-40GC
EW0104-41GC
EW0104-42GC
EW0104-43GC
0
50
100
150
200
250
300
Depth (centimeters below seafloor)
WR

Figure V-6

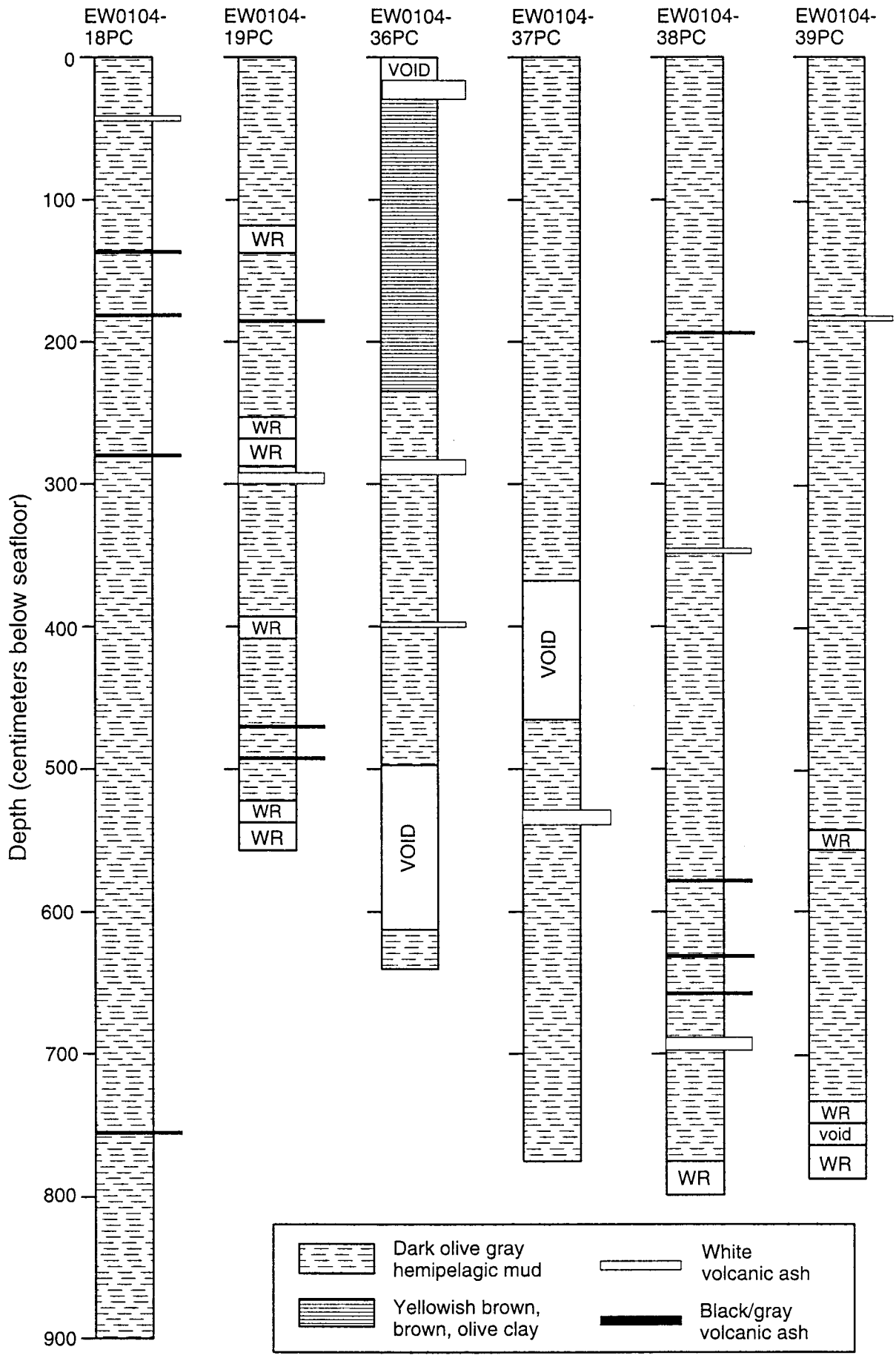
EW0104-18PC
EW0104-19PC
EW0104-36PC
EW0104-37PC
EW0104-38PC
EW0104-39PC
Depth (centimeters below seafloor)
0
100
200
300
400
500
600
700
800
900
VOID
WR
WR
WR
WR
WR
VOID
VOID
WR
WR
void
WR
Dark olive gray hemipelagic mud
Yellowish brown, brown, olive clay
White volcanic ash
Black/gray volcanic ash

Figure V-7

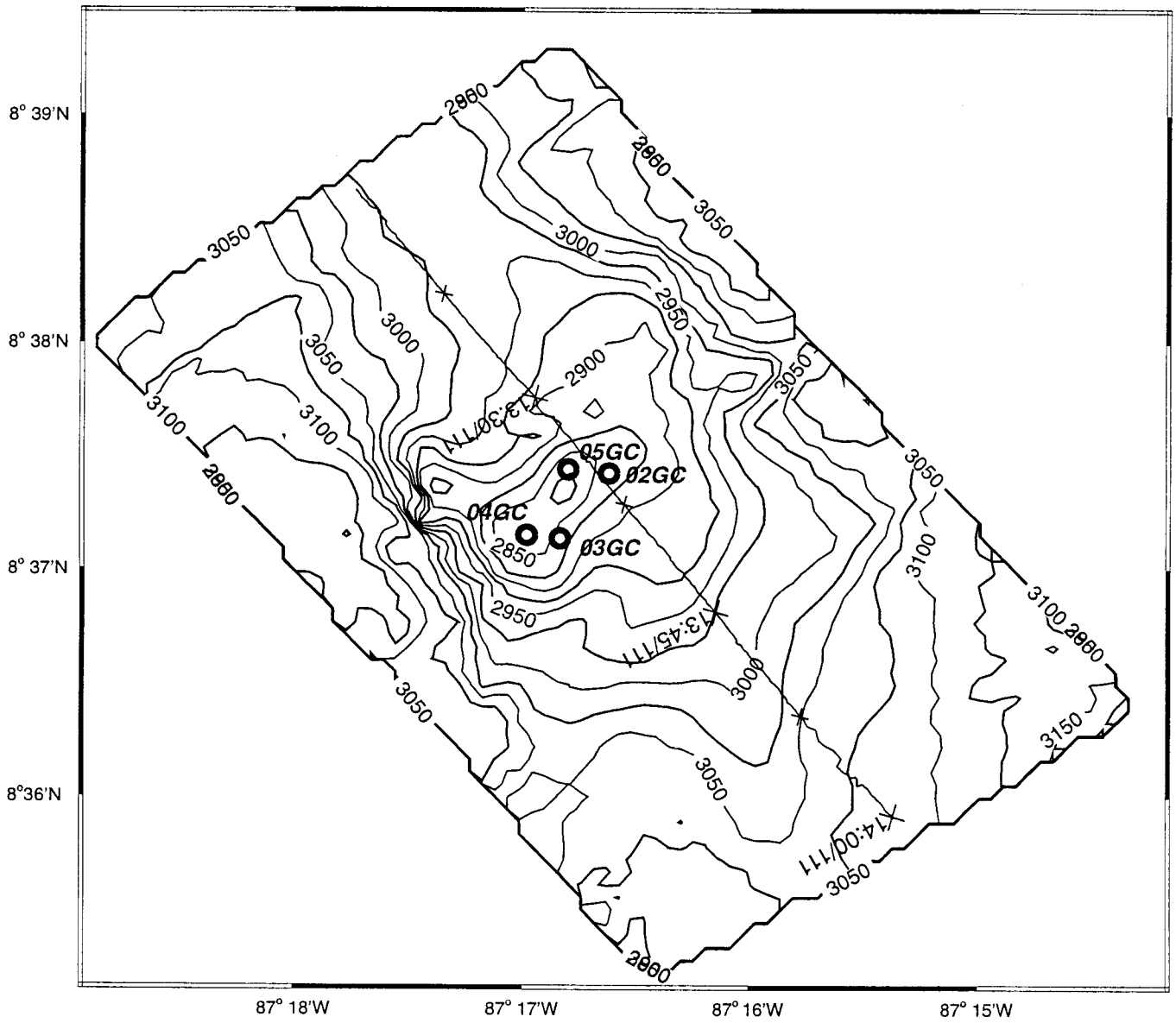
8° 39'N
8° 38'N
8° 37'N
8°36'N
87° 18'W
87° 17'W
87° 16'W
87° 15'W
05GC
02GC
04GC
03GC
2850
2900
2950
3000
3050
3100
3150
13:30/111
13:45/111
14:00/111

Figure V-8

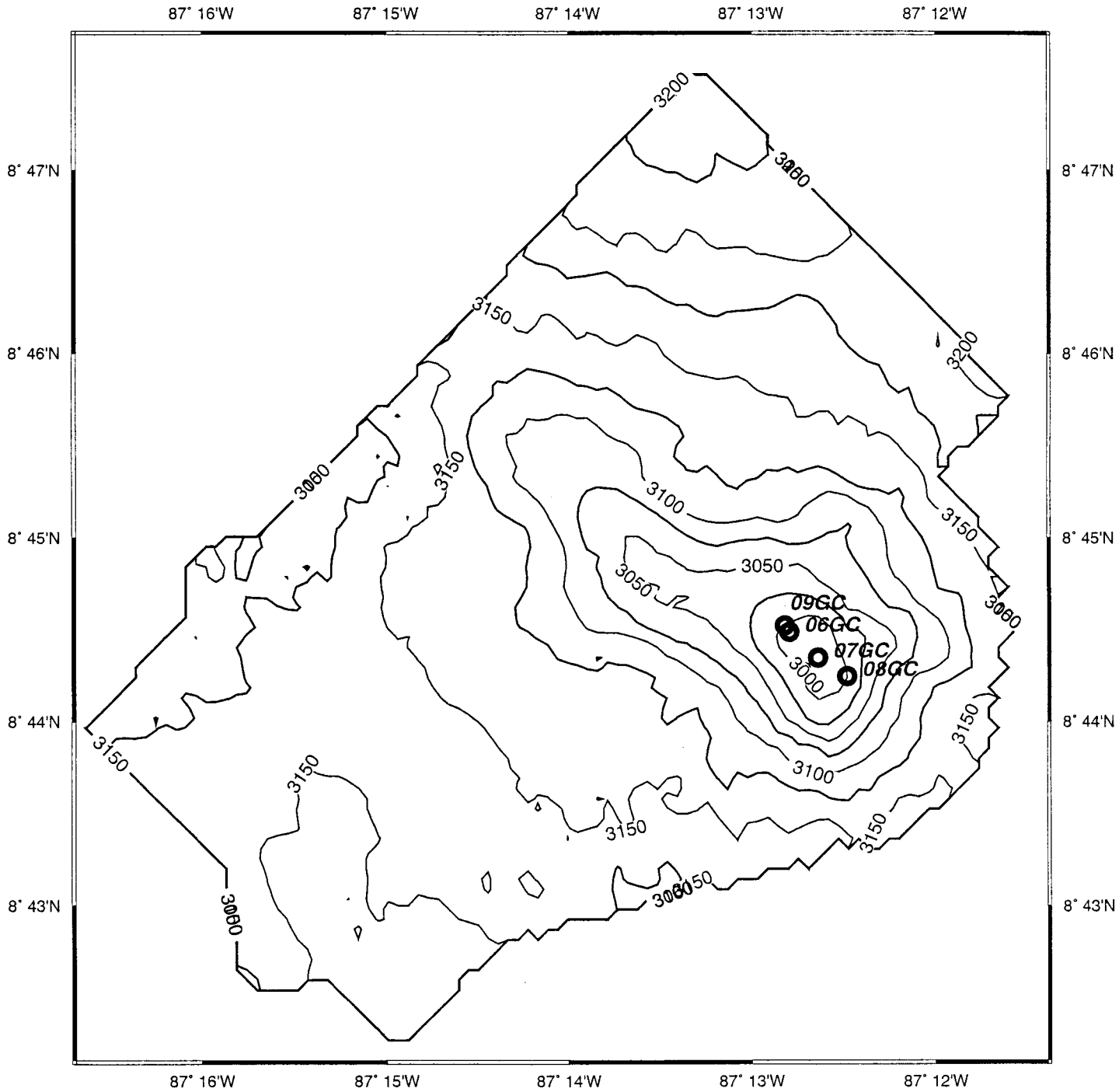
87° 16'W
87° 15'W
87° 14'W
87° 13'W
87° 12'W
8° 47'N
8° 46'N
8° 45'N
8° 44'N
8° 43'N
3200
3150
3100
3050
3000
09GC
06GC
07GC
08GC

Figure V-9

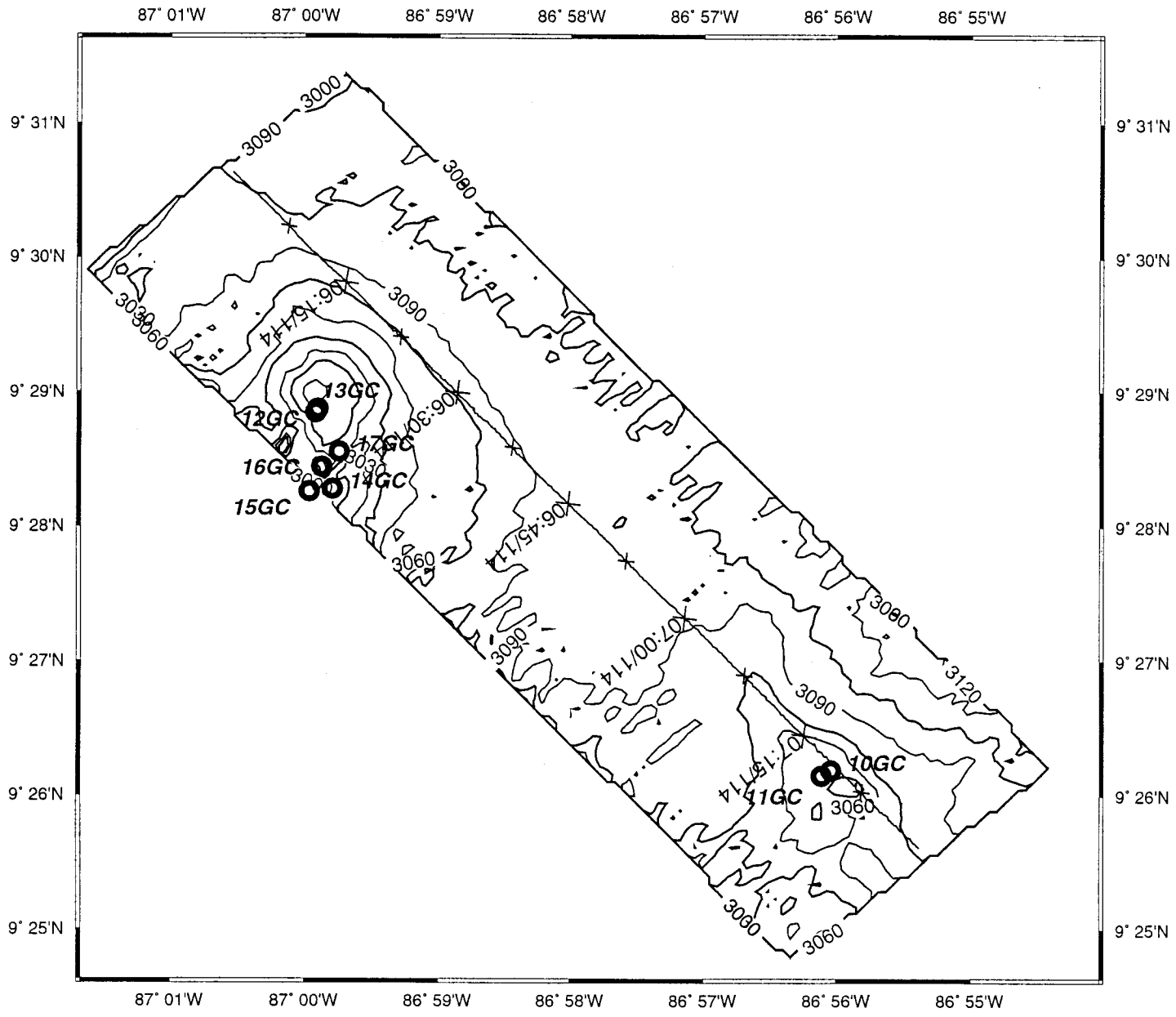
87° 01'W
87° 00'W
86° 59'W
86° 58'W
86° 57'W
86° 56'W
86° 55'W
9° 31'N
9° 30'N
9° 29'N
9° 28'N
9° 27'N
9° 26'N
9° 25'N
3000
3030
3060
3090
3120
06:15/14
06:30/14
06:45/14
07:00/14
07:15/14
13GC
12GC
17GC
16GC
14GC
15GC
10GC
11GC

Figure V-10

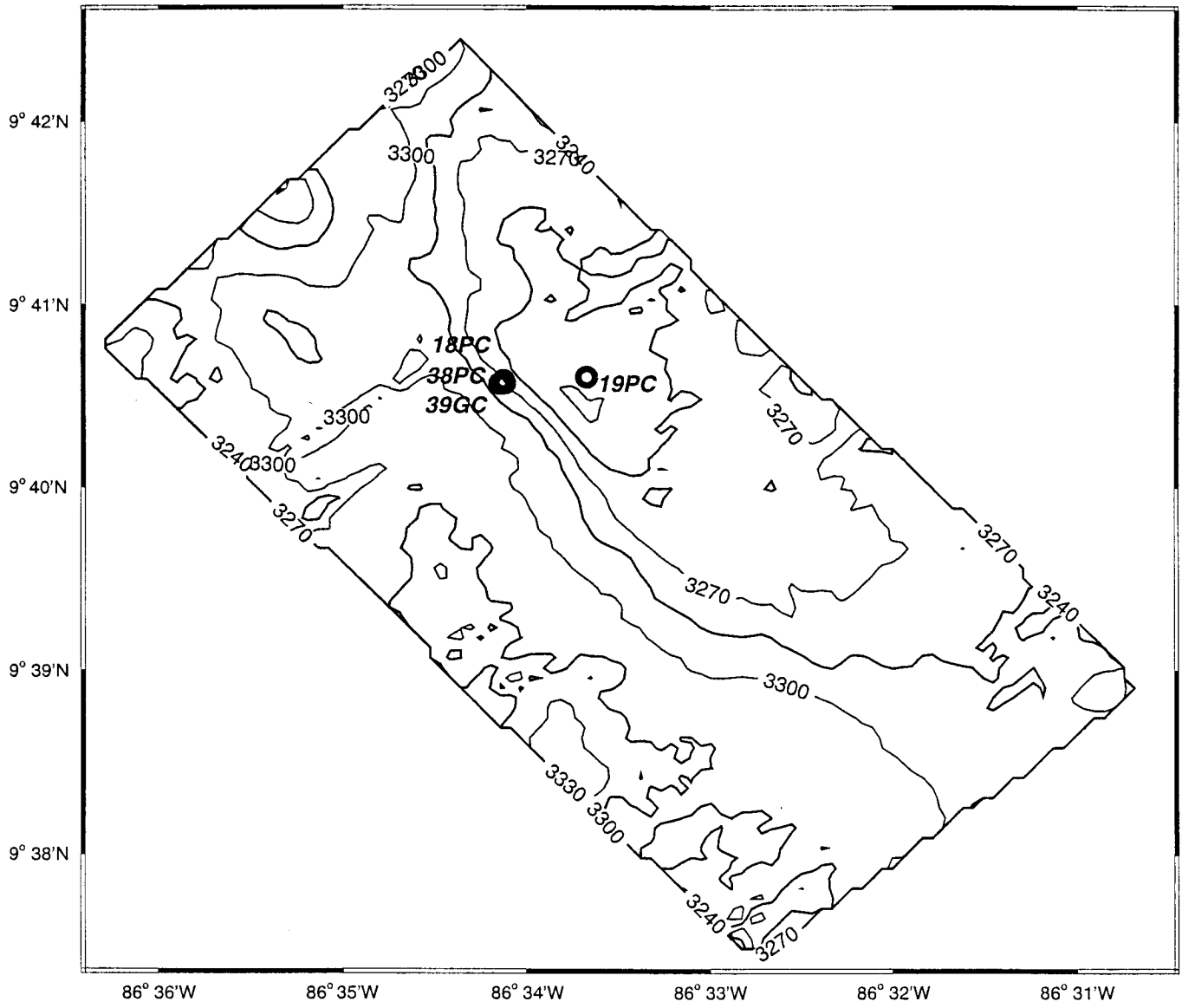
9° 42'N
9° 41'N
9° 40'N
9° 39'N
9° 38'N
86° 36'W
86° 35'W
86° 34'W
86° 33'W
86° 32'W
86° 31'W
18PC
38PC
39GC
19PC
3300
3270
3240
3330

Figure V-11

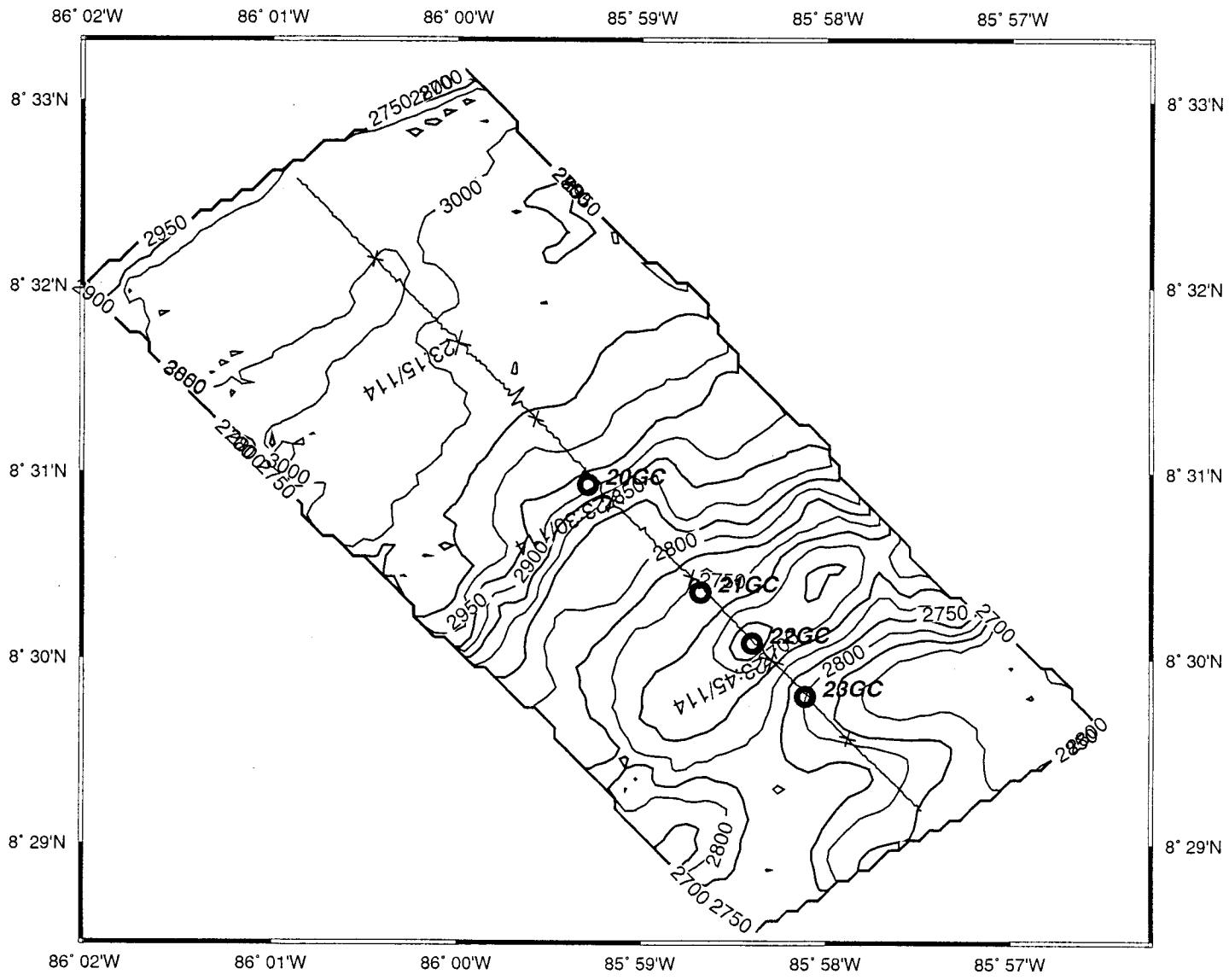
86° 02'W
86° 01'W
86° 00'W
85° 59'W
85° 58'W
85° 57'W
8° 33'N
8° 32'N
8° 31'N
8° 30'N
8° 29'N
20GC
21GC
28GC
26GC
2700
2750
2800
2850
2900
2950
3000

Figure V-12

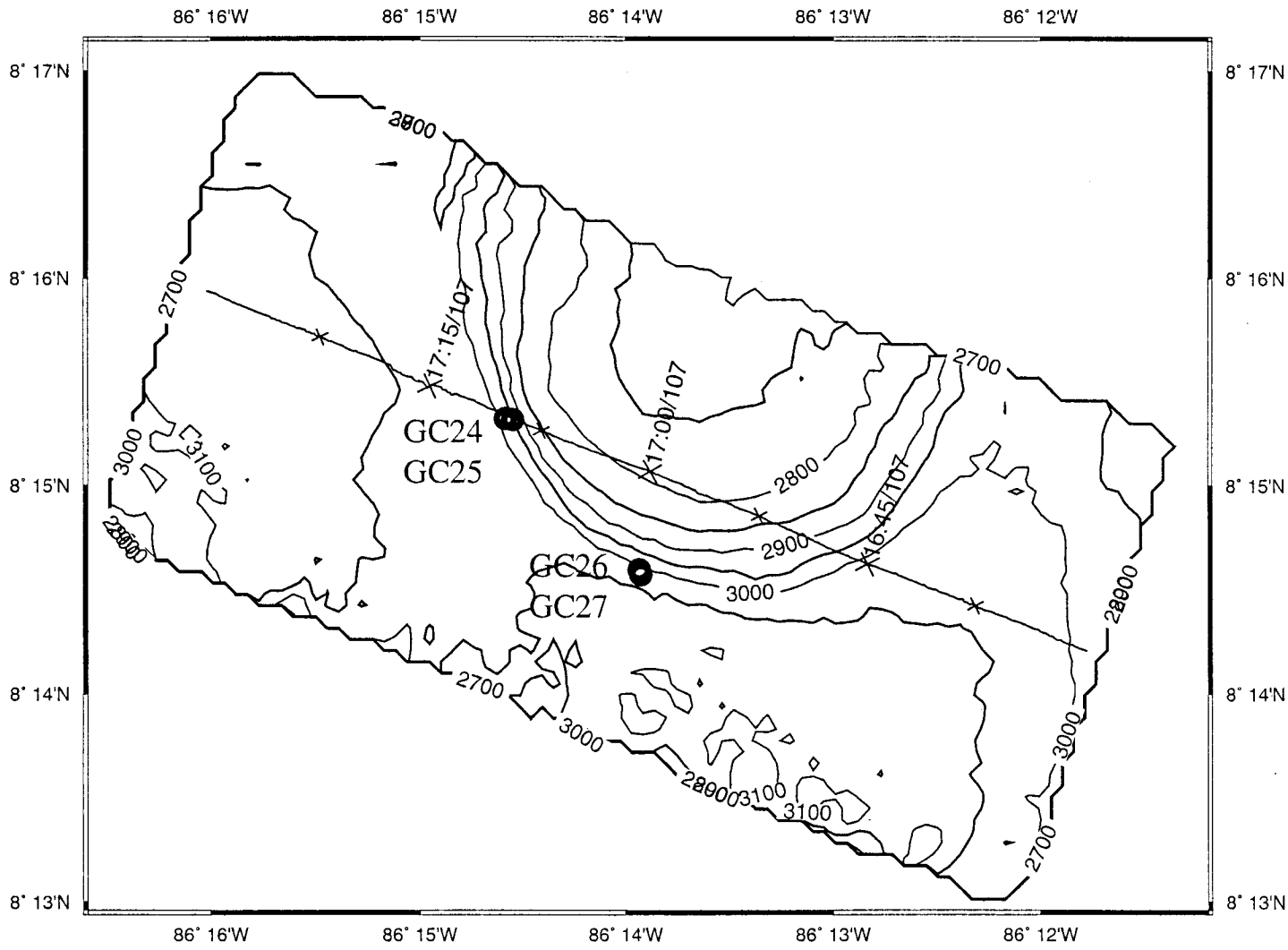
86° 16'W
86° 15'W
86° 14'W
86° 13'W
86° 12'W
8° 17'N
8° 16'N
8° 15'N
8° 14'N
8° 13'N
GC24
GC25
GC26
GC27
17:15/107
17:00/107
16:45/107
2700
2800
2900
3000
3100

Figure V-13

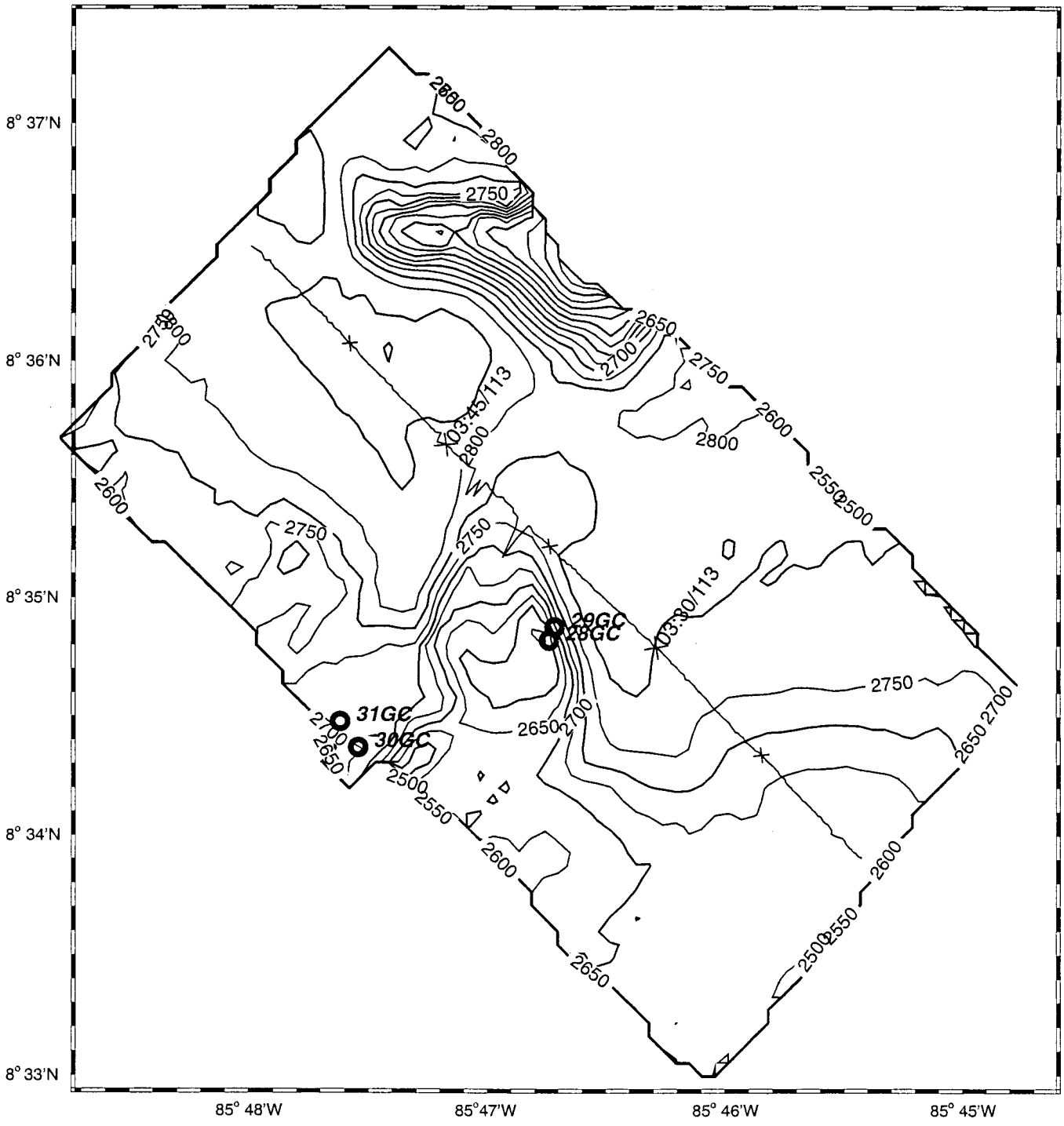
8° 37'N
8° 36'N
8° 35'N
8° 34'N
8° 33'N
85° 48'W
85°47'W
85° 46'W
85° 45'W
2800
2750
2700
2650
2600
2550
2500
03:45/113
03:30/113
29GC
28GC
31GC
30GC

Figure V-14

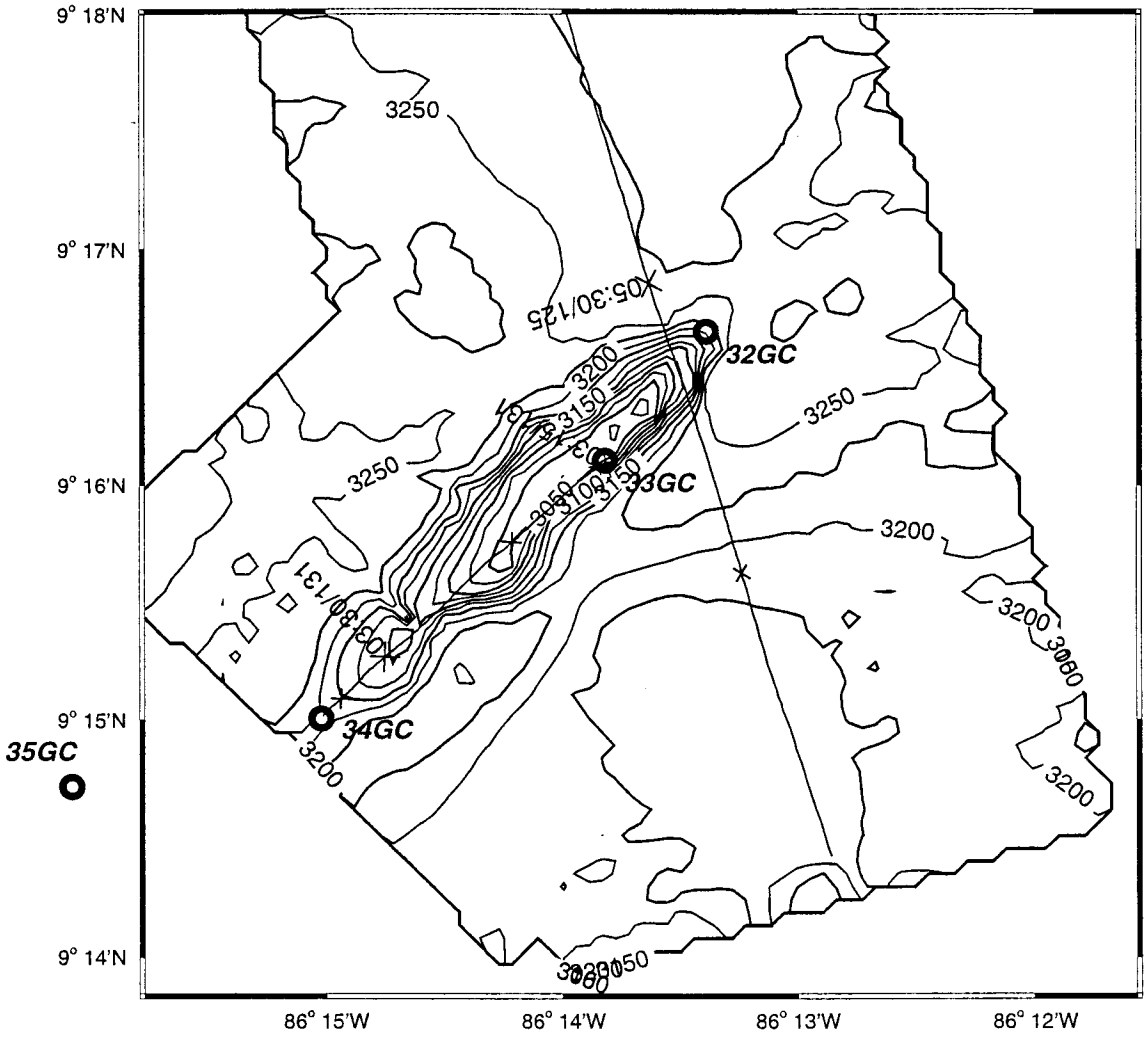
9° 18'N
9° 17'N
9° 16'N
9° 15'N
9° 14'N
86° 15'W
86° 14'W
86° 13'W
86° 12'W
32GC
33GC
34GC
35GC
3250
3200
3150
3100
3050
3000
05:30/125
05:30/131

Figure V-15

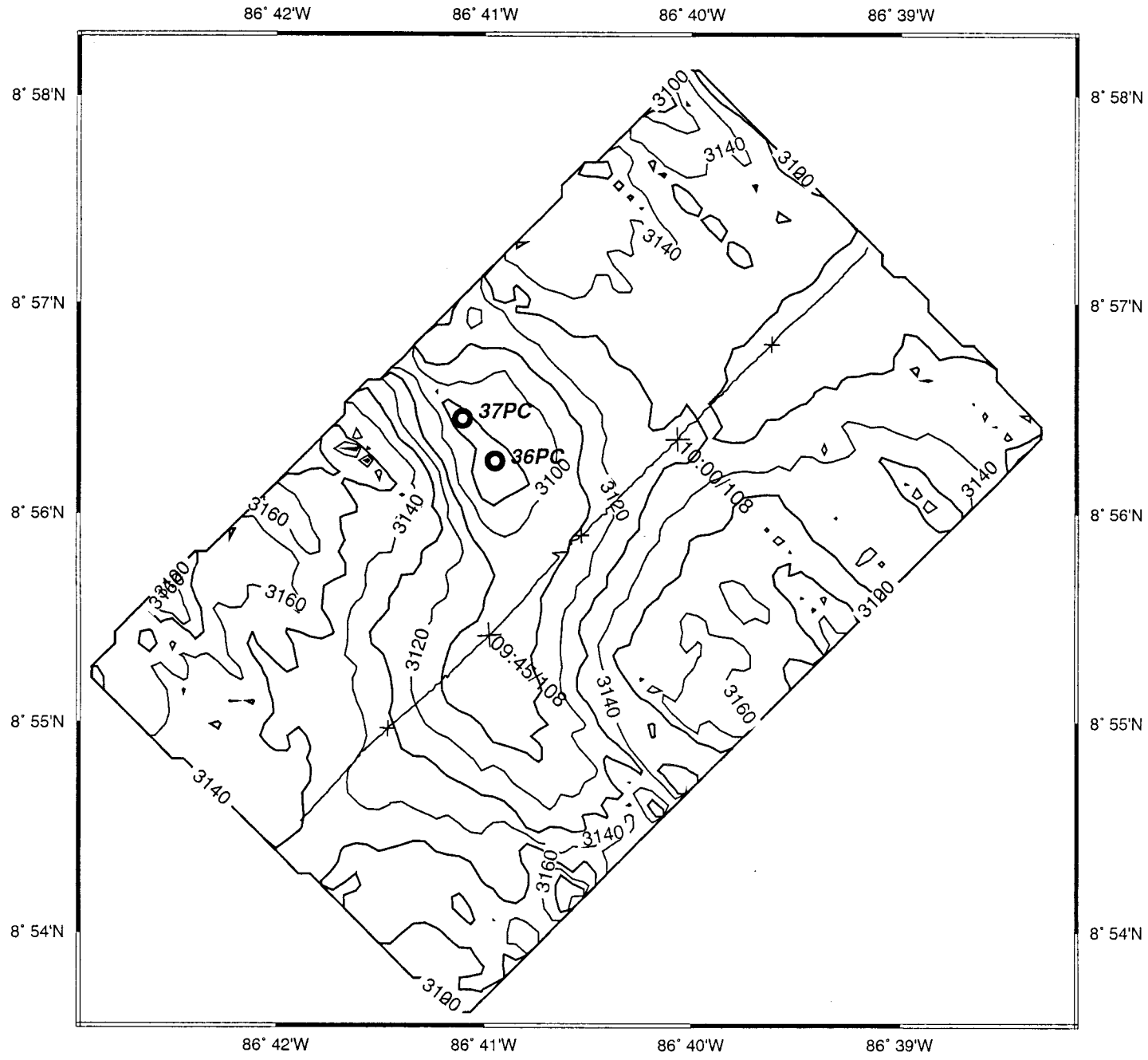
86° 42'W
86° 41'W
86° 40'W
86° 39'W
8° 58'N
8° 57'N
8° 56'N
8° 55'N
8° 54'N
37PC
36PC
10:00/108
09:45/108
3100
3120
3140
3160
3180

Figure V-16

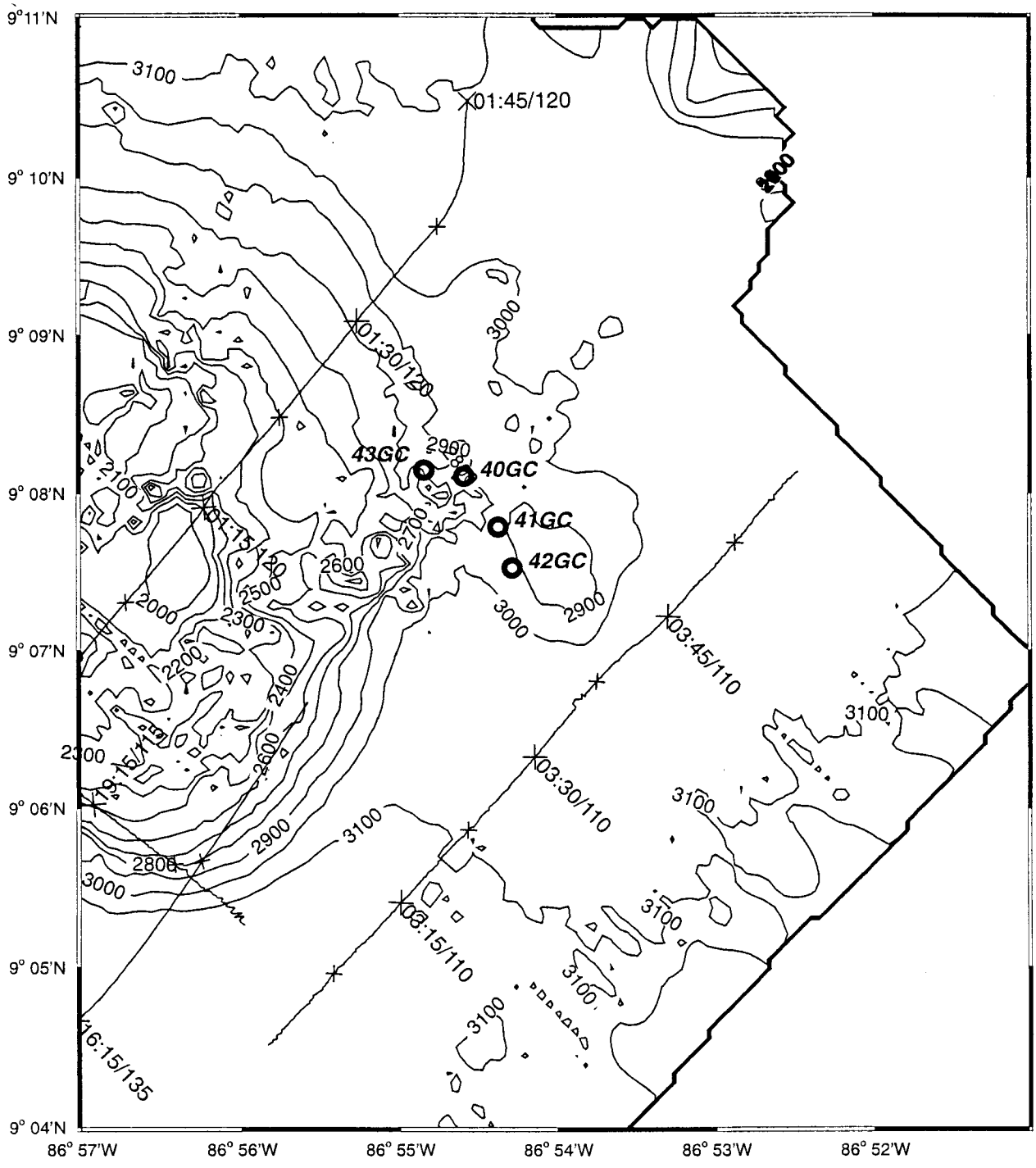
9°11'N
9° 10'N
9° 09'N
9° 08'N
9° 07'N
9° 06'N
9° 05'N
9° 04'N
86° 57'W
86° 56'W
86° 55'W
86° 54'W
86° 53'W
86° 52'W
01:45/120
01:30/120
01:15/120
03:45/110
03:30/110
03:15/110
16:15/135
43GC
40GC
41GC
42GC
3100
3000
2900
2800
2600
2500
2400
2300
2200
2100
2000

Figure V-17

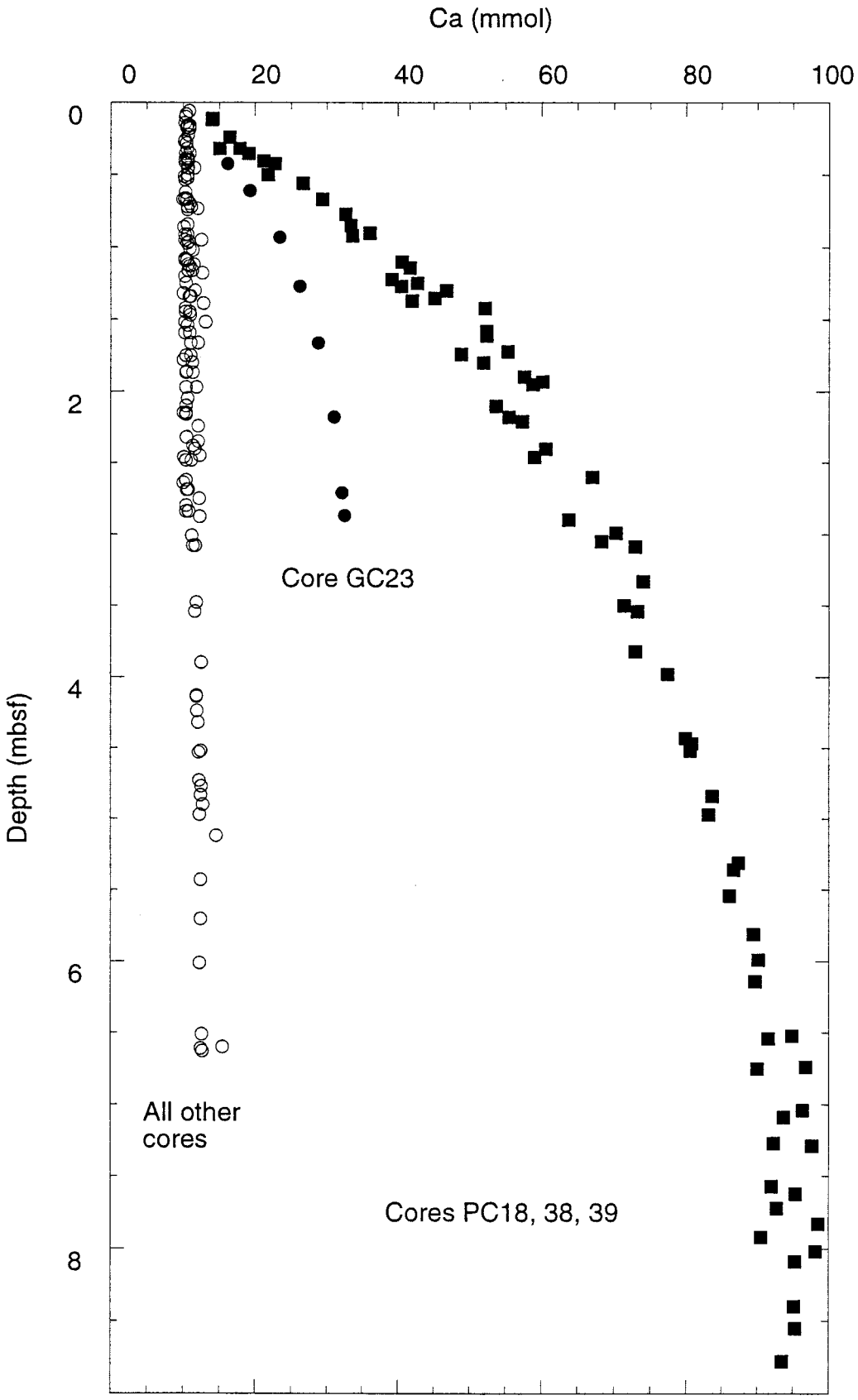
Ca (mmol)
0
20
40
60
80
100
0
2
4
6
8
Depth (mbsf)
Core GC23
All other cores
Cores PC18, 38, 39

Figure V-18